Technical Report
TR-18-13
December 2018

Some mechanisms that influence bentonite erosion in a KBS-3 repository – an exploratory study

Ivars Neretnieks
Luis Moreno

SVENSK KÄRNBRÄNSLEHANTERING AB

SWEDISH NUCLEAR FUEL
AND WASTE MANAGEMENT CO

Box 3091, SE-169 03 Solna
Phone +46 8 459 84 00
skb.se

SVENSK KÄRNBRÄNSLEHANTERING

ISSN 1404-0344
SKB TR-18-13
ID 1694827
December 2018

Some mechanisms that influence bentonite erosion in a KBS-3 repository – an exploratory study

Ivars Neretnieks, Luis Moreno
Royal Institute of Technology, KTH

This report is a result of a joint project between Svensk Kärnbränslehantering AB (SKB) and Posiva Oy. The conclusions and viewpoints presented in the report are those of the authors. SKB and Posiva may draw modified conclusions, based on additional literature sources and/or expert opinions.

A pdf version of this document can be downloaded from www.skb.se.

Abstract

Current modelling suggests that bentonite clay that expands into fractures in crystalline rock with low ionic strength water, below the critical coagulation concentration, CCC, will solubilize and carry away the colloidal size montmorillonite particles as sol. However, in recent experiments the particles in the sol have been found to form flocs. The flocs can also be carried by seeping, even very dilute water. The flocs sediment to the lower side of a horizontal or semi-horizontal fracture and in more sloping fractures they sediment to the bottom of the fracture. Thus clay can be lost from deposition holes by sedimentation also in stagnant water. The rheological properties of the flocs, floc suspensions and sediments influence how fast and how far into the fracture network they migrate. It is shown that the flocs of the primary montmorillonite particles will age and gradually rearrange the network of primary particles to make the flocs stronger. They form gel-like structures strong enough to stop their further movement in fractures. This also impedes water flow in the regions with gel.

Gel formation in waters below CCC is a novel finding in the context of montmorillonite migration in fractured rocks. This can considerably impact the expansion of clay and formation of colloids at the gel/water interface. Models and earlier observations and experiments on the rheology of dilute montmorillonite suspensions are revisited. It is shown that for suspensions with more than about one percent by volume of montmorillonite the shear strength is strongly nonlinear with respect to the shear rate. In some simple scoping experiments it is found that even in very dilute suspensions the montmorillonite flocculates, sediments and forms gel. These observations and data suggest that even several mm large aperture fractures will impede movement of the sedimented montmorillonite. However, when the expanding clay reaches the sediment it will overcome its shear strength and will be destroyed. The expansion rate will not be much impeded.

Another process that has not been quantitatively addressed earlier is the fate of detritus material in the bentonite clay used to protect radioactive waste repositories. In addition to the main mineral, montmorillonite, the clay also contains 10 % or more of much larger accessory mineral particles. When the clay expands into narrow fractures the detritus particles are captured in the narrow portions of the fractures and clog them. Experiments show that filters with pores as large as 0.1 mm are rapidly clogged.

Mechanisms and models for quantitative modelling of such clogging are discussed. Simulations suggest that such clogging can be quantitatively modelled based on independent measurements of natural fracture aperture distributions and of detritus size distributions. The modelling and the experimental evidence strongly suggest that detritus material will clog fractures and strongly reduce the loss of bentonite.

Another aspect of the results of this study is that fractures that are filled with immobile gel and/or detritus material to distances larger than a few decimetres can considerably decrease the mass transfer (nuclide release) from the waste to the seeping water in the fractures. This may be of special importance for the performance assessment of vault repositories where it is more difficult to avoid intersections with more prominent fractures and with small fracture zones.

Sammanfattning

Nuvarande modellering tyder på att bentonitlera som expanderar in i vatten i sprickor i kristallint berg med jonstyrka under den kritiska koagulations-koncentrationen, CCC, kommer att solubilisera och föra bort kolloidala montmorillonitpartiklar som sol i vattnet. Nyligen genomförda experiment visar att partiklarna i solen slås ihop och bildar flockar. Flockarna kan också föras iväg av sipprande vatten. Dock sedimenterar flockar till undersidan av horisontella sprickor och i mer sluttande sprickor sedimenterar de till botten av sprickorna. Därvid kan lera förloras från deponeringshål för radioaktivt avfall även i stagnant vatten. Flockars, floc-suspensioners och sediments reologiska egenskaper påverkar hur snabbt och långt in i spricknätverket montmorilloniten kan vandra. Flockarna med montmorillonitpartiklarna åldras vilket gör flockarna starkare. De bildar geliknande strukturer som är tillräckligt starka för att stoppa fortsatta vandring i sprickorna. Detta hindrar också vattenströmning i områden som fyllts med gel. Gelbildning i vatten under CCC har tidigare inte beskrivits i samband med montmorillonitmigration i sprickor. Gelbildning kan väsentligt påverka expansionen av lera och kolloidbildning. Tidigare modeller, observationer och reologiexperiment av utspädda montmorillonit-suspensioner gås åter igenom. Det visas att för suspensioner med mer än omkring 1 volymprocent montmorillonit är skjuvhållfastheten starkt icke-linjärt beroende av skjuvhastigheten. I några enkla orienterande experiment visas att även i mycket utspädda suspensioner bildar montmorillonitsol sediment och gel. Dessa observationer och data tyder på att även flera mm stora sprickaperturer kommer att hindra rörelsen av sedimenterande montmorillonitgel. Emellertid kommer den expanderande leran att bryta upp flockarna när den når dessa. Lerans expansion kommer inte nämnvärt att påverkas.

En annan process som inte har behandlats kvantitativt tidigare är vad som sker med detritusmaterialet i bentonitlera som användes för att omge radioaktivt avfall i slutförvar. Förutom det viktigaste mineralet, montmorillonit, innehåller lera också 10 % eller mer av större partiklar av andra mineral. När leran expanderar ut i tunna sprickor fastnar detrituspartiklarna i de trängre delarna av sprickorna och täpper igen dessa. Experiment visar att filter med porer så stora som 0,1 mm snabbt blir igensatta och hindrar ytterligare montmorillonit att passera. Mekanismer och modeller för sådan igensättning diskuteras.

Orienterande modellering tyder på att sådan igensättning kan simuleras kvantitativt baserat på oberoende mätningar av naturliga sprickors aperturfördelning och av storleksfördelning hos detritusmaterialet. Modelleringen och experimentella resultat tyder starkt på att detritusmaterialet kommer att kunna täppa till tunna sprickor och minska förlusten av bentonit.

En annan aspekt av resultaten av denna studie är att sprickor som är fyllda med gel och/eller detritusmaterial längre ut än några decimeter avsevärt kan minska massöverföringen till det sipprande vattnet utanför (nuklidutsläppet) från det avfall som skyddas av bentoniten. Detta kan vara av särskild betydelse för avfallsförvar i långa bergrum där det är svårare att undvika att bergrummen skärs av större sprickor och av små sprickzoner. Det senare kan ha stor betydelse för säkerhetsanalysen.

Contents

1 Aims and scope 7

2 Introduction and background 9
2.1 Structure of the report and description of some terms used 9
2.1.1 Structure of report 9
2.1.2 Use of some terms in this report 9
2.2 Overview of properties and behaviour of bentonite clays related to the present problem 10
2.3 Some observations related to the problems in this study 12
2.3.1 Observations in tubes and slots with stagnant water 13
2.3.2 Observations in slots with seeping water 15
2.4 Questions asked and approaches to address them 18

3 Mechanisms and models of bentonite properties and behaviour 19
3.1 Rheology of bentonite slurries and Mt sols 19
3.1.1 Rheology and viscosity 19
3.1.2 Bentonite clay properties 19
3.2 Expansion and sol formation of Mt in bentonite 20
3.3 Compression of sol by gravity and phase separation of sol 22

4 Flocculation and floc migration 25
4.1 General 25
4.2 Flocculation 26
4.2.1 General 26
4.2.2 Particle and floc sedimentation rates 27
4.2.3 Modelling flocculation kinetics and floc strength 28
4.3 Some cases considered 29
4.3.1 Horizontal fracture 29
4.3.2 Sloping fracture with stagnant water 29
4.4 Modelling non-Newtonian flow in slots 30

5 Some scoping experiments in testtubes 33
5.1 Yield strength and minimum slot aperture for gravity induced flow 35

6 Viscosity and shear strength of montmorillonite suspensions in low ionic strength water 37
6.1 Experimental data on viscosity and shear strength of montmorillonite in dilute water 37

7 Flow of powerlaw and H-B fluid in a slot 41
7.1 Commencement of flow 41
7.2 Flow after mobilisation 42

8 Possible causes and consequences of phase separation of sol at low ionic strength and dilute waters 45
8.1 Impact of positively charged edges 45
8.2 House of cards structure of gel 45
8.3 Impact on expansion of clay from the source 46
8.4 Conclusions on the impact of gel formation in below CCC waters 47

9 Impact on clay expansion by detritus material in bentonite 49
9.1 Movement of detritus particles 49
9.2 Conventional filtration processes in nature and industry 49
9.3 Filtration techniques 49
9.3.1 Membrane filtration 49
9.3.2 Deep bed filtration 50
9.4 Basic mechanisms of filtration 50
9.5 Overview of concepts and mechanisms 51

9.6 Colloid transport in porous media and fractured rocks 52
9.6.1 Experimental evidence for clogging of pores by expanding bentonite 52

10 Quantitative modelling of filtration 55
10.1 Continuum-based models 55
10.1.1 Filtration coefficient concept 55
10.1.2 Filtration coefficient magnitude 57
10.1.3 Tentative conclusion regarding the use of filtration coefficient models 57
10.2 Population balance models 57
10.2.1 Example to illustrative the idea of the PTMC 59
10.3 Discrete pore network modelling 60
10.4 SP flux driven by expanding Mt 61
10.4.1 Example with filtration coefficient model 62
10.4.2 Example to illustrate Population balance model. 64
10.4.3 Further comments on the PTMC model 66

11 Discrete element modelling of particle transport 67
11.1 Possible clogging simulations of a variable aperture fracture 67

12 Some possible future modelling approaches and experimental demonstrations of clogging of rock fractures around a repository 69
12.1 Sol flocculation, gel formation and clogging of fractures 69
12.2 Clogging by detritus 69
12.2.1 Filtration coefficient concept 70
12.2.2 Population balance model(s) 70
12.2.3 Discrete element modelling of particle transport 70

13 Discussion and conclusions 71

References 73

Appendix A Summary of the equations used to simulate straining of SP by the filtration coefficient model 77

Appendix B Summary of the central equations for the population balance model 79

Appendix C Summary of some recent erosion experiments 83

Appendix D Exploratory modelling of forces in house of cards structures 85

1 Aims and scope

In this exploratory study we want to address and explore what will be the fate of eroding colloidal size montmorillonite fraction of bentonite clays when this intrudes fractures in crystalline rocks at repository depth and how this will influence clay transport and water seepage in fractures. We also want to address the fate of the accessory mineral particles in the clay and how these may be captured in the variable aperture fractures. Clogging of fractures may also influence the water seepage and may impede the erosion itself. We do this by revisiting earlier SKB and Posiva investigations and papers in the open literature and by performing some simple scoping experiments and some simulations.

2 Introduction and background

In SKB and Posiva present clay erosion modelling it is shown that when the clay can form gel, which it can, when ion-concentrations in water are higher than a few 10´s mM the gel will not erode although it may expand into fractures. In more dilute waters the montmorillonite, Mt, in the bentonite can form stable sol that can be carried away by seeping water. Both phenomena have theoretical support and have been verified by experiments. Details of the further fate of the eroded sol were not considered in the previous modelling. Recent experiments show that the sol is not stable and forms flocs that sediment. A suspension of flocs can be expected to develop much higher viscosity with time and possibly form non-flowing gel.

Clogging of fractures by the eroded material could influence the flowpaths around a repository. Such potential clogging is therefore of interest for those who are concerned with hydrological aspects and solute transport in the rock in the near- as well as in the far-field hydrology. Some of these problems have recently been addressed (Neretnieks and Moreno 2018).

For the benefit of those who are not familiar with bentonite clay properties and modelling we summarise and highlight some of the relevant basic concepts, models and observations of clay properties, expansion and erosion in Chapters 3 and 4. This information is relevant for the subsequent chapters.

If not otherwise mentioned, the purified montmorillonite is from Wyoming bentonite “MX-80”.

2.1 Structure of the report and description of some terms used

2.1.1 Structure of report

The report addresses two different mechanisms that impact the expansion of bentonite clay in fractures namely gel formation in low salinity water and the fate of detritus particles in bentonite. The present Chapter 2 summarises some basic properties of bentonite clays and their behaviour in relation to their use to protect nuclear waste in repositories. Chapter 3 outlines the main mechanisms and processes that influence bentonite mobility. Chapter 4 describes flocculation and floc mobility and aging. These chapters also give background to the discussions in later chapters. Chapter 5 describes some novel experiments that show that what is commonly thought to be stable montmorillonite sols are not stable and within weeks or months form gel that clogs fractures. Chapters 6 and 7 discuss rheologic properties of gels and bentonite pastes and their mobility in fractures. Chapter 8 discusses possible causes of the instability of “stable” montmorillonite sols.

Chapters 9 and 10 discuss mechanisms of filtration of fine particles by filters and porous media, conceptual models for particle retardation and capture and also modelling that could be used to quantify the capture of particles in variable aperture fractures. In Chapter 11 a modelling tool, hardly discussed in conventional filtering literature, discrete element modelling, DEM, is shortly described. Its merits and potential to simulate clogging of real fractures is discussed. Chapter 12 summarises the effects of gel and detritus clogging and possible ways forward.

2.1.2 Use of some terms in this report

- Aggregate refers to a group of particles that are quite strongly bound together whereas agglomerates refer to looser, larger structures of primary particles or aggregates.
- By agglomerate fluid, AF, is meant a suspension of agglomerates that can be gel-like under some conditions but can flow under other conditions. The AF may be considered as an elasto-plastic material, which only deforms under mild stress but can flow under large stress.
- Floc is a small agglomerate.
- Gel is a semi-rigid 3-dimensional structure of particles (colloids) in a continuous phase. An example is jelly. An agglomerate, if strong, can behave like a gel.

- Sediment is a collection of particles, aggregates and agglomerates generated by settling in a gravity field. It has been compressed by gravity and can be fluid or behave as a gel depending on the stress.
- Sol is a stable suspension of colloidal size solid particles.
- Stack is a face-to-face aggregate of two or more clay sheets.

2.2 Overview of properties and behaviour of bentonite clays related to the present problem

In the KBS-3V design of the repository for spent nuclear fuel deep in crystalline rock, copper canisters surrounded by compacted bentonite clay are emplaced in vertical deposition holes in tunnels. The tunnels and drifts of the repository are backfilled with a sand-bentonite mixture. Bentonite clay consists mostly of montmorillonite, Mt, a smectite mineral and on the order of 10 % of other accessory minerals, here called detritus. The montmorillonite crystals are extremely thin sheets, 1 nm thick, built up of a three layers of oxides. The middle layer of Al_2O_3 is sandwiched between two SiO_2 layers. Al and Si atoms share oxygen bonds. The sheets are typically 200–300 nm in the other directions. The sheets are highly negatively charged because some Al(III) atoms are substituted for Mg(II) or some other divalent atom and some Si(IV) atoms for Al(III). The surplus negative charge is compensated by the presence of Na^+ and Ca^{2+} ions bound to the surfaces of the sheets. Also lower concentrations of Mg^{2+} and K^+ and other ion contribute. In dry clay the sheets are arranged in stacks on the order of hundred(s) of sheets. The accessory minerals are on the average much larger than the sheets. The size ranges typically from 1–100 μm, but also larger particles are present.

The description below outlines the conventional concept of gel and sol formation and behaviour of montmorillonite clay according to the DLVO theory (Evans and Wennerström 1999). See also Birgersson eta al. (2009) and Neretnieks et al. (2009) where the clay properties are directly related to problems in KBS-3 repository conditions. We will later discuss another attractive force than the van der Waals, vdW, force, which may change the above picture for the conditions of interest here.

Bentonite clay takes up water and swells strongly when the cations bound to the surfaces of the sheets by electrostatic forces dissolve in the water intruding between the sheets. These charge-compensating ions still remain near the surface of the sheet in a diffuse double layer, DDL. The negative charges make up one layer and the cations dissolved in the water make up the other layer. The term diffuse indicates that nearest the surface the ion concentration is high and drops off with distance. The sheets repel each other with a swelling pressure that can be up to ten MPa at the high compaction at which the clay is emplaced. When the clay has room to expand the sheets distance themselves from each other and the swelling pressure between them decreases. The swelling pressure at a given distance between sheets, which also can be expressed as volume fraction of montmorillonite ϕ, is also influenced by the ion concentration in the intruding water. Swelling pressure decreases with increasing ionic strength but is also influenced by the kind of cations that dominate the composition. At total concentration of ions below some tens of mM monovalent cations the colloidal size Mt sheets could expand "forever" and fill out all available volume and form a stable sol in water. At some point of expansion the swelling pressure between sheets is no longer large enough to push the mostly uncharged detritus mineral particles before them and these are left behind. In a gravity field the Mt particles still continue to distance themselves because the Brownian diffusion can be stronger than the restraining force by gravity. The larger detritus particles, however, can sediment and will no longer be influenced by the, now weaker swelling pressure of the expanding Mt colloidal sol. This will happen at volume fractions ϕ of Mt on the order of 1 %. The repulsive forces described above are called DDL forces.

In higher than a few tens mM monovalent cation concentrations the swelling pressure decreases more rapidly with increasing distance between the sheets than the attractive van der Waals, vdW, forces do. At some distance the attractive and repulsive forces become equally strong and expansion stops. The Mt forms a stable gel. The volume fraction of montmorillonite of the gel at this point is on the order of five percent and is larger at higher ionic concentration. The lowest ion concentration at which sol is not stable and gel forms is called the critical coagulation concentration, CCC.

Figure 2-1 illustrates swelling stages of montmorillonite in which sodium ions dominate the swelling. At high compaction the sheets are very close to each other, about 1 nm distance between faces. When allowed to expand and swell the distance between sheets increases. When the intruding water is above the CCC, the swelling stops and a coherent gel forms because the repulsive DDL force becomes equal to the attractive vdW force. Then individual particles are not spontaneously released to the water and shear rates generated by the seeping water cannot tear off colloidal particles from the gel.

In dilute waters on the other hand, such as rainwater and typical drinking waters, the repulsive DDL forces dominate over the attractive vdW forces and gel does not form by the face-to-face repulsion/ attraction balance. In a stable sol the particles can distance themselves and fill out all available volume, were it not for the effect of gravity. In a vertical testtube e.g., the particle concentration will be larger near the bottom.

It may also be noted that the above is the conventional description of the processes involved. It is somewhat oversimplified. It does not apply when the charge compensating ions are mostly divalent such as calcium ions. Ca^{2+} ions are the most important in this context. Figure 2-2 illustrates such conditions where stacks of montmorillonite sheets in calcium dominated conditions do not disperse but form stable aggregates (stacks) in which the sheets are very strongly held together at a distance of about 1 nm. This is also the case in extremely dilute waters, including de-ionised water. It should be noted that the stacks repel each other and that compacted calcium dominated clays also expand with a high swelling pressure. The expansion is much more limited than for sodium dominated clays and the stacks are too massive to be released as colloids. However, in a gravity field the stacks are released and "rapidly" sediment (Schatz and Akhanoba 2017).

Figure 2-2 also illustrates the presence of accessory minerals (detritus). The detritus particles are mostly much larger than the smectite sheets. The detritus particles are pushed along by the swelling clay until, as in sodium-dominated clays in dilute waters, the Mt forms sol and releases the detritus. The detritus particles can then sediment in a gravity field. It is also illustrated in the figure that in calcium dominated clays the Mt forms stacks of particles and swelling will stop earlier.

It should also be noted that during the expansion of the clay in a variable fracture the detritus particles may be captured in narrow passages of the fracture and potentially clog the fracture slowing down the clay expansion. This is one of the processes that will be specifically addressed in this report.

Figure 2-3 shows the size distribution of detritus particles from the MX-80 bentonite (Neretnieks et al. 2009). It also indicates the apertures of fractures expected to intersect a deposition hole. The size of smectite sheets is also indicated by the location of the vertical downward pointing arrow close to the y-axis.

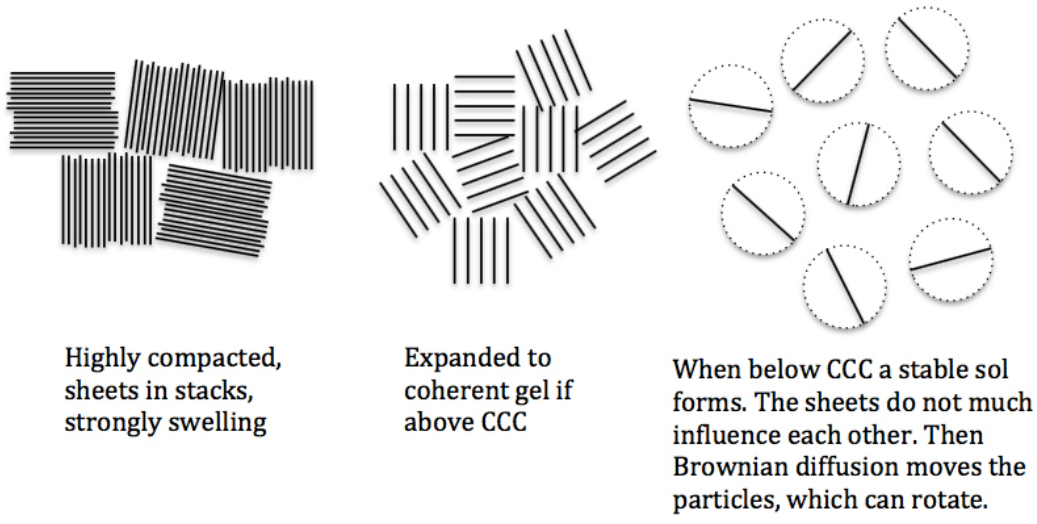

Figure 2-1. *Different stages of swelling Na dominated montmorillonite.*

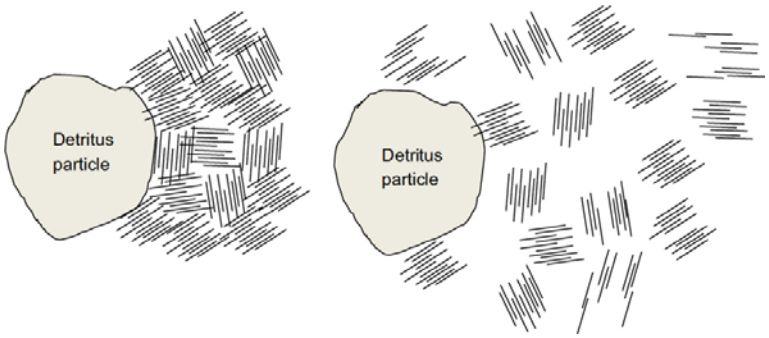

Figure 2-2. *Conceptual picture of swelling untreated Ca-bentonite clay. Left figure shows highly compacted clay with stacks of sheets arranged for low porosity. Right part of figure shows expanding clay where stacks distance themselves from each other and partly break apart at the weak spots in the stacks. The stacks repel each other.*

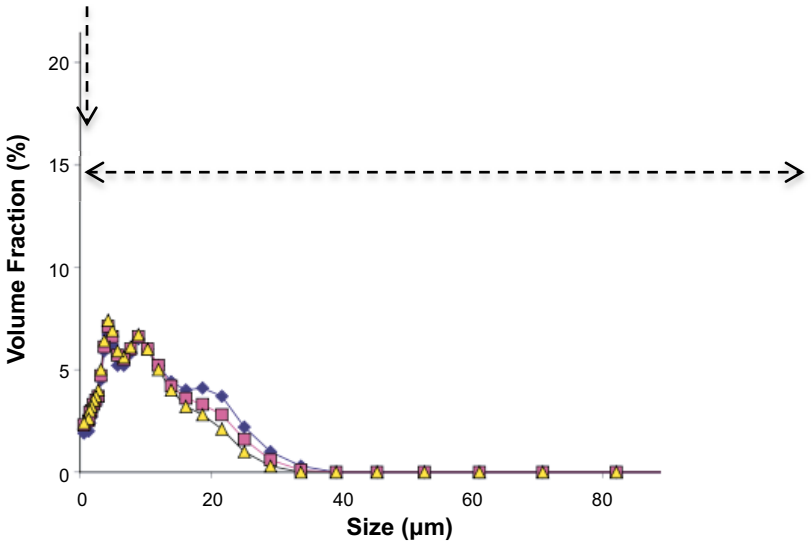

Figure 2-3. *Particle size distribution for accessory mineral particles measured on three different batches. The horizontal dashed arrow shows the range of mean fracture apertures expected to intersect deposition holes. The vertical dashed arrow close to the vertical axis indicates the size of the thin Mt sheets.*

In addition to the DDL and vdW forces between the flat sheets specific coulombic forces can be important. The edges of the sheets can be positively charged, which can lead to edge-to-face attraction and formation of lose flocs of sheets also when the ion concentration is below what is expected to be CCC (Hedström et al. 2016). When newly formed, the agglomerates are quite flexible and can change their form and penetrate through narrow passages in e.g. a narrow net, to reform into larger agglomerates after passing. The agglomerates or flocs are denser than water and sediment in a gravity field.

2.3 Some observations related to the problems in this study

The bentonite in a deposition hole and the bentonite or a bentonite-sand mixture in the drifts and tunnels swells by the water intruding from the fractures in the water filled rock. Water can also migrate in the connected pores of the unfractured rock matrix. The expanding clay fills the available volume and also expands into the water filled fractures in the rock. As described above the montmorillonite can expand until its volume fraction decreases to about 1 % at the gelling front if the ion concentration is above the CCC, or it could expand "forever" if below CCC according the DLVO theory. The colloidal size montmorillonite particles can pass through passages that are smaller than

a few μm (Birgersson et al. 2009). They do this with the same ease as they pass lager pores and their movement does not seem to be influenced by wall friction when they expand into the water in the fractures (Neretnieks et al. 2009).

Under below CCC conditions, the loss rate of clay from a deposition hole intersected by a horizontal fracture, neglecting gravity effects and clogging effects by detritus, decreases only slowly over time. This is when the expansion is into fractures that extend far into the rock as well as when the expansion is into a fracture that connects to a three-dimensional fracture network (Neretnieks at al. 2017). Over very long times the loss could be considerable. In water below CCC the particles at the clay/water interface solubilise to sol, which can be carried away by seeping water. This can further increase the loss rate above that which fills the fractures and remains there. Furthermore, it has been found that the sol that forms in flowing fractures rapidly agglomerates forming loose flocs that also can be carried away by the water. The flocs sediment in sloping fractures, which increases the rate of loss (Schatz et al. 2013, Schatz and Akhanoba 2017). The floc formation speeds up the release of new colloid particles (Neretnieks et al. 2017).

2.3.1 Observations in tubes and slots with stagnant water

Montmorillonite flocs formed by agglomeration of numerous individual montmorillonite sheets can form large structures and fill fractures. Floc formation is facilitated by weak shear forces, which help the individual particles to come in contact, so that attractive forces can form bonds. At higher shear rates the bonds can break. The flocs are flexible and can navigate through narrow passages when driven by some force e.g. gravity, as they are slightly denser than water. Figure 2-4 shows an example of this. These simple tests were made where a small amount of clay (0.2 g) was put into the bottom of testtubes. 10 ml water was poured onto the clay, which was allowed to swell and expand in the water giving a volume fraction of Mt of 0.74 %. A thin very fine net with nominal hole size of 10 μm was fastened in the tube on top of the suspension. The tubes were then filled to the rim with water with different compositions. After one day the tubes were turned upside-down. The response was easy to observe within 5 minutes. Depending on water composition, either the clay dispersed and started to fall through the net or else it stayed above the net (Jansson 2009). Discrete flocs were not visible to the eye after the one-day rest before inverting the tubes but have formed because individual smectite sheets are not mobilized by far so rapidly by gravity as will be shown later.

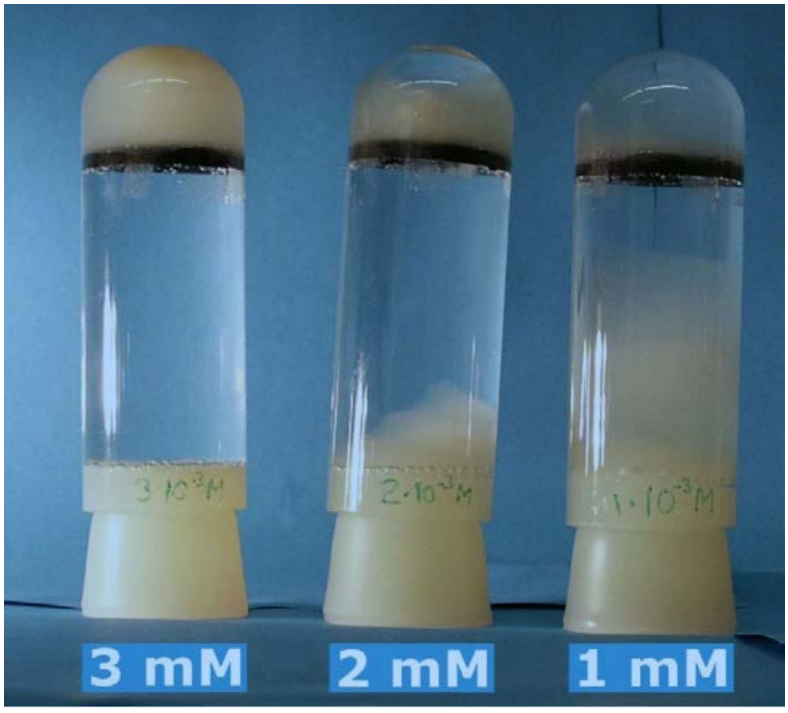

Figure 2-4. *Sedimentation of montmorillonite clay flocs through a fine net at different concentrations of* $CaCl_2$.

Figures 2-5 to 2-7 show an experiment in which bentonite clay had expanded upward in a smooth-walled slot in de-ionised water. After some days, when swelling had stopped, the slot was turned upside down. After some hours the sediment (black) developed "fingers" pulled by gravity as shown in Figure 2-5.

Figure 2-6 shows an enlargement of the flocs. The small dark spots are detritus particles. One floc, about 1 mm in size has just been released and moves slowly downward. It is probably in touch with the walls.

Figure 2-7 shows another floc under different lighting conditions.

It was found that natural MX-80 bentonite as well as MX-80 washed of the calcium sulphate in the detritus could release clay flocs into initially de-ionised water. In different experiments the water after some time in contact with the clay had acquired Na and Ca concentrations ranging from 0.42 to 2.9 and from 0.02 to 1.02 mM respectively.

The above examples show that flocs readily form in dilute waters and are mobilised by gravity. The examples also show that the flocs carry detritus material with them.

Figure 2-5. *Upside down turned sediment in 1 mm aperture fracture 24 hours after turning the slot upside down. Floc fingers are slowly pulled downward by gravity. Small flocs are released and very slowly move downward. The whole picture is about 4 cm high.*

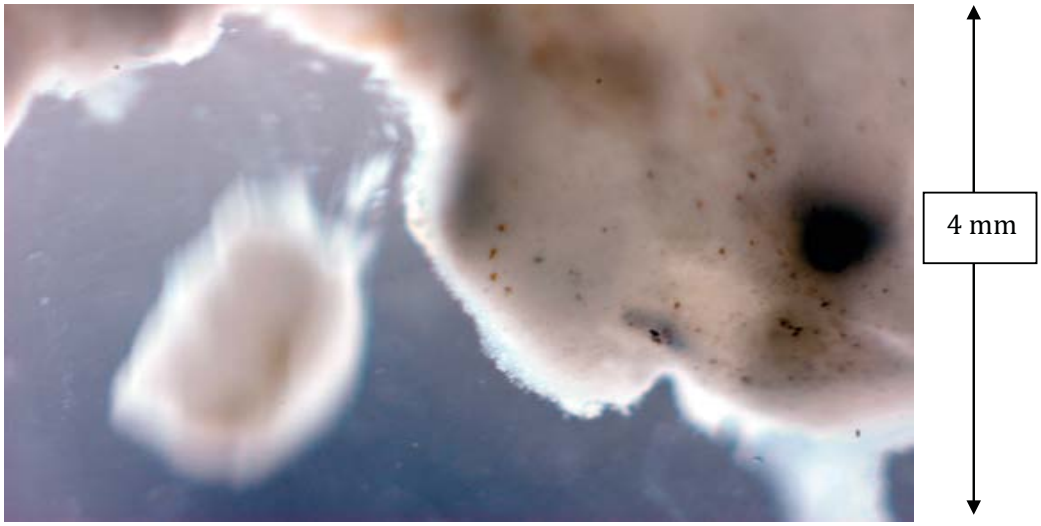

Figure 2-6. *A floc just released and sedimenting in a vertical fracture. Large and small black particles are clearly seen in the floc that is forming.*

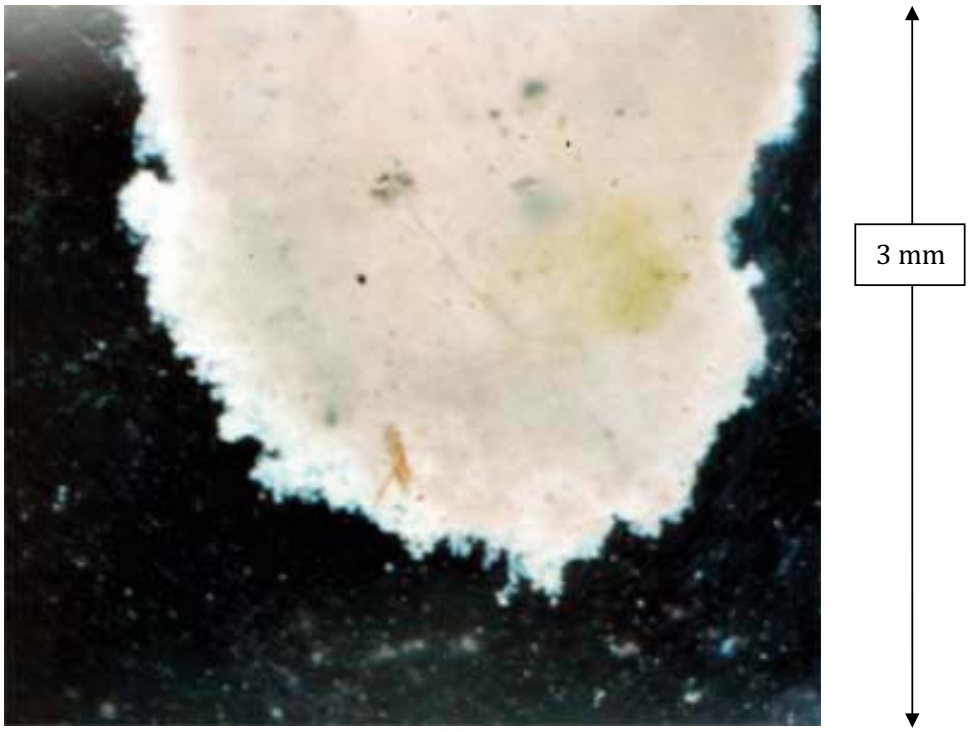

Figure 2-7. *Another floc with different lighting. Small dark detritus particles are clearly identifiable.*

2.3.2 Observations in slots with seeping water

Below follow a series of pictures from Schatz et al. (2013). They illustrate the floc formation when compacted homo-ionic Mt pellets free from detritus are subjected to flowing de-ionised water in horizontal narrow slots. It is also shown that when the slot is turned vertical the flocs sediment. It is also seen that the flocs become grainier with time. A number of other similar experiments that address the fate of flocs in sloping fractures are reported in Schatz and Akhanoba (2017). In one experiment detritus-free, homo-ionic NaMt in de-ionised water was used. See Figure 2-8. Flocs are beginning to be seen after 144 hours in frame d. The floc structure becomes coarser with time and is quite grainy after 456 hours as seen in frame f. Dye injection showed that the flocs moved essentially with the same velocity as the water outside the floc region. When the slot was turned vertically the flocs sedimented and formed a heap at the bottom of the fracture.

Figure 2-8 shows a series of photographs of how homo-ionic detritus free montmorillonite is released from a compacted pellet to water flowing in a narrow horizontal slot.

Figure 2-9 shows an enlargement of a section in frame f.

When the slot was turned to vertical the flocs sedimented. An example is shown in Figure 2-10. It is seen that initially small flocs and very narrow streams of particles are released. They seem to collect to a larger coherent “sheet” after a short distance. This sheet fills the slot between its two walls. The sheet is in contact with both walls of the slot, which slows the sedimentation. At the lower end of the sheet new small flocs are released. If the migration of the agglomerate fluid, the sheet in this case, cannot move away due to wall friction as rapidly as it is fed from above, this would eventually clog the fracture.

The formation of agglomerate sheets is also seen in Figure 2-11, right column, where the flocs sedimenting in a 0.1 mm slot form coherent sheets after a short distance. This was not the case in a 1mm slot, left column.

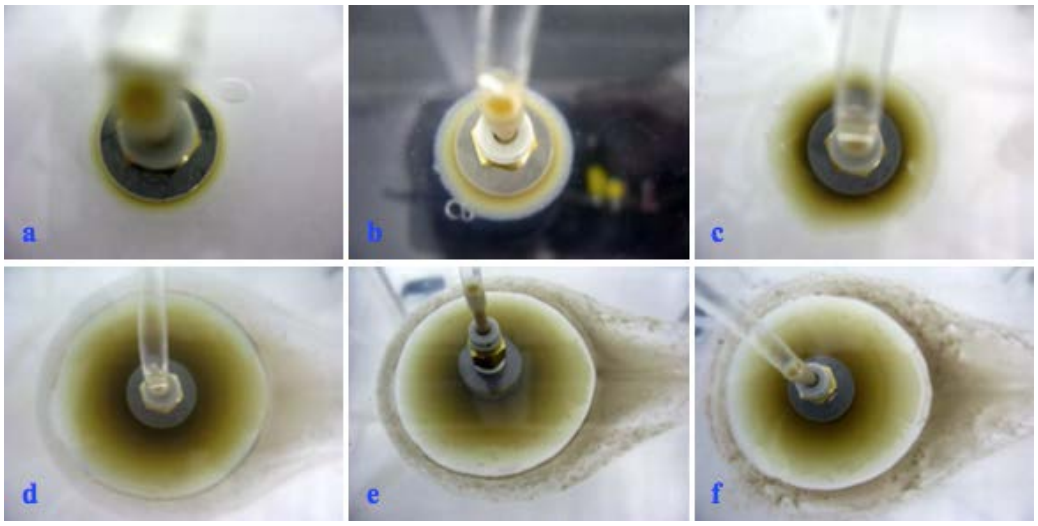

Figure 2-8. *Overhead photographic images of test with NaMt and DI at a) 1 h, b) 4 h, c) 24 h, d) 144 h, e) 312 h, and f) 456 h; the direction of flow in the 1 mm fracture is from left to right. Note the porous frit (diameter = 2 cm) at the centre of each image for scale.*

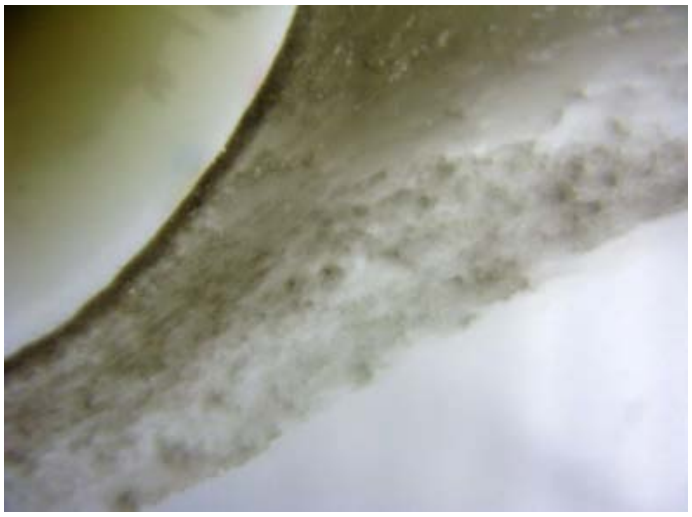

Figure 2-9. *Enlargement of a section in frame f in Figure 2-8. Grainy flocs are clearly visible.*

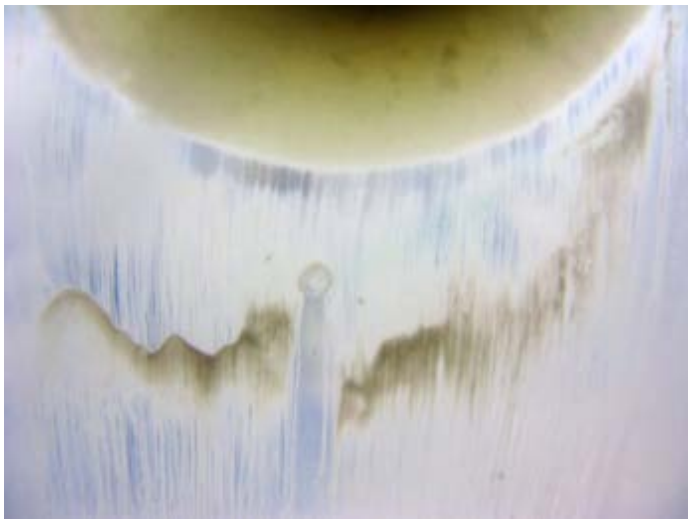

Figure 2-10. *Close-up photographic image of test with a 50/50 mix of CaMt and NaMt at 90° rotation from a horizontal fracture position to vertical.*

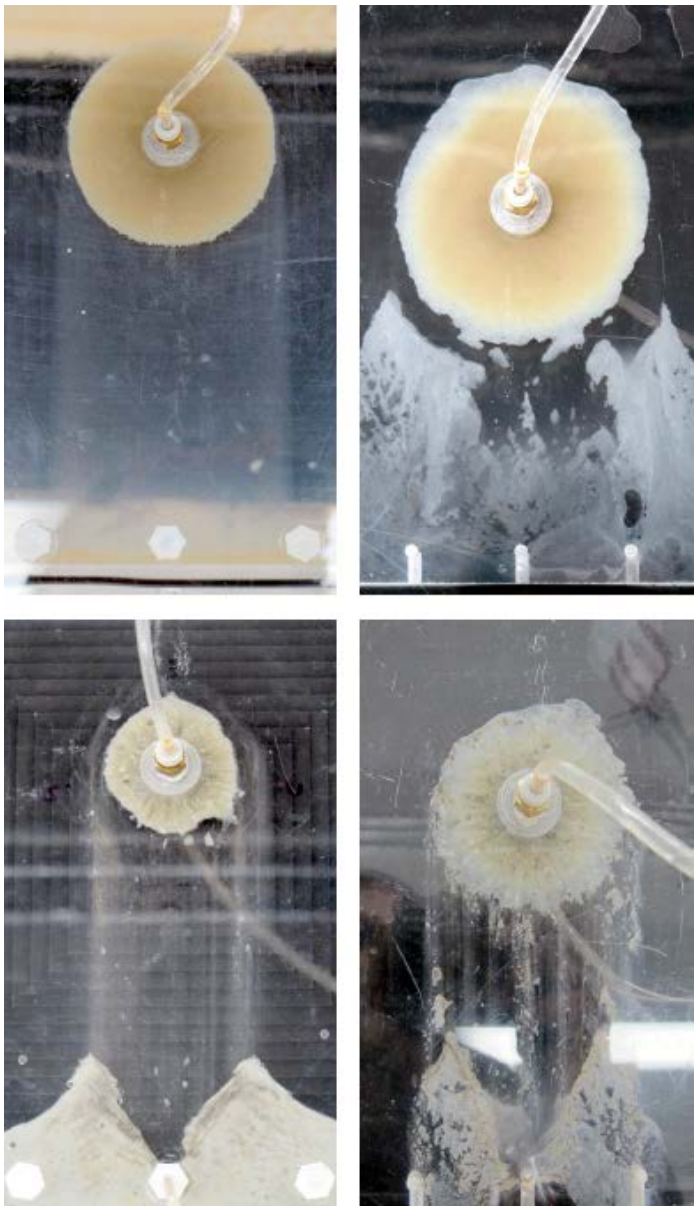

Figure 2-11. *Images of extrusion and mass loss of sodium montmorillonite (top row) and Wyoming bentonite (bottom row) in 45° sloped fractures with 1 mm apertures (left column) and 0.1 mm apertures (right column). Clockwise from top left, the corresponding test times are 72, 720, 504 and 336 h, respectively. The tests with sodium montmorillonite were performed under stagnant water (no flow)*

Figure 2-12 shows sedimentation experiments in a 45° sloping 1 mm aperture fracture after 720 hours in stagnant water into which a compacted clay pellet expands.

The slopes of the sediment heap suggest that the sediment may have a friction angle of about 45° and the sediment cannot readily flow as a liquid horizontally once it has settled.

In sloping fractures gravity can pull flocs and agglomerates of Mt particles downward and give room for release of new flocs. The sedimentation rate of flocs as an agglomerate fluid AF, which in narrow fractures, < 0.1 mm, is in contact with both walls of a fracture is on theoretical ground thought to be proportional to the fracture aperture to the third power (Neretnieks et al. 2017).

Recently (February 2018) a preliminary report on expansion and erosion of bentonite clay in narrow fractures has been submitted to SKB (Alonso et al. 2018). The results are quite different from those of Schatz et al. (2013) as no flocculation was observed under what seems to be nearly identical conditions. A summary of the findings is reported in Appendix C.

Figure 2-12. *Image of extrusion and mass loss of Wyoming bentonite in a 45° sloped fracture after 720 h. The test was conducted in a 1 mm aperture fracture filled with stagnant water with 0.68 and 0.14 mM, Na^+ and Ca^{2+} respectively. The sample was initially emplaced at a dry density of ~1.6 g/cm^3 (Schatz and Akhanoba 2017).*

2.4 Questions asked and approaches to address them

Main aims of this exploratory study are to find ways to understand and quantify the processes involved in agglomerate formation and flow in fractures and in the formation of filters by the detritus material. The following questions are posed and addressed in the report.

- Will flocs form in well-below CCC water?
- Can the rate of floc formation be quantified?
- Can the rheological properties of floc suspensions be understood and quantified?
- Can/will filters of detritus material form in natural variable aperture fractures and will they seriously influence the rate of clay penetration into the fractures?
- Could such understanding be used to formulate and develop credible and reliable simulation tools?

We have made some simple scoping experiments. A survey of recent publications on filtration and filtration modelling was also made.

Furthermore it is explored whether recent developments in the field of discrete element modelling, DEM, coupled to finite element modelling FEM as well as molecular dynamics modelling MD might be useful for the above purposes. It is recognised that at present there exist no ready made model tools that can account for individual particle movement and simultaneously consider the impact of the forces on the molecular level that depend on surface chemical effects present in the colloidal size gels/sols.

3 Mechanisms and models of bentonite properties and behaviour

3.1 Rheology of bentonite slurries and Mt sols

3.1.1 Rheology and viscosity

Fluids such as water with or without dissolved salts and low molecular weight organic molecules such as alcohols and hydrocarbons have a viscosity that does not depend on shear rate. These are called Newtonian fluids. The presence of rigid particles in the liquid increases the viscosity of the slurry above that of the liquid. At low particle concentrations the increase in viscosity is linear but becomes increasingly non-linear at higher concentrations. When particles can agglomerate as the Mt can, the slurry become non-Newtonian, which means that the apparent viscosity depends on shear stress and/or shear rate and that, it may vary over time.

We are especially interested in the following types of non- Newtonian behaviour. The *Bingham body/fluid* behaves like a solid when subject to low shear stress but flows at higher stresses. A typical example is Ketchup. It is a gel and does not flow until the bottle is strongly shaken. Then it rapidly flows. Having landed on the plate or food, it again behaves like a gel and does not flow away as a Newtonian liquid would. The rapid recovery of a high, in this example extremely high viscosity, is a characteristic of *thixotropic fluids*. Another example of a thixotropic fluid is modern paints that behave like gel when at rest, but flow when sheared by the brush. The paint's viscosity slowly increases and it has smaller tendency to drip. One can understand the reasons for this behaviour as follows. The fluid contains particles e.g. Mt sheets, that attract each other by weak forces and with time form a complex three-dimensional increasingly strong network. This structure is strong enough to behave like a gel. When subject to large stress, bonds break and particles become free to move in relation to each other. When the stress is decreased the particles gradually rearrange themselves to form gel again.

3.1.2 Bentonite clay properties

Viscosity measurements of clay slurries and sols have been performed and reported in Birgersson et al. (2009) and Hedström et al. (2016) for different bentonites and purified Mt's in different clay concentrations and different water compositions for raw bentonites and sodium as well as calcium exchanged clays for conditions of interest for this report. We first discuss conditions where the clay concentration is so low that the suspensions are Newtonian, i.e. the shear stress is proportional to shear rate. This is found at clay concentrations less than about 25 to 50 g/l (or volume fractions less that 1 to 2 %). These are roughly the conditions under which sols start to form in dilute waters (Birgersson et al. 2009, Neretnieks et al. 2009, 2017, Hedström et al. 2016)

Liu (2011) used data from Birgersson et al. (2009) and other sources from the literature to develop a model that shows how the viscosity depends on Mt concentration and sodium ion concentration. Figure 3-1 shows how the sol or suspension viscosity increases with volume fraction of smectite. The experiments in Birgersson et al. (2009) and Hedström et al. (2016) suggest that at around a volume fraction of 1 % there is a tendency for the slurry to have a high viscosity, which decreases as the shear rate increases. The slurry becomes non-Newtonian. With increasing volume fraction the change is more pronounced.

One of the central questions is this report is if the flocs that form at the clay/water interface can be expected to develop so strong agglomerates that the agglomerate fluid will not be mobilised in the fractures by the gravity or by the hydraulic gradient. Alternatively, even if such no-flow conditions cannot be proven to result, the increasing viscosity of the agglomerates will decrease the transport rate of the agglomerate fluid. This might set an upper bound on the rate of erosion.

Rheology measurements by Birgersson et al. (2009) of clay slurries at different volume fractions and ion concentrations relevant for the present study have been performed. However, the measurements were made a short time after preparation of the slurry and the slurry was also shaken to ensure homogenisation of the slurry before measurement. Furthermore, the shear rate induced in

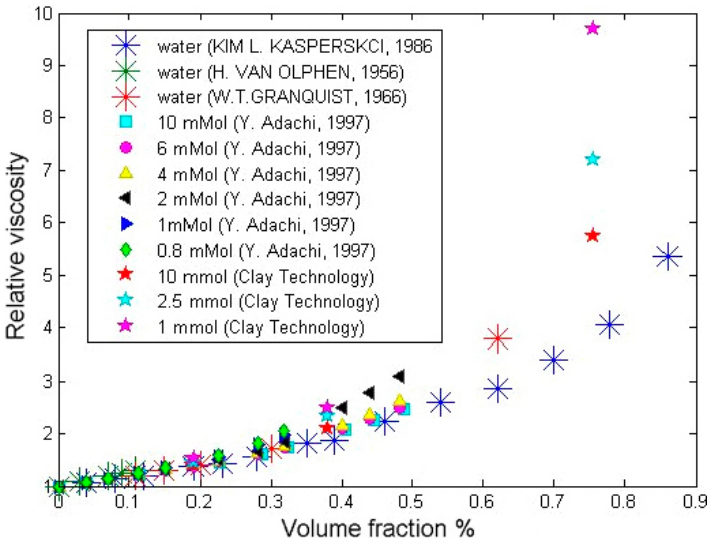

Figure 3-1. *Relative viscosity as a function of volume fraction from different sources (Liu 2011).*

the viscometer may have broken important bonds in any flocs that formed. Such measurements do not give information on the shear stress needed to break bonds in the flocs that have had time to grow and mature. In the same report, it was shown that in other experiments that studied the time aspect the viscosity of suspensions increased continuously with the time the slurry rested before the measurements. In Chapter 5 more information on rheologic properties is presented in connection with modelling of non-Newtonian fluid models.

Flocculation is commonly used in drinking water purification and it is well known that floc formation and growth is promoted by low shear rates. When flocs grow, sediment and gradually compress under gravity the denser sediment becomes more viscous. To make it flow to the exit of the equipment higher shear rates i.e. more vigorous stirring is used in the sediment. This breaks bonds in the denser agglomerate fluid and allows it to flow. This is mentioned here to prepare the reader for later discussions of experiments that show that the Mt flocs behave like this and especially to show that the floc strength can over weeks become strong enough to withstand deformation and flow by gravity.

3.2 Expansion and sol formation of Mt in bentonite

This section summarizes some of the basic mechanisms that influence the expansion, release, and sedimentation of bentonite clays. For more details please consult Neretnieks et al. (2009), which gives the background for later discussions of experimental observations and expectations of Mt sol and sediment behaviour in fractures.

The expansion in space over time of Mt in water can be described by a diffusion equation in which the diffusion coefficient of the Mt particles in the Mt paste/dispersion depends of volume fraction of Mt and ion concentration[1].

Figure 3-2 shows the diffusivity coefficient for different concentrations of NaCl in the water.

We are mainly interested in the region where $c_{ion} < 10$ mM. Consider a case with $c_{ion} = 1$ mM and a clay that initially has a volume fraction at the clay/water interface ϕ_R larger than 0.03. The diffusion coefficient is on the order of 3×10^{-10} m^2/s. The clay particles migrate out into the water but as they do the diffusion coefficient decreases as the volume fraction decreases and the particle in the dilute region cannot move away as rapidly as clay in the region with larger volume fraction expands. A sharp clay concentration front that is pushed outward will develop.

[1] The terms paste and dispersion are used here because we wish to emphasise that the diffusion concept can be used for the entire range of volume fractions of Mt/water ratio from very compacted clay to extremely dilute sol.

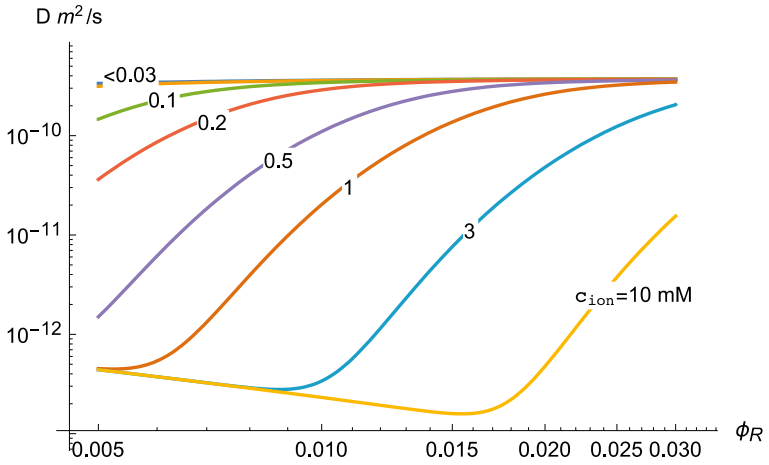

Figure 3-2. *Diffusivity coefficient influenced by volume fraction ϕ_R and sodium ion concentration c_{ion}. Mt sheet diameter is 200 nm. Based on the dynamic expansion model (Neretnieks et al. 2009).*

This is illustrated in Figure 3-3 where experimental results are compared with those predicted by the dynamic clay expansion model. A pellet of compacted as-received bentonite clay (MX-80) expands in de-ionised water. During the experiment salts in the untreated clay as well as small amounts of the clay itself are dissolved. In this experiment, the ion concentration along the path could not be experimentally followed. To account for this in the modelling the ion concentration in the model was adjusted to improve the fit between experiment and model. Without this fitting, the prediction was still quite good and influenced mainly the time scale. The fitted concentrations are shown because they give values in the range found in post-mortem measurements in other experiments with the same clay. For additional examples with purified clays and no adjustment of ion concentration in the modelling see Neretnieks et al. (2009). The expansion experiments in Figures 3-3 and 3-4 were performed by Dvinskikh and Furó (2009).

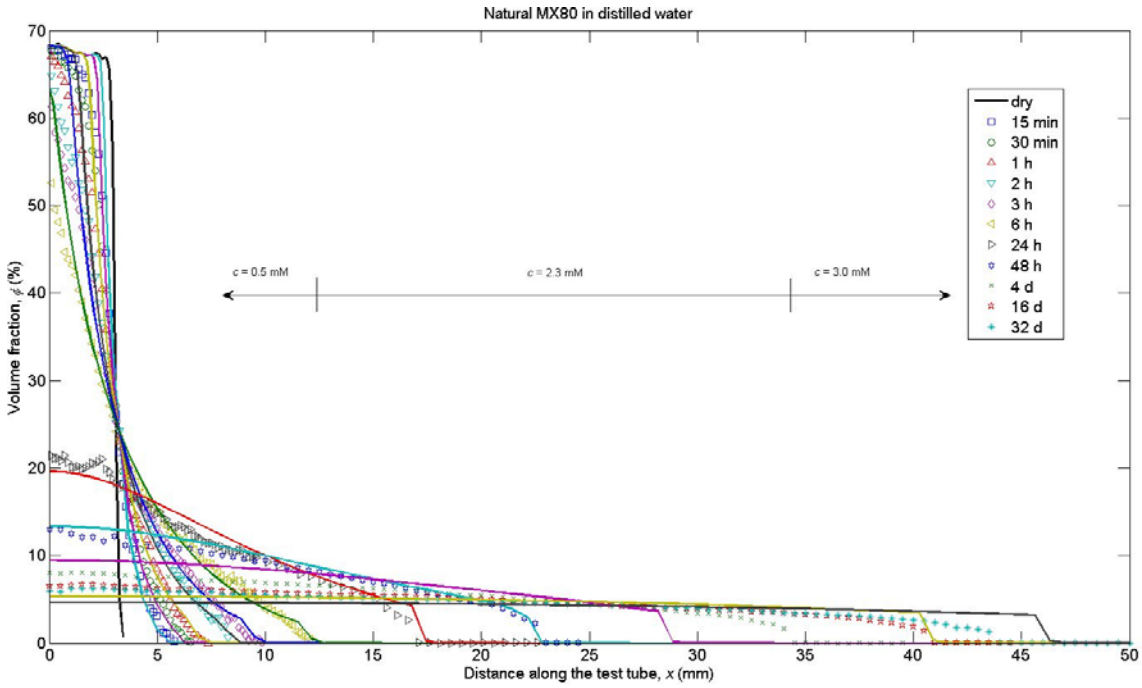

Figure 3-3. *Expansion of a bentonite pellet in water. Predicted/fitted (lines) and experimental results (symbols). (Neretnieks et al. 2009)*

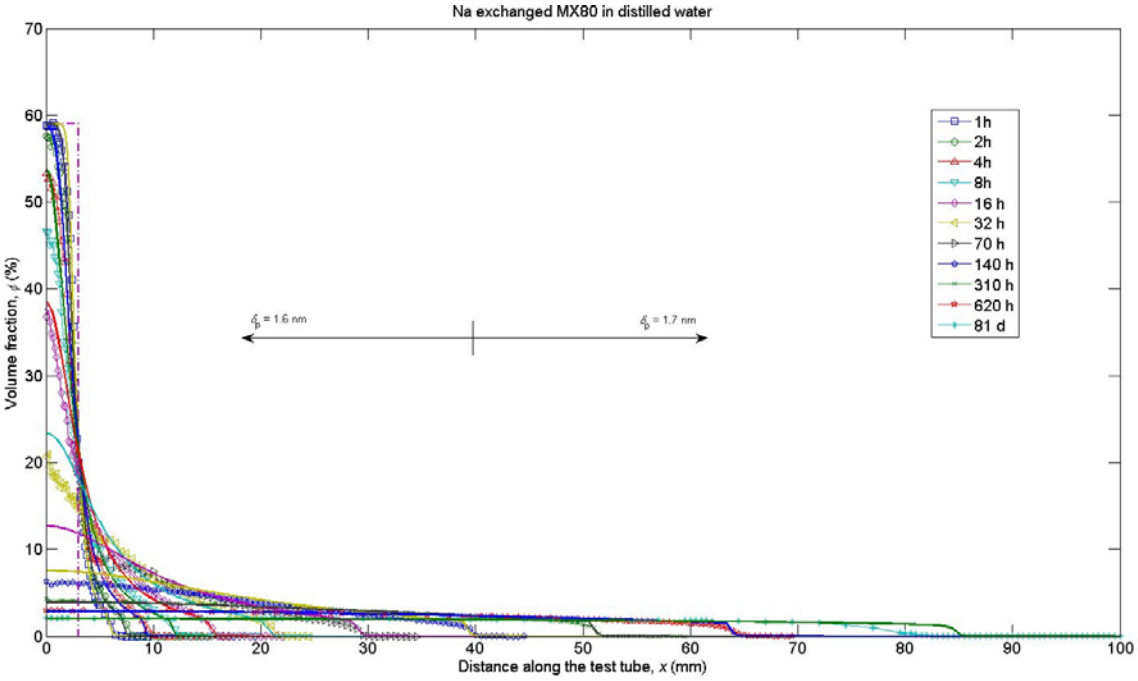

Figure 3-4. *Expansion of an Mt pellet in distilled water. Predicted/fitted (lines) and experimental results (symbols) (Neretnieks et al. 2009).*

Figure 3-4 shows the experimental and predicted/fitted expansion of sodium homo-ionic NaMt. To obtain a better fit, Mt particle mean thickness was adjusted as shown in the figure. This suggests that on average 1.6 to 1.7 sheets had formed thicker particles. Seemingly also with only a mono-valent counterion some stacking of the sheets takes place.

These examples show that the dynamic clay expansion model captures the expansion phase quite well and also shows that the untreated bentonite will supply ions to the water, which influences the diffusion. One may further note that the above expansion would continue unimpeded in the horizontal direction predicted by the model. It may be noted that in these experiments friction against the walls of the tube in which the pellet expands has not impeded the expansion.

For a deposition hole intersected by a sloping fracture, gravity will try to restrain the expansion in the upward direction but will aid the expansion in the downward direction. It may be noted, however, that if there were no agglomeration of the individual Mt sheets, the influence of gravity will be negligible. The settling velocity of a 300 nm Mt particle is on the order of 10^{-7} m/s. It would take 4 months to drop 1 m and a few weeks to drop 10 cm. See also Section 5.2.2 on sedimentation rates.

3.3 Compression of sol by gravity and phase separation of sol

Here we discuss Mt behaviour in well below CCC water when it remains a sol. Figure 3-5 shows the volume fraction profile that would result at equilibrium after a long time expansion or settling of Mt in a vertical tube or slot. The figure shows how the volume fraction of Mt in sediment would evolve in a sequence of steady states as more and more mass, which settles is added. The left-most curve shows that when there is only little mass in the system that has settled, the volume fraction at the bottom is $\phi = 0.005$. As more mass is added the sediment at the bottom is compressed by the overburden. As even more mass is added, at the bottom the sediment will be compressed to a larger volume fraction, which increases the swelling pressure. As the swelling pressure increases very much with increasing volume fraction even very large height of sediment still would be only moderately compressed. This is shown in Figure 3-6 where the sediment is 15 m high but the volume fraction at the bottom has increased to only 0.03 and the front is very sharp.

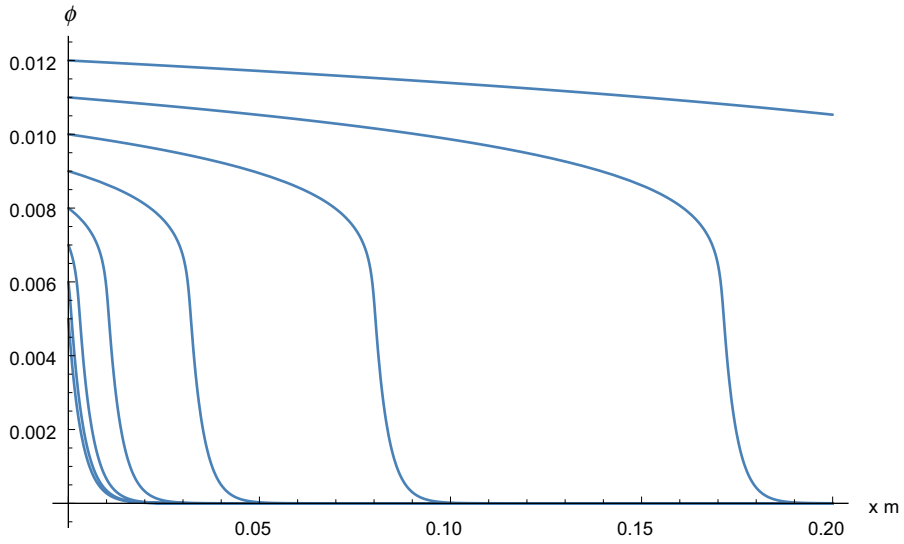

Figure 3-5. *Steady-state volume fraction of solids, ϕ as function of height x for c = 1 mol/m^3 NaCl and particle thickness $\delta_p = 1 \times 10^{-9}$ m in a gravity field.*

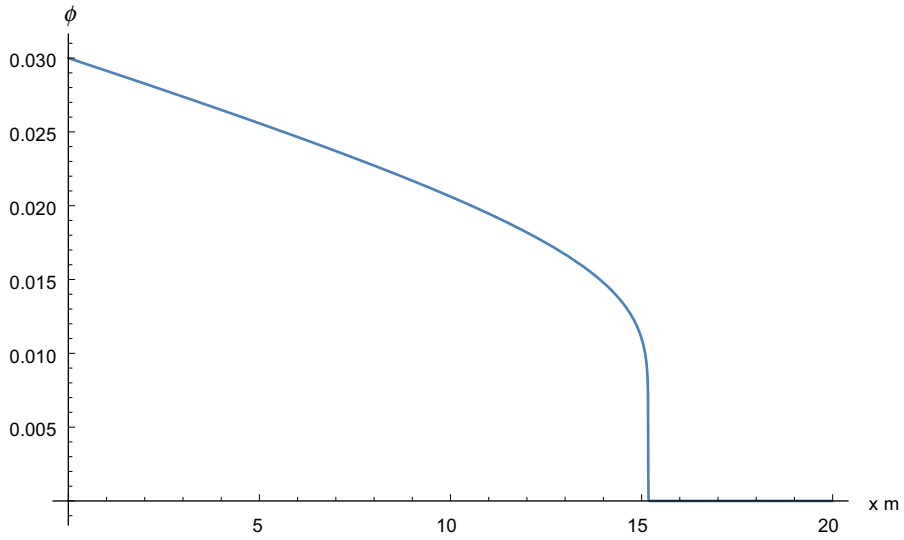

Figure 3-6. *Steady-state volume fraction of solids, ϕ as function of height x for c = 1 mol/m^3 and particle thickness $\delta_p = 1 \times 10^{-9}$ m in a gravity field.*

It should be noted that at a volume fraction exceeding about 1 % the viscosity of the sediment increases very sharply and may even behave like a Bingham body/fluid. This implies that the sediment cannot be dislodged by the hydraulic gradients, less than a few percent, that can be expected at repository depth and also that the sediment, once formed cannot be mobilized by gravity. See also Section 4.1 on viscosity of the agglomerate fluid. We preempt the discussion on the properties of the sediment formed by individual Mt sheets as described above and those of flocs that form a sediment by mentioning that the loose flocs, at least when recently formed, may behave differently than a sol of individual Mt particles at the same volume fraction.

Figures 3-5 and 3-6 show that in a gravity field a suspension is expected to sediment notwithstanding that it is a sol of colloidal size particles. The reason is that below about 1 % by volume the repulsion forces a very weak and is over-powered by gravity forces. If gravity is “deactivated” by turning the testtube horizontally the sol expands to fill the length of the tube. The sol will, in this case, remain a sol. This is what is meant by a stable sol. This somewhat idealized concept is universally accepted and would be valid for also for the negatively charged montmorillonite according to the DLVO theory on which our dynamic clay expansion model is based.

However, this model does not consider the increasingly strong evidence that the thin montmorillonite sheets can have positive charges at the edges that allow very complex larger three-dimensional agglomerates to form by binding to the negative faces, given time. These agglomerates sediment and form gel-like structures, which are sufficiently strong to withstand at least weak shear forces. Such sedimented agglomerates or just sediments have been reported. See Chapters 5 and 6. The rheology of the Mt sediments does not seem to have been systematically studied although there are numerous studies of the rheology of clay suspension under different conditions. This is a key issue in the present study and we will try to utilize the insights from rheology studies on montmorillonite especially at conditions relevant to our aims.

4 Flocculation and floc migration

4.1 General

It was illustrated in Chapter 2 that Mt flocs form when compacted homo-ionic sodium montmorillonite, NaMt, is subjected to flowing de-ionised water. Also pellets with 50/50 % of NaMt and CaMt behave in the same way. Such floc formation is also observed in waters with ion concentration below about 10 mM of NaCl. It was also shown that the flocs form sediment in sloping fractures.

The formation of flocs under these conditions is itself at first surprising because under these conditions when the ion concentration in the water is below the critical coagulation concentration and in stagnant water, the clays are known to expand and release individual colloidal Mt particles. According to the traditional DLVO theory, they should form a stable sol and not flocculate (van Olphen 1977, Evans and Wennerström 1999, Birgersson et al. 2009, Neretnieks et al. 2009).

Bergaya et al. (2006, p 141) qualitatively describe the complex behaviour of clay particles in water under different conditions and for different clay types. They present what may be called phase diagrams, which intend to show under what ion concentrations and clay particle concentrations one can expect gel and sol formation and when the clay is attractive or repulsive. Coagulation and floc formation under different conditions and the underlying mechanisms are discussed as well as how different structures of clay-clay agglomerates and aggregates have been observed to form. The book has numerous references. The book shows that clay and smectite clay behaviour is still not so well in hand that it can be used to set up quantitative models for the properties of interest in this report.

It is known that the thin, highly electrically negatively charged montmorillonite sheets have positive edge charges under some conditions and that house of card-like and other complex structures can form and be quite strong. With this as a starting point, a thorough discussion supported by numerous experiments on gel and sol formation of homo-ionic Mt is presented in Hedström et al. (2016). They found more complex behaviours than what is commonly reported in the literature. Besides the well known swelling at high Mt concentrations, and that Mt forms a stable gel in water above CCC and sol below CCC, the paste, sol, gel and sediments could behave differently in different cases. Paste could form sediment of Mt but not turn to gel at seemingly comparable Mt concentration. The boundary between the more concentrated phase and sol could be diffuse in some combinations of NaCl and Mt concentrations and sharp in other. It is thought that some of these observations may be caused by floc formation, which was not considered specifically in that report.

Hedström et al. (2016) found that very stable gels formed due to edge-to-face interactions in waters with at least about 5 mM sodium in Mt prepared from some bentonites but needed higher concentrations for bentonites from other sources. The CCC values found in these experiments were well below what DLVO theory predict and are also much lower than what face-to-face gel formation predicts (Liu et al. 2009). The observations reported in Hedström et al. (2016) suggest that the face-to-edge binding is a key process in Mt suspension behaviour because it allows many different structures to form compared to what is the case for the DLVO model, which assumes only face-to-face interaction for the thin smectite sheets.

Kranenburg (1999) showed that face-to-edge binding can lead to complex floc formations and that flocs can settle to form stable structures at different particle concentrations and that they grow in strength with time. His results also suggest that such flocs, once formed, probably need not restructure to the global free energy minimum but can remain stable at some local free energy minimum. This implies that the formation conditions, e.g. the local shear rate during formation can influence the later behaviour of the system. It is hypothesised that this can be an important reason for the varied behaviour observed by Hedström et al. (2016) and for some of the observations described later.

When favourable conditions for flocculation exist, gentle stirring increases it. This allows the particles to approach each other more frequently than if they move only by diffusion (Brownian motion). Stirring enhances the frequency at which a positively charged site on one particle can approach a negative site on another particle. Under non-sheared conditions, the particles tend to

be arranged in parallel, due to the DDL repulsion, until they are so distant that they have room to rotate. With particle dimensions of 200 nm, rotation induced by Brownian motion would start at around the same distance between particles as their diameter. As the thickness of the particles is 1 nm this would be at a volume fraction of around 0.5 %. The volume fraction can even be smaller in low ionic strength waters because the extent of the DDL increases the effective diameter of the particles.

In water flowing in narrow slots, the velocity profile is parabolic and particles will continuously try to rotate. They will also move with different velocities at different distances from the walls. This will facilitate edges to impact faces. One may speculate that an edge will "penetrate" the DDL layer and attachment can result from the coulombic attraction between the positive edge and locations on the negative surface. It has been found experimentally with saponite, which is another smectite mineral with many properties similar to montmorillonite that unexpectedly stable structures form. Monte Carlo simulations have shown that with plausible charge distributions on the smectite sheets flocculation can result (Angelini et al. 2014). In that paper, it is also shown that the floc strength increases with time.

4.2 Flocculation

4.2.1 General

Floc formation, properties, settling, and compaction have been studied extensively in connection with drinking water purification, wastewater treatment and sedimentation of natural flocs in lakes and rivers. Some general theories on floc behaviour and properties have been formulated and validated by experiments. Generally, it is found that flocs form complex fractal structures but with considerable variation of fractal dimensions. The binding can be caused by different attractive forces between the primary particles that make up the flocs including vdW, coulombic and gravity forces and is influenced by velocity gradients in laminar flow and in turbulent vortices. In chemical engineering applications such as mine water treatment and water purification, inorganic and organic flocculants are commonly used. In natural waters, bio-organic matter and microorganisms themselves play an important role. Bentonite clays are also used as flocculants because its Mt particles readily form flocs in water and these occlude many undesired constituents that later can be separated by sedimentation of the flocs.

In the present application, the fate of the Mt itself in dilute waters is of interest where the flocculation is not due to face-to-face attraction by vdW forces but probably by edge-to-face binding. Practically no papers in the open literature on Mt floc formation, strength, viscosity and other properties in waters with ion concentrations below about 10 mM sodium have been found. However, it may be possible to learn something from flocculation and floc behaviour from other areas that have been much more extensively studied. One such area is water purification. Another is kaolinite clay flocculation. In effluent and drinking water purification bacteria, virus, microscopic solid particles, organic material, heavy metals etc. are removed by adding iron or aluminium sulphate to generate flocs that sediment and can be removed. Cat- and anionic organic polymers can be added in other applications. Flocculation is promoted by slow stirring. Voluminous flocs can, after sedimentation, be broken up by more vigorous stirring to obtain more compact sediments. The sizes and strength of the flocs and the viscosity of the floc slurry will influence the formation and handling of the slurry of flocs. In the recent literature, only a few papers in which these phenomena have been discussed in more general terms, based on detailed underlying mechanisms have been found. Most papers usually treat very specific applications and it is not obvious how the results could be used to gain quantitative insights into the montmorillonite system. Only one paper from 1999 was found to apply a broader view (Kranenburg 1999). He tries to formulate some more general principles and to quantify these. His observations showed that flocs tend to form self-similar structures and that the number of bonds in a critical yield plane in such structures does not depend on the size of the flocs. This was used to formulate a model for the viscosity of a dense suspension of flocs. Apparent viscosity in Kranenburg's model is inversely proportional to the shear rate $\dot{\gamma}$ and proportional to the yield stress of the gel τ_y. The term gel, in this case, is to be understood as the coherent space-filling structure of the bonded primary particles. The model was compared to a number of kaolinite suspension experiments with shear rates between $\dot{\gamma} = 1$ and 100 s^{-1}. His model agrees fairly well with experiments in

the lower range of shear rates. However, the suspensions are about two orders of magnitude denser (300–600 kg/m^3) than the suspensions expected for the bentonite system of interest in this report.

Jarvis et al. (2005) present a review of floc strength, and breakage and different techniques to measure floc properties. It gives some insights into various processes that influence formation, strength, and breakage and emphasises the importance of shear rate. None of the specific results from the above and other sources could be directly transferred to the Mt system of interest here.

4.2.2 Particle and floc sedimentation rates

This section treats the sedimentation rate of particles. It is used to estimate the time it will take for particles and flocs of different sizes to sediment in experiments and in rock fractures.

Particles denser than the liquid sediment and the settling velocity can be estimated by Stokes law when the particles are not very close to each other and under laminar settling. This is valid for the cases of interest here (Neretnieks et al. 2009). With minor modification, Stokes law, which is derived for rigid spherical particles, can also be used for thin sheets such as the Mt particles.

The settling velocity u_p is

$$u_p = \frac{d_p^2(\rho_p - \rho_w)g_c}{18\eta_w} \tag{4-1}$$

d_p is the sphere diameter, ρ_p is the particle density, ρ_w and η_w are the water density and viscosity respectively. g_c is the gravitational constant. For very thin coin-like sheets

$$d_p = \frac{2}{\pi} d_{coin} \tag{4-2}$$

d_{coin} is diameter of the sheet.

For flocs, the particle density depends on the volume fraction of Mt, ϕ and is

$$\rho_p = \rho_w(1 - \phi) + \rho_s\phi \tag{4-3}$$

ρ_s is the density of Mt mineral and is about 2 700 kg/m^3. The volume fraction ϕ in flocs and AF of interest here is expected to be between 0.001 and 0.02.

The settling velocity for individual Mt sheets with diameter 200 nm in water at 10 and 20 °C is 1.2×10^{-8} and 1.5×10^{-8} m/s. This is 0.36 and 0.47 m/yr. respectively. This is about 1 mm per day. This suggests that over a few days or weeks one would hardly be able to observe the settling of a suspension of individual Mt particles in 10 cm high testtubes or slots.

Figure 4-1 shows the floc density as function of volume fraction.

Figure 4-2 shows the settling velocity of flocs as function of floc diameter with different volume fractions. Stokes equation is not valid for larger velocities and particle sizes than the highest value in the figure because the Reynolds number then would exceed 1.

Figure 4-3 shows the time for flocs with different volume fractions to sediment 0.1 m.

The above figures illustrate that the free settling velocities can vary over a very large range. During the sedimentation, the flocs can grow, which will influence the behaviour of the floc slurry. Also the volume fraction in the flocs can change if the flocs are compacted underway, which to some degree can be expected as they probably are subject to shear forces. This may lead to rearrangement of the individual particles in the flocs. Nevertheless, the figures may give some guidance in experimental design and interpretation. In the scoping experiments, presented later, the duration of the settling experiments in 5 and 15 cm high testtubes ranged from a few days up to several months.

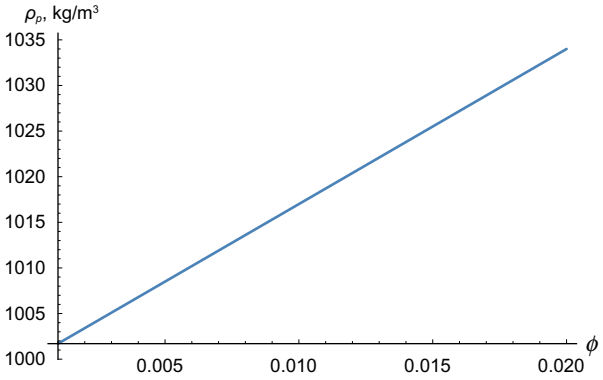

Figure 4-1. *Floc density as function of volume fraction.*

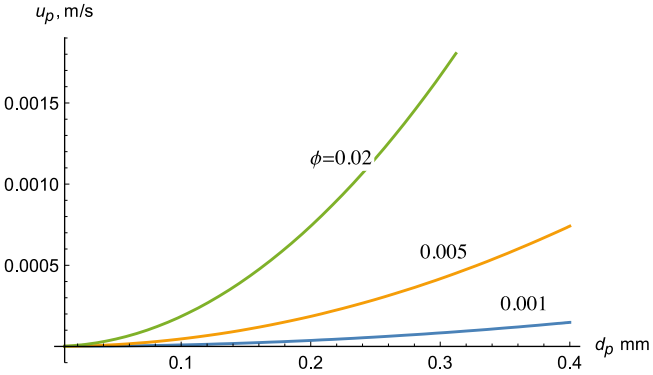

Figure 4-2. *Settling velocity of flocs as function of floc diameter with different volume fractions.*

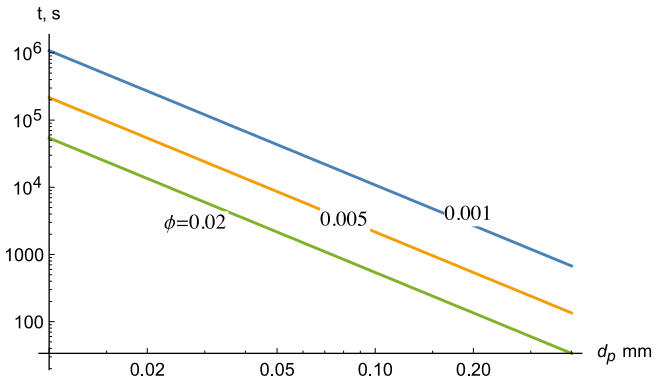

Figure 4-3. *Time for flocs with different volume fractions Mt to sediment 0.1 m as function of floc diameter.*

4.2.3 Modelling flocculation kinetics and floc strength

Flocs form when primary particles such as a Mt sheet bind to another sheet forming dimers with number density[2] n_2, which by binding to an additional sheet forms n_3 or when two n_2 collide and bind to form n_4, etc. This process can be generalized using a population balance of all possible combinations of n_x and n_y. One needs to account for how often two flocs collide and of the probability of combining to a larger floc. This, in turn, depends on the forces and velocities involved and also on the form of the flocs and how they collide. The process is further complicated by the fact that the trajectories of the flocs depend on the flow geometry and the hydraulic gradient. At low flow veloci-

[2] Number density nx is the number of particles consisting of x primary particles per volume of water.

ties and gradients also Brownian motion and gravity settling become important. Not surprisingly it has been difficult to devise models that can account for all these processes and mechanisms in a quantitative manner. Nevertheless, some general semi-empirical expressions have been derived that can be used to describe how the total number density of flocs evolves over time. See e.g. Sato et al. (2004) where it is shown that the temporal evolution of the total number concentration is reduced to the first order equation

$$\frac{dN(t)}{dt} = -Const \times N(t) \times \dot{\gamma} \qquad (4\text{-}4)$$

$N(t)$ is the number density of flocs and $\dot{\gamma}$ is the shear rate. The constant will in practice have to be determined by experiments. Equation (4-4) does not account for the breakage of large flocs, which will increasingly become important when weak flocs brake into smaller flocs. In modelling, this can be accounted for by adding a disintegration term, but this, of course, adds another empirical constant. The equilibrium number density of flocs and thus also their mean size can experimentally be determined in different ways. One simple method is by the Couette equipment in which a nearly constant shear rate is generated in the slot between two concentric tubes, one stationary, the other rotating at known speed. Direct observations of floc structures and sizes are possible if the outer tube is transparent. Alternatively, samples can be withdrawn from the apparatus to determine size, structure, and strength. Information of floc strength is obtained from their size and the shear rate. There are also other methods to determine floc strength See e.g. Kranenburg (1999) who shows that the strength can be estimated based on maximum size of the flocs and their settling velocity.

4.3 Some cases considered

In the situations of interest here the primary Mt particles released from the expanding bentonite clay form flocs that migrate carried by seeping water or sediment under the influence of gravity. The migration takes place in a variable aperture fracture connected to other fractures in a three-dimensional network.

4.3.1 Horizontal fracture

In a horizontal narrow fracture with seeping water, the parabolic velocity profile across the aperture will promote floc growth. Gravity lets the particles settle toward the lower face of the sloping fracture. A floc that has grown to the same size as the local fracture aperture will touch the walls and will be subject to friction and shear. Its velocity will slow down compared to the local water velocity. When the floc reaches a narrower part of the fracture it will be forced to deform to be able to pass. It will be slowed down. Smaller, more rapidly moving flocs will catch up with the slower and may become amalgamated, forming a larger floc, which blocks the region to water flow. The agglomerate suspension can be treated as a non-Newtonian viscous fluid or a gel-like structure with a yield strength for which the friction force against the walls must be overcome to mobilise it. We will later see that some simple models exist that can describe a fluid with an apparent viscosity that changes with shear rate and also has a distinct yield strength.

4.3.2 Sloping fracture with stagnant water

In the sloping fracture, the released primary particles agglomerate to flocs by Brownian movement and also by the sedimentation induced velocity gradient in the sloping fracture. We suggest that the agglomeration process could develop as follows. Larger flocs sediment more rapidly, catch up with smaller and eventually form large “blobs” between the two fracture surfaces. In the same way, as for the gradient driven flow, the movement of the AF can slow down and even stop. This can be seen in Figures 2-10 and 2-11 where large coherent regions have formed. This is quite interesting because a slow-moving or rigid AF has formed in the slot by friction against the walls without another impediment, such as physical constriction. An additional interesting phenomenon is also seen in Figure 2-10. At the lower rim of the AF, new flocs are released in the same way as from the primary source.

An additional case may now be considered. If the AF approaches or becomes a Bingham body/fluid and is mobile in a vertical or steep fracture it might not be mobile in a less sloping fracture in which the driving force is smaller. In such a fracture in the network of fractures or channels in fractures, its movement would stop. The slope of the sediment heap seen in Figure 2-12 suggests that the sediment does not *flow* sideways at least not as rapidly as new sediment collects.

As in the case of flowing fractures the Newtonian and/or non-Newtonian properties is of interest to determine. Floc strength and its evolution over time is probably a key factor to study.

4.4 Modelling non-Newtonian flow in slots

The viscosity, μ of Newtonian fluids is independent of the shear rate and shear stress τ. For such fluids, there is a simple relation between shear stress, τ, and velocity gradient $\frac{du_x}{dy}$, also called shear rate $\dot{\gamma}$.

$$\tau = -\mu\frac{du_x}{dy} = -\mu\dot{\gamma} \tag{4-5}$$

Non-Newtonian fluids for which the viscosity depends on shear stress and/or shear rate are modelled with the same formalism but empirical relations for the dependence of an apparent viscosity on shear rate, shear stress and time must be determined. Such relations cannot be derived based on only fundamental physics; but valuable insights can be gained from theoretical considerations of stress-strain relations and physics and chemistry of solutions of large molecules and suspensions of particles (Bird et al. 2002). Below we present some commonly used empirical models that are used to describe non-Newtonian fluid properties.

A very simple and often used relation for a non-Newtonian fluid behaviour is the powerlaw fluid. For shear thinning, such as bentonite fluids $n_{PL} < 1$, which implies that the shear stress increases less than in proportion to the shear rate.

$$\tau = K_{PL}\dot{\gamma}^{n_{PL}} \tag{4-6}$$

K_{PL} is a constant. The apparent viscosity at a given shear rate

$$\mu_a = K_{PL}\dot{\gamma}^{n_{PL}-1} \tag{4-7}$$

The apparent viscosity will seem to decrease with increasing shear rate. For very low shear rates the apparent viscosity will seem to go to extremely high values.

Another type of body/fluid is that described by the Bingham model.

It is solid when $\tau < \tau_o$, the yield stress, and a fluid with constant viscosity when $\tau \geq \tau_o$. The sediment will not move at all unless a sufficiently strong force is applied and then it flows like a Newtonian fluid.

Another common model is the Herschel-Bulkley model. This model combines the properties of the powerlaw and the Bingham models.

$$\tau = \tau_o + K_{HB}\dot{\gamma}^{n_{HB}} \tag{4-8}$$

With the relation between viscosity and shear rate $\tau = \mu_a\dot{\gamma}$, the apparent viscosity for this model is

$$\mu_a = \tau_o/\dot{\gamma} + K_{HB}\dot{\gamma}^{n_{HB}-1} \tag{4-9}$$

Numerous other empirical relations have also been proposed. Only the powerlaw, the Bingham, and the Herschel-Bulkley model will be discussed. As will be shown there is experimental evidence that the studied gel/sediment has shear strength and that once mobilised can be well fitted to the powerlaw model.

For the present problem the dependence on $\dot{\gamma}$, τ and time must be considered. The observations that the floc-sediment seems to have constant slope when settled suggest that there may be a minimum shear stress, the yield stress τ_o below which it will not flow in the slot. This could be due to that it has formed a gel and minimum stress is needed to mobilise it.

In the powerlaw and Hershel-Bulkley models, it is assumed that the fluid has no memory. This is not generally true for bentonite pastes, gels, and suspensions. Bentonites and their main mineral, montmorillonite becomes more viscous with time but regains lower viscosity when agitated. The Bingham model shows the extreme for this. The time dependence of the rheological properties of the bentonite is of special interest for this report because of the observed aging of the sedimented flocs. This will be discussed in the next section in which a very important observation is discussed, namely that sol that is supposedly stable when the water has ionic strength below CCC, phase separates into a nearly particle free-water phase and a gel. The consequences of this phase separation, although reported (van Olphen 1977) do not seem to be discussed in the literature in the context of Mt migration in fractures.

5 Some scoping experiments in testtubes

Some simple scoping experiments were made using as-received MX-80 and de-ionised water. The idea was to explore how flocs form, sediment and compact in testtubes and if the sediment becomes so rigid that it will not readily deform by gravity forces. The experiences from these experiments may give some guidance to more elaborate experiments. The aim of the experiment was to 1) explore and confirm that agglomerates of Mt that potentially become gels in very dilute water (low ionic strength), 2) to observe if the agglomerates might become gel-like and deform only slowly subject to compression or shear by gravity and 3) to observe if gentle agitation can influence the rate of flocculation and floc structure.

For the scoping experiments, 10.5 g of MX-80 in 500 ml de-ionised water was vigorously shaken for 25 minutes and set to sediment for 3 hours and 15 minutes. The opaque supernatant was decanted leaving about 30 ml sediment, which was evaporated and dried. It contained 3.86 g solid matter. The supernatant thus contains 6.64 g montmorillonite with a negligible amount of detritus particles. This gives 14.1 g/l, and a volume fraction of 0.52 %. Microscope pictures of evaporated drops of the supernatant showed very few very small particles in contrast to what was seen in the samples from the 30 ml first sediment.

The pH in of the supernatant with particles drifted between 6.7 and 7.2, the conductivity between 450 and 630 µS/cm and the salt content between 310 and 440 mg/l. The variation was probably caused by the presence of the charged Mt particles. After settling, the Mt free supernatant had a pH of 8.6 and contained 408 mg/l salts and had a conductivity of 563 µS/cm. The previously observed drift was not noticed anymore. If the salt would be only NaCl this would give a concentration of 7.0 mM. This is below CCC for MX-80 bentonite.

In one experiment 5 ml supernatant stock suspension, **#2**, was mixed with 5 ml DI in a testtube. This results in a salt concentration of about 3.5 mM, even more below CCC. This tube is numbered **#3**. The tube was set vertical to sediment. Another tube, **#5**, with 1 ml of the stock suspension **#2**, and 9 ml DI was prepared after shaking **#2** vigorously. **#5** thus has a salt concentration of about 0.7 mM, which is even further below CCC. In both tubes sediments with 1–2 % volume fraction had settled after less than one weak. This is shown in Figure 5-4. The Mt amount in **#5** is 5 times less than in **#3**. In both cases when the tubes were turned nearly horizontal the sediment did not move for many hours but some time overnight it has slid down. This is shown in the rightmost picture in Figure 5-4.

These simple experiments confirm that formation of gel-like structures occur in ion concentrations well below what is conventionally thought to be CCC. They also show that the sediment of the flocs has become extremely viscous, even if not a fully stable gel, after a few days of consolidation.

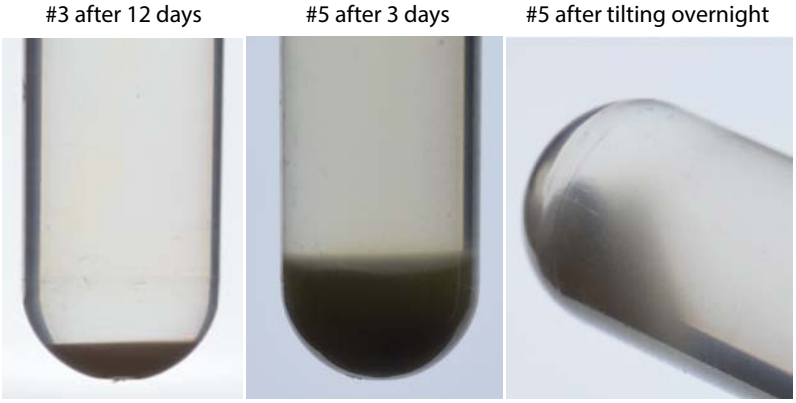

Figure 5-1. *Sediments in water with about 3 mM (left) and 0.7 mM ion concentrations, right two pictures.*

Another testtube **#4** was prepared with the stock solution, **#2**. It differs from the other two, in that no dilution was done and that the testtube was gently rolled back and forth during one hour to promote agglomeration. No flocculation was observed during the rest of the day but a loose sediment had formed overnight in the tube set at an angle of 45°. Tilting from 45° to vertical did not change the slope of the sediment during the rest of the day. The slope changed later but it was not noted when. Six days later the tube was tilted to a nearly horizontal position.

Figure 5-2 shows pictures of the bottom of the tube **#4** at different times.

The sediment was rigid at first but after some time lost coherence and flowed out. When again tilted vertically the sediment "immediately" settled to give horizontal upper surface. However, the sediment seemed to have become a little less dense. Titling it vertical again, after about a week re-formed a horizontal gel/water interface with the earlier height. Two months later it had gained such strength that tilting the tube horizontally, the interface remained vertical. This suggests that it takes more than a week to form a gel that does not collapse under its own weight. It also shows that a disturbed sediment regains its strength after a few weeks.

Note that the tilt was chosen to be such that the air/water interface is above the upper part of the sediment. The slightly denser sediment than water has a driving force to move downward and displace and "lift" the water. The force is proportional to the density difference between sediment and water. This was enough to break the strength of the sediment but only after many hours.

The situation is different if instead of water there is air in contact with the sediment and the driving force is the full weight of sediment. The disrupting force would then be much larger. This is explored with tube **#3**.

The tube was turned nearly horizontal and no deformation of sediment is seen. The gel remains rigid. This is shown in Figure 5-3 in the left-hand picture.

The tube was then tilted with bottom upward so that the air bubble is in contact with the sediment. Immediately the sediment deforms as shown in the right-hand picture.

After a few minutes, the sediment "body" split in two and the lower part slid downward as shown in Figure 5-4.

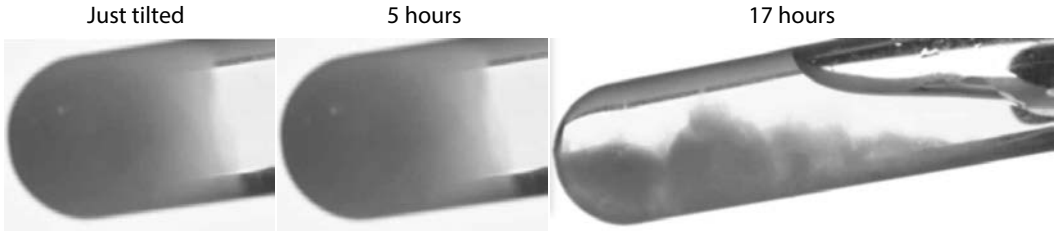

Figure 5-2. *Behaviour of sediment in tube **#4** after tilting. Ion concentration is about 7 mM.*

Figure 5-3. *Behaviour of sediment in **#3** after tilting*

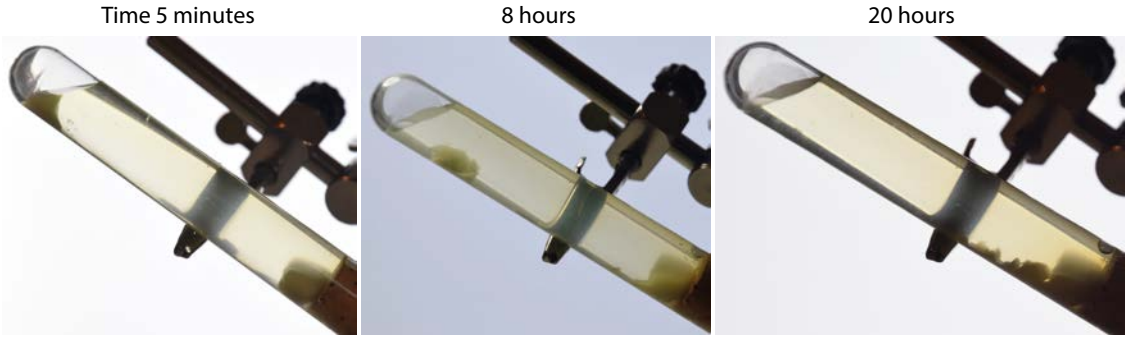

Figure 5-4. *Sliding of sediment in #3 after tilting.*

These results suggest that the sediment behaved largely as the gel that can resist gravity-induced stress, but only for hours to a day.

Table 5-1 summarises the data on concentrations and volume fractions in the tests.

Table 5-1. Summary of test tube concentration data

Sample #	Mt conc g/l	Volume fraction, initial %	Volume fraction, final %	Ion concentration mM
2	14.1	0.52	About 1.7	7.0
3	7.1	0.26	1–2	3.5
4	14.1	0.52	1–2	7.0
5	1.4	0.052	1–2	0.7

5.1 Yield strength and minimum slot aperture for gravity induced flow

In this section, we use the above simple experiments to roughly estimate the yield stress and also to assess the aperture width of a vertical slot at which the gel could be mobilised by gravity.

When in the horizontally tilted tube the vertical boundary between the sediment and water interface stays stable, the lower bound of the shear strength, τ_o, of the sediment can be approximately determined from the pressure difference between sediment and water at the bottom of the sediment height, h_{sed}. It is

$$\tau_o = (\rho_{sed} - \rho_w)\, g_c h_{sed} \tag{5-1}$$

The sediment density ρ_{sed} can be estimated from Equation 4-3. In the tilting experiments when the sediments did not deform ($\rho_{sed} - \rho_w$) was on the order of 20 kg/m^3 and h_{sed} one to two cm. This gives τ_o to a minimum of 2–4 Pa.

When tilted in such a way that the other medium was air instead of water the density difference ($\rho_{sed} - \rho_{air}$) is about 1 000 kg/m^3. As the sediment then flowed it implies that τ_o < about 100 Pa.

In a vertical water-filled fracture that is gradually filling with sedimenting flocs, the weight of the sediment would increase and the stress at the bottom of a metre or two of sediment would be sufficient to make it start to spread sideways in the fracture. The rate of spreading will depend on the viscosity of the mobilised sediment and how the friction against the walls of the slot restrains the movement.

For flow of the mobilised fluid in the vertical fracture, the driving force F_g induced by gravity must overcome the shear stress F_τ against the walls. A force balance gives

$$F_g = \Delta\rho\, LW d_B g Sin(\alpha) \tag{5-2}$$

d_B is the aperture that just allows flow to occur, L and W are length and width of the sediment in the fracture

$$F_\tau = 2LW\tau_o \tag{5-3}$$

From this for an example with τ_o = 2 Pa and $\Delta\rho$ = 20 kg/m^3.

$d_B = \frac{2\tau_o}{\Delta\rho\, gSin(\alpha)} = \frac{2 * 2.}{20\ 9.81\ 1}$ = 0.02 m = 20 mm

For illustration, the reader may consider that many soft food products, mayonnaise, ketchup, yoghurt, mustard, etc. have τ_o from tens to hundreds Pa.

The observations in the simple experiments can also be used to make a rough estimate of the apparent viscosity of the sediment. We assume that the sliding "blob" has an apparent viscosity μ_a at the shear rate that is generated by internal circulation in the blob as it moves down an inclined wall.

The force balance between gravity force and restraining viscous force gives

$$F_\tau = \mu_a LW \frac{du}{d\xi} = F_g = \Delta\rho\, LW\delta g Sin(\alpha) \tag{5-4}$$

$\frac{du}{d\xi} = \frac{u}{\delta/2}$ is an approximation of the velocity gradient across half the blob in which the fluid circulates. δ is the thickness of blob, L and W are the length and the width, u the sliding velocity along the wall, ξ a coordinate perpendicular to the wall, g the gravitation constant and α the angle to the horizontal. $\Delta\rho$ is the density difference between the blob and the surrounding fluid.

This gives $\mu_a = \frac{\Delta\rho\, \delta^2 g Sin(\alpha)}{2u}$

As an example: In the experiment #5 it took at least 4 hours for the 8 mm high (once turned) sediment to slide down the 10 cm long tube after the tube had been tilted to about 30°. The velocity was about 220 m/yr, the thickness δ was about 8 mm and $\Delta\rho$ = 20 kg/m^3. The apparent viscosity is about 450 Pas. This is about 450 000 times larger than that of water. It is noted that the shear rate was about 0.002 s^{-1}, which is well below shear rates commonly reported in rheology measurements of bentonite gels and slurries.

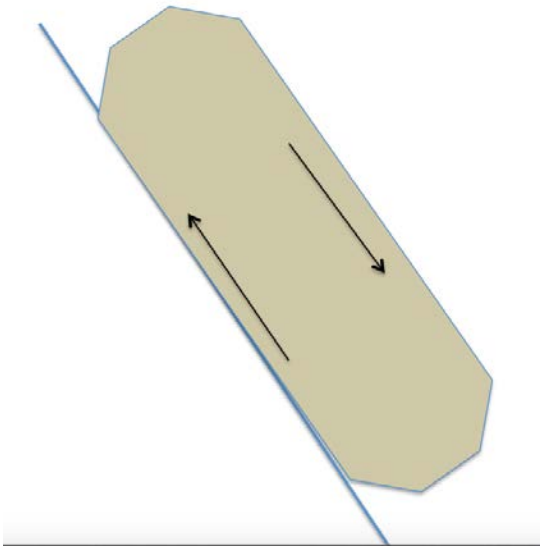

Figure 5-5. *A viscous " blob "slides" down an inclined wall.*

6 Viscosity and shear strength of montmorillonite suspensions in low ionic strength water

Numerous methods to measure floc strength have been devised (Jarvis et al. 2005). There is a large number of publications on the viscosity and yield strengths of clay-rich slurries at different solids concentrations and ion concentrations. Practically always they show that at high ionic strengths gels form with yield strengths larger than many Pa or even tens to hundreds of Pa when the slurry contains hundreds of g/l or more. Such slurries need considerable pressure or hydraulic gradients to be mobilised. Once mobilised, the slurry (or paste) can flow. The apparent viscosity of the mobilised slurry is high at low shear rates but can decrease dramatically at higher shear rates. Only a few studies have been found for montmorillonite suspension rheology at a low ionic strengths and solid concentrations around 1–3 volume %. This is the region of interest for the present study.

A detailed study of the rheology of freshly prepared suspensions of Mt in waters with different Mt and ion concentrations down to deionised water are reported in Birgersson et al. (2009). The data show that at low ionic strength and for volume fractions below about 1 % (water ratios above 25–30 (mass water/mass Mt) the suspension is Newtonian and that the viscosity increases with Mt concentration and with decreasing ionic strength. The data in this region together with other published data were used by Liu (2011) to develop a viscosity model for ion concentrations below the CCC. The viscosity was Newtonian and increased by up to a factor of ten up to about 1 volume % Mt. For higher Mt volume fractions the apparent viscosity was clearly non-Newtonian and could be fitted to shear rate by a power-law model.

A few measurements of shear strengths were made with suspensions aged 1 and 21 days by Birgersson et al. (2009). These showed an increase in shear strength for by a factor 2–3 by aging.

6.1 Experimental data on viscosity and shear strength of montmorillonite in dilute water

There is a large number of publications on the viscosity and yield strengths of clay-rich slurries at different solids concentrations and ion concentrations. Most studies concern sedimentation in riverbeds, lakes, and oceans. However, the solid material and clay in these sediments contain only minor amounts of swelling clays such as Mt and the solid concentration in the sediments is much larger than a few volume percent, practically always they show that at high ionic strengths gels form with yield strengths larger than many Pa or even tens to hundreds of Pa when the slurry contains hundreds of g/l or more.

We have found only one systematic experimental investigation in dilute waters by which we mean less than 5–10 mM, for montmorillonites that have been allowed to age before or during the measurements and for solid concentrations less than 8 % by weight (Pujala 2014). (In the sections below weight % will be denoted “W%” and volume % by V% for short). These are the conditions of interest for the present report. Pujala measured yield strength and apparent viscosity of suspensions of purified montmorillonite in deionized water.

The viscosity increases with resting time when the solids concentration is higher than 2.5 W% (0.9 V%). Below this concentration, aging does not influence the viscosity. The viscosity increases gradually from that of water up to ten times that of water in this range of concentrations. The suspension is a sol. This is in full agreement with the findings in Liu (2011) who also found that above

this solids concentration the fluid is no longer Newtonian. At higher concentrations, the fluid is non-Newtonian and starts to have yield strength. The Pujala results show a "rapid" aging already after days to weeks. The apparent viscosity increases ten to hundredfold after a few weeks. The increase is larger for the more concentrated suspensions. This can be exemplified by the following. At 4 W% the relative viscosity is nearly 40 times that of water and at 5 W% it is 120 and at 6 W% it is 300 times larger than water after 15 days rest.

The aging is caused by the build-up of larger and stronger 3-dimensional networks of individual Mt sheets generating a gel with an increase of yield strength over time. When the gel is subject to a shear force larger than yield strength the gel breaks up at weak locations. With higher shear rate (velocity gradient) stronger and stronger bonds in the suspension break and the viscosity decreases. A balance between the rate of breaking of bonds and reformation of bonds will result for any imposed shear rate. Decreasing the shear rate will result in a more viscous fluid. It should be noted that this idealized picture is marred by the fact that the suspension can show hysteresis and may not return to the earlier viscosity at the same shear rate.

The shear rates in the experiments covered a range 0.1 to 1 000 s^{-1} and Mt concentrations 3–6 W% in steps of 0.5. The results were found to fit very well to the Herschel-Bulkley model Equation (4-8). Figure 6-1 shows a summary of the results fitted to the experimental data for three different Mt concentrations using the Hershel-Bulkley model.

The exponent n_{HB} is 0.45. The yield stress increases with W% Mt according to

$$\tau_o = 0.2\ (\mathrm{cMt})^3 \tag{6-1}$$

where τ_o has units Pa and cMt is Mt concentration with units W%

$$K_{HB} = 1.3\ \mathrm{cMt} - 2.3 \tag{6-2}$$

With these relations, we have emphasised the agreement for the lower cMt over the higher Mt concentrations for which the apparent viscosity is somewhat under-predicted at the lower shear rates. The reason for this is that it is expected that the sediment settled from the floc suspension in the fractures will not compact much. The suspensions in Pujala's experiment were prepared by making the slurry to have a given cMt and not by settling it out from a less concentrated suspension. This would not have been possible because such slurry is swelling and would not allow phase separation.

Figure 6-2 shows a plot of τ vs. $\dot{\gamma}$ for the Pujala experiments

Figure 6-3 shows the yield stress τ_o as $\dot{\gamma} \rightarrow 0$ as function of c_{Mt}.

The Pujala data can be summarised well by the Hershel-Bulkley model

$$\tau = \tau_o + K_{HB}\dot{\gamma}^{0.45} \tag{6-3}$$

with τ_o from Equation (6-1) and K_{HB} from (6-2).

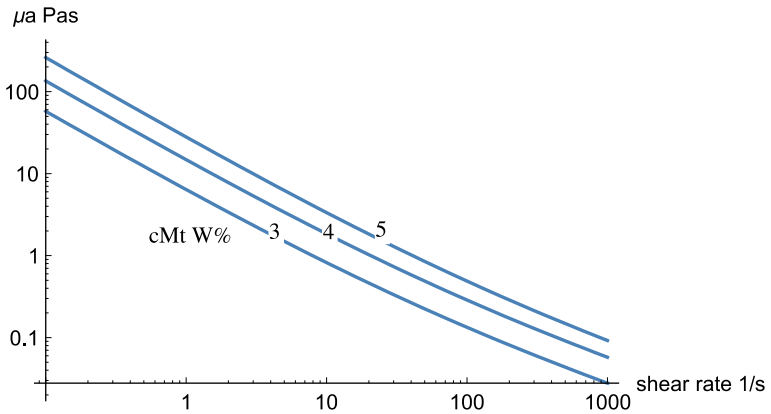

Figure 6-1. *Summary of Pujala´s results fitted to the Herschel-Bulkley model. The exponent n_{HB} = 0.45.*

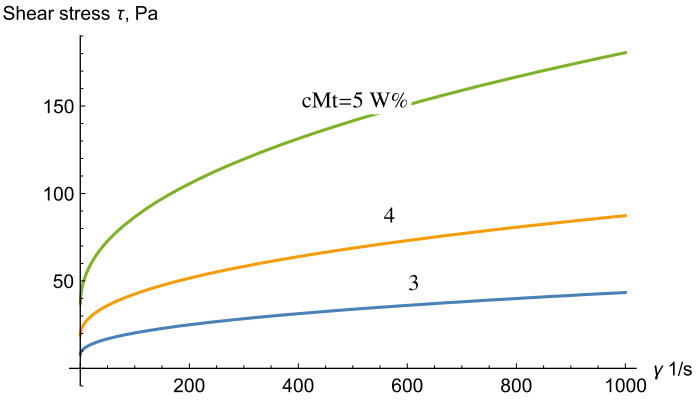

Figure 6-2. *Shear stress vs. shear rate for different c_{Mt} one-year aged suspension.*

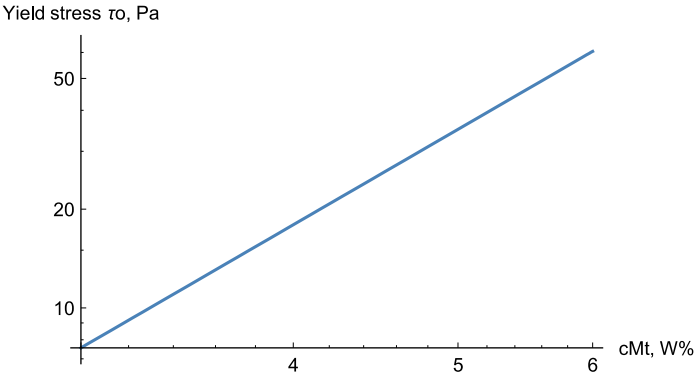

Figure 6-3. *Yield stress vs. c_{Mt} for one year aged suspension.*

It may be noted that at low shear rates, the apparent viscosity is totally dominated by the yield stress τ_o as shown in Figure 6-4 where the dotted line is $\mu\alpha = K_{PL}\dot{\gamma}\, n^{PL-1}$ with $n_{PL} = 0.83$. Thus for low shear rates the powerlaw model also gives a fair or even good fit to the data but it cannot account for yield strength, which would be predicted to be infinitely large.

The Pujala data could also be fitted well by the powerlaw expression $\mu\alpha = K_{PL}\dot{\gamma}\, n^{PL-1}$. n_{PL} decreases from 0.17 to 0 when c_{Mt} increases from 3 to 5.5 W%. K_{PL} increases from 6 to 120 for the same increase in c_{Mt}. μ_α has units Pas. For $c_{Mt} = 4$ W% (1.5 V%), $K_{PL} = 30$ and $n_{PL} = 0.1$.

The evaluation of the yield strength in the scoping experiment in Section 5.1 gave τ_o to a minimum of 2–4 Pa at cMt around 3 W%. The apparent viscosity was 450 Pas. The shear rate was about 0.002 s^{-1}. Extrapolating the shear rate to 0.1 s^{-1} the apparent viscosity would be about 20 Pas, which is not very far from the about 50 Pas found by Pujala.

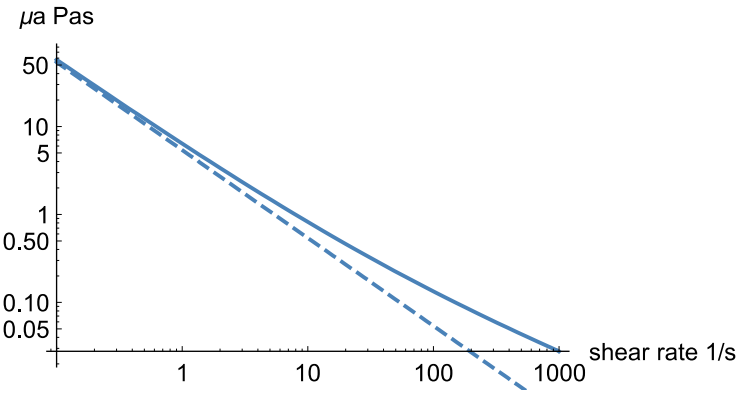

Figure 6-4. *Apparent viscosity vs. shear rate for cMt = 3 W%. Dotted line is for powerlaw fluid $\mu_\alpha = K_{PL}\dot{\gamma}\, n^{PL-1}$ with $n_{PL} = 0.17$.*

7 Flow of powerlaw and H-B fluid in a slot

7.1 Commencement of flow

A powerlaw fluid will start to flow at infinitesimally low pressure gradients although with infinitesimally low velocity. A Bingham fluid and a H-B fluid needs a minimum stress to be mobilised.

The minimum aperture for flow start is obtained from the force balance in the slot

$$d_{Bmin} = \frac{2\tau_o}{\frac{dP}{dz}} \tag{7-1}$$

$\frac{dP}{dz}$ is the pressure gradient . For the buoyance driven case in a vertical slot

$$d_{Bmin} = \frac{2\tau_o}{\Delta\rho\, g} \tag{7-2}$$

$\Delta\rho$ and g are density difference and gravitational constant respectively.

Example: Vertical fracture and buoyancy driving force

Figure 7-1 shows the smallest aperture d_{Bmin} where an H-B fluid with density difference to water would be mobilised as function of τ_o.

Even very low shear strength of the gel formed from the AF will immobilise it in a slot. Thus any fractures in which the AF has phase-separated and formed gel will essentially be closed to flow. This could potentially clog many of the flow paths in the vicinity of a deposition hole or a vault repository that earlier were available for hydraulically driven water flow.

Example: Expanding clay pushes the gel

If the gel has formed a tiny distance outside the expanding clay the expanding clay will "soon" overtake the gel and build up pressure on the "inside of the gel. If the gel has formed a layer d_{gel} m thick the swelling pressure will dislodge the gel when the pressure difference over it has reached P_{crit}. Figure 7-2 shows P_{crit} as function of τ_o.

Gel in a 0.1 mm aperture with shear strength 1 Pa is mobilised for a swelling pressure at the paste/gel interface of only a few kPa. With a shear strength of 10 Pa a pressure of 20 kPa is needed to mobilise the gel. The swelling pressure of the expanding sodium bentonite is on the order of 1 000 kPa at V% = 50, 100 kPa at V% = 22 and 50 kPa at V% = 17 (Börgesson et al. 1988). This agrees with the data from the dynamic expansion model for dilute pore water conditions (Neretnieks et al. 2009) shown in Figure 7-3. The figure also shows that the swelling pressure sharply drops to very low values in higher pore water concentrations of sodium.

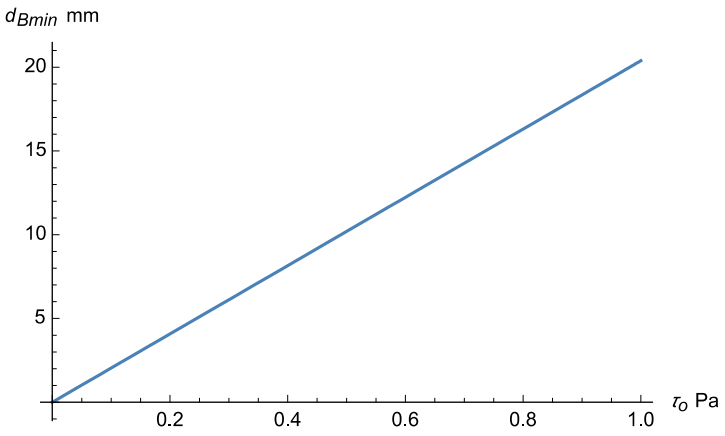

Figure 7-1. *Smallest fracture aperture for buoyance flow to set on*

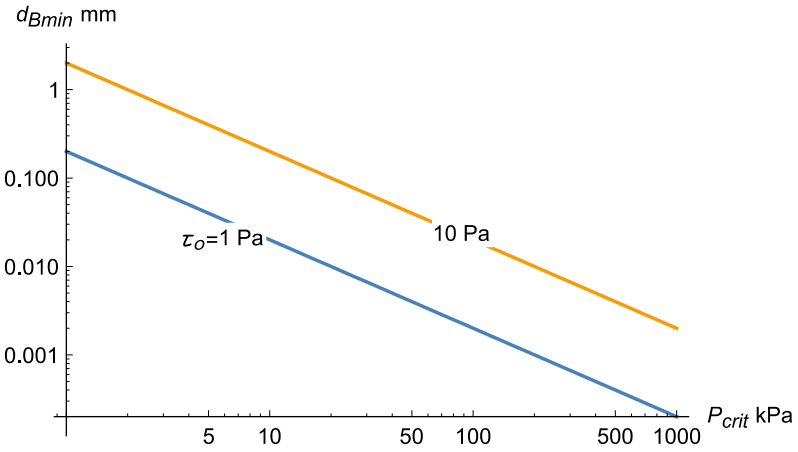

Figure 7-2. *Smallest fracture aperture filled with d_{gel} = 0.1 m long gel to be mobilised by the swelling pressure of expanding clay at the clay/gel interface.*

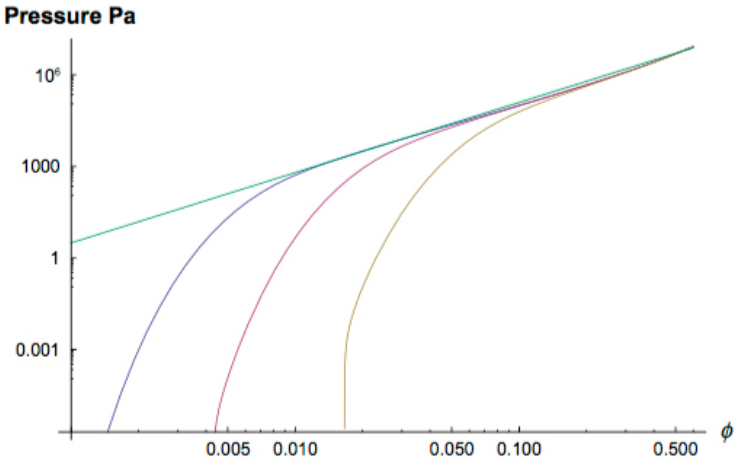

Figure 7-3. *Swelling pressure as a function of the volume fraction for different sodium ion concentrations. From left to right 0.1, 1 and 10 mM. The straight line is given by $P_{swell} = 2.5 \times 107 \times \phi^{2.4}$ (Neretnieks et al. 2009).*

This suggests that in very dilute waters, < 1 mM, the expanding clay easily can push the gel in front of it but at 10–20 mM, still below CCC, the gel in the narrow fractures could slow down or stop the expansion.

7.2 Flow after mobilisation

The H-B fluid, once the shear stress is larger than τ_o starts to flow. The velocity distribution in a slot and the flowrate of a powerlaw fluid have been derived and can be found in Bird et al. (2002, Equations 8.3–13 and 8.3–14 respectively).

The equations are shown as Equations 7-3 and 7-4. In the vertical slot the pressure $\frac{dP}{dz} = \Delta\rho\, g$

$$u_z = \left(\frac{dP}{dz}\frac{b}{K_n}\right)^{\frac{1}{n}} \frac{b}{\frac{1}{n}+1}\left(1 - \left(\frac{x}{b}\right)^{\left(\frac{1}{n}+1\right)}\right) \qquad \text{valid for } 0 \le x \le b \qquad (7\text{-}3)$$

u_z is fluid velocity, b is half fracture aperture, x is distance from centre of fracture, n and K_n are constants determined from experiments.

$x = 0$ at centre of the slot. The volumetric flowrate Q is

$$Q = \frac{2Wb^2}{\frac{1}{n}+2}\left(\frac{dP}{dz}\,\frac{b}{K_n}\right)^{\frac{1}{n}} \qquad \text{in the region valid for } -b \le x \le b \tag{7-4}$$

Note that $2b \le d_{Bmin}$. For the H-B fluid the equations can be used for the region $b_{min} \le |x| \le b$. In the region $0 \le |x| \le b_{min}$ the velocity is constant equal to that at b_{min} provided the pressure gradient is sufficiently large to mobilise the fluid, otherwise the fluid does not move.

However, if the gel that formed has settled near the expanding clay in the fracture and the clay expands with a high, and over time, growing swelling pressure at the clay/water interface the pressure on the gel will gradually increase and mobilise the gel. The expanding clay in the present concept is a swelling paste whereas the AF forms a gel after phase separation of a previously released sol after some "maturing" time outside the paste/sol interface. As the expanding paste overcomes the gel the swelling pressure could either compress the gel or could mobilise the gel, disrupt its 3-D structure and return it to repulsive swelling paste. Remember that the sol contained about 3 W% smectite, which formed the AF. This AF phase separated in a 10 W% gel and "clean" water. One can speculate about the properties of the remobilised gel. If the bonds in the 3D gel structure are disrupted it would become a swelling paste again with DDL forces expanding the paste in the same way as the original paste with the same volume fraction Mt. At present it cannot be excluded that the only effect will be that the gel returns to be a swelling paste and expansion goes on, just somewhat retarded.

In the regions below the source where the AF has sedimented this may have taken place at some distance, below the expanding clay/sol interface. The gel may clog the fractures below the repository long before the expanding clay has reached those regions.

We refrain at present from using Equation (7-4) to calculate the flowrate of the H-B gel as influenced by the expanding clay because the pressure gradient over the gel $\frac{dP}{dz}$ entirely depends on the extent of the gel length which is influenced by many unknown factors.

8 Possible causes and consequences of phase separation of sol at low ionic strength and dilute waters

8.1 Impact of positively charged edges

It is long known that under acidic and probably neutral pH conditions the edges of Mt particles can be positively charged and that one can expect a complex house of cards structures to develop to form gel-like structures (van Olphen 1997). Hedström et al. (2016) showed that such Mt gels formed in semi-dilute waters (15 mM Na^+) could be stable and support their own weight for many years. They also found that aggregates are formed in the sol phase even when the clay is dispersed in deionized water. They report that the aggregates have limited size, do not form a network that spans the available space, and have no yield strength. Over long time periods, aggregates may accumulate at the bottom of a vessel as sediment. The sediment has no observable yield strength. This is mentioned here because there is other increasingly strong evidence that the sediments can have considerable yield strength, which is of paramount importance for the fate of eroding clay in dilute waters.

Pujala (2014) found that there was a distinct jump in the phase separation of dilute Mt suspensions in deionised water. Above 2.5 W% no separation took place. However, at 2.5 W% sediment had formed to a height in the tube that is about 20 % of the original suspension height after 3.5 years. The other phase was essentially clear water. There was a sharp boundary between the phases. This implies that the sediment has on the order of 15 W% Mt (about 5 V%). The same Mt concentration in the sediment resulted also starting with suspensions with 0.3, 0.5, 1, 1.5, and 2.0 W%. This is an unexpectedly high solids concentration. Our own scoping experiments described earlier give similar results and also show that the sediment has considerable yield strength.

Below we explore a possible reason for this behaviour. It is based on the idea that when the sol is sufficiently dilute Brownian motion can make the particles rotate. This occurs at around 1 V% (Neretnieks et al. 2009). The system becomes self-organising, forming an attachment between the negatively charged faces and positively charged edges, EF, which gradually leads to formation of a space-filling structure of particles bound to each other. One such structure is conceptualised as a house of cards, HoC. The particle density in such a structure can be estimated as well as its strength, assuming that the EF bond is formed by Coulomb forces. Experiments and Monte-Carlo simulations have shown this for synthetic Laponite clay (Ruzicka et al. 2010). See also Shalkevich et al. (2007) who discuss cluster, glass, and gel formation and viscoelastic phase separation.

8.2 House of cards structure of gel

Figure 8-1 illustrates the idea of house of cards structure in two dimensions

The volume fraction ϕ of the solid platelets is estimated in the following way. The water volume between the platelets in the 3D configuration is on the order of $V_w \approx d_p(\frac{d_p}{2})^2$ for the voids between the six platelets. The volume of the parts of the 6 circular platelets with thickness δ belonging to the void is approximately $V_p \approx \frac{\left(2\left(\frac{d_p}{2}\right)^2 + 4\frac{d_p}{2}d_p\right)}{2}$. The "/2" means that each side of the void is shared with one neighbouring void.

Then $\phi = \frac{5\,\delta}{d_p}$. For typical platelet dimensions of Mt, δ = 1 nm and d_p = 200 nm the volume fraction ϕ = 0.025 (about 7 W%). This is surprisingly close to what was found in our scoping experiments as well as in those by Pujala (2014). Some exploratory modelling on the strength of a HoC is presented in Appendix D.

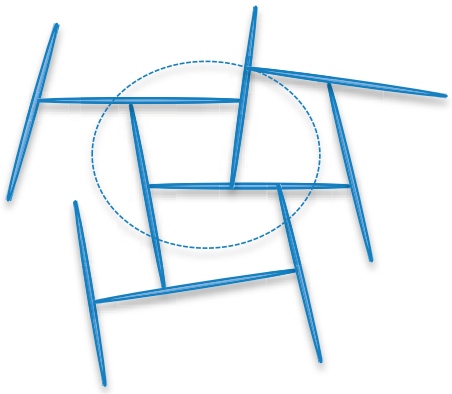

Figure 8-1. *Illustration of "House of cards" structure in 2D. The dotted circle suggests how a third dimension could be added.*

8.3 Impact on expansion of clay from the source

In this section we explore how the formed gel may influence the expansion of the bentonite from the source. Several questions arise. Will a mobilised gel re-form again once disrupted? How long is the region filled with the gel? How far "downstream" from the expanding bentonite/sol interface will the phase separation occur? A few exploratory examples are presented and discussed.

The sediment cannot be mobilised by gravity in fractures with apertures smaller than a few centimetres, sic. As the sediment cannot move away by gravity the expanding clay behind it will start to exert a pressure on the sediment. The pressure at the swelling clay/sediment interface will increase over time until the pressure gradient over the sediment is sufficiently large to mobilise it as shown in Chapter 7.

The largest mean fracture apertures expected intersecting a deposition hole is on the order of 0.1 mm. The swelling pressure of the compacted clay in the source in a KBS-3 repository is on the order of 5 MPa for a long time.

The reader is reminded that the detritus free swelling clay, which has not formed gel in the fractures, may not be restrained by friction against the fracture walls because the swelling is caused by the DDL forces forcing the smectite particles apart and their rate of movement is restrained by their friction against the water moving in the other direction in the fracture to exactly replace the volume vacated by the particle with an identical volume of water (Neretnieks et al. 2009). There is thus no net movement of the clay "paste", just exchange of location between colloid particles and water. This can be seen by the analogue of two different liquids in contact with each other in a fracture, one consisting of large molecules (the colloidal particles) mixing with a small molecule liquid, water, by molecular diffusion. The *mixture* does not flow. It is just gradually diluted by water with the colloidal particles, "diluting" the water.

It is so far not clear at which fracture apertures also the expanding, detritus free Mt, will be influenced by wall friction, although it is probable that apertures smaller than a few smectite sheet diameters, i.e. around some μm will start to be influenced by the presence of a wall. In contrast, the sediment-gel formed by flocculation and aging has attained yield strength and is pushed by the expanding clay. The sediment is a gel and has no internal swelling pressure, as the swelling clay has, even at the same smectite concentration. The sedimented gel will resist the rising pressure (stress) exerted by the expanding clay due to friction against the walls. The gel will be mobilised in smaller and smaller fractures as the pressure at the swelling clay/sediment interface increases. It thus seems likely that the gel will not be able to withstand the expansion pressure of the Mt that continues to expand into the fracture from the source. In the disrupted gel the smectite particles are released and can be subjected to the same forces as in the expanding paste. Not being a gel anymore and having a volume fraction of 3–4 % it expands and releases colloids into the water forming a sol. This phase separates and forms gel somewhere downstream and the process is repeated.

8.4 Conclusions on the impact of gel formation in below CCC waters

Neretnieks et al. (2017) derived detailed and also simplified models adapted for PA calculations of bentonite clay expansion and erosion in fractures with seeping water for conditions that may be expected for a KBS-3 repository. In the present report new information is presented on the behaviour of montmorillonite sol, which needs to be considered for the modelling. The sol is not stable, forms flocs that grow with age and form gel. The gel clogs fractures somewhere below and downstream of the source. The formed gel is not mobilised by gravity or by natural hydraulic gradients. The information available at the time for the report by Neretnieks et al. (2017) showed that the flocs were carried away by the seeping water and new sol formed at the clay water interface. It was shown that in narrow fractures the flocs cannot move away as rapidly as new floc form and that the flocs will fill the fracture and potentially slow down new floc formation. It was not explicitly modelled how the settled flocs would be influenced by the expanding clay behind them. As is considered in this report.

When the flocs, or gel formed by the flocs, is overtaken by the expanding clay the gel is disintegrated and mobilised. The mobilised gel reverts to a swelling montmorillonite paste. It can again release sol, which flocculates near the rim. The process can then be repeated. The flocs/gel are pushed in front of the expanding clay. The shear strength of the gel and apparent viscosity of the disrupted gel only marginally slows down expansion of the clay. There is no erosive loss of montmorillonite as sol. All clay lost from the source remains in the fracture.

A similar case was modelled for the conditions that exist for swelling montmorillonite above CCC conditions described in Neretnieks et al. (2017). That model also applies to the present case. The results are shown below.

The mass loss over time, $M(t)$, is summarised in the following equation. M is in kg, the aperture δ is in metres and t is time in years.

$$M(t) = \delta(93.74\,\mathrm{t} - 0.0004521\,\mathrm{t}^2 + 2.236 * 10^{-9}\mathrm{t}^3) \qquad (8\text{-}1)$$

For details of this equation please refer to Neretnieks et al. (2017)

Figure 8-2 shows the mass loss over time for a 0.1 mm fracture.

The recent experiments at Ciemat summarised in Appendix C that showed no floc formation under conditions very similar to those described earlier, raises the question of the impact of *absence* of floc formation. This case was also considered and modelled earlier.

The model(s), the instructions how to use them, and conclusion described in Chapter 4 in Neretnieks et al. (2017) are therefore still applicable for pure montmorillonite clay.

We deem the main weakness on the models to be that the impact of the presence of 10 % or more of detritus material in the bentonite is not considered. This is discussed next.

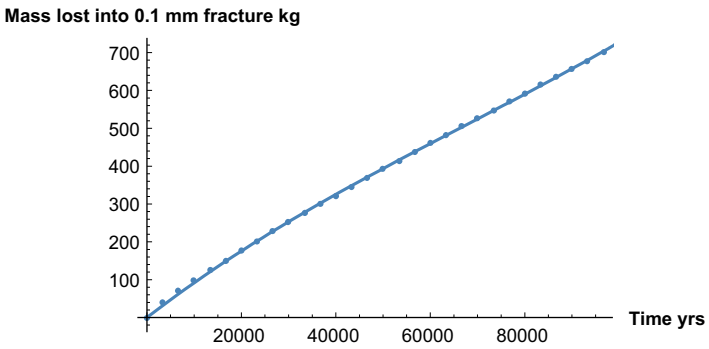

Figure 8-2. *Mass loss as function of time. The fitted full line can hardly be distinguished from the simulated results by the model, the points.*

9 Impact on clay expansion by detritus material in bentonite

9.1 Movement of detritus particles

Detritus particles in the clay can be transported by the AF. They can also move downward by gravity in the AF and/or in Mt free water. The detritus particle size is in the same range as that of the expected apertures and if the particles are captured in the narrow passages this will decrease the sizes of the passages and further increase the resistance to flow. We start with a simplistic discussion on what may happen to a detritus particle that is either carried by the expanding clay or is sedimenting by the impact of gravity.

The simple mechanistic approach here is that a particle propagated by some directed force, e.g. gravity, migrating in a section of the fracture that narrows down to the size of the particle, gets trapped. The next particle can choose to pass the previous on either side and be trapped where its size does not allow it to move on. The trapped particles change the aperture distribution generating increasingly narrower "pores", trapping smaller and smaller particles. Eventually, if the particle size distribution is favourable a pore size distribution may develop through which only the smallest of even the montmorillonite can navigate through the "filter" that has developed by the captured detritus. Such tight filters have been experimentally found to build up rapidly when filtering a bentonite suspension through paper filters as well as sintered metal filters with pore sizes as large as 100 μm. This is reported in an analysis of a number different experiment with clays with and without detritus material that were made by different research groups in the BELBaR project (Neretnieks and Moreno 2018).

In an experiment, Reid et al. (2015) studied clay expansion in a replica of a natural fracture and showed that a filter of the detritus formed, expanded, and finally clogged the fracture.

9.2 Conventional filtration processes in nature and industry

Filtration is a process that separates solid particles from gases or liquids. It has applications in a wide range of areas including chemical, oil & gas industry, environmental, pharmaceutical and medical applications, mechanical and household appliances etc. One common industrial problem is that filters become clogged after some time and the aim is to avoid this. This is the opposite of the theme of this report where the aim is to ensure that clogging will occur. There is another important difference between the approaches, namely that in many industrial applications in which a valuable or undesired component is to be separated by filtration from gas or fluid. Then when the function of the filter is seen to degrade, remedial action can be taken. That is not the case for the deep underground repository, which will be closed after the waste has been deposited. The function must be assured beforehand.

9.3 Filtration techniques

The main purpose of filtration can be to purify the fluid from the solid particles or to concentrate and collect the solid material. Two main filtration techniques, membrane and deep bed filtration are used.

9.3.1 Membrane filtration

In membrane filtration, a thin porous membrane e.g. a paper filter, synthetic woven cloth or similar constructs with pores smaller than those of a large fraction of the particles to be separated is used. The suspension is pressed through the filter membrane, which lets the fluid pass but retains the solid particles. The particles are retained by straining at the pore entrance and build up a porous layer of particles around the pores. After a short initial time, during which the smallest particles pass the growing bed, it lets increasingly less of the small particles to pass. These are trapped in the winding pores between the already deposited particles. As this happens the bed thickness and

the pressure drop increases. This is partly because the bed becomes thicker and partly because the smaller particles that are trapped decrease the pore size of the conduits. Another, often important effect, especially for non-rigid particles such as flocs, is that the pressure drop compresses the bed, which further decreases the pore sizes and increases the pressure drop further. Then the operation must stop and the membrane must be exchanged or cleaned.

The membranes can either be flexible and then need to have a support or be rigid e.g. made up of tiny glass or metal particles that are sintered together. Such filters have a three-dimensional network of pores with a narrow size distribution of winding pores. Such filters will also trap particles inside the filter, as in deep bed filters, not only on the surface where the slurry enters.

The entrance to the smaller rock fractures can be likened to the pores of a membrane into which the particles cannot enter. In fractures that are at least locally larger than the particles small particles can enter the fracture but may be strained in narrow sections further in. This can be likened to deep bed filtration described in the next section.

9.3.2 Deep bed filtration

In many applications where the concentration of particles is low, e.g. drinking water treatment, deep bed filtration is used. The filter then consists of a tall bed of sand grains. The particles are trapped when they are too large to navigate the narrow passages between the grains but also, and more importantly because they attach to the sand grains by vdW, electrostatic and other attraction forces. A thin layer of the material to be removed from the water increasingly coats the grains. In e.g. drinking water purification this often consists of flocs of aluminium or iron hydroxide, which were added to the water to occlude unwanted material such as virus, bacteria, heavy metal precipitates etc. The flocs are often loosely bound to the surface of the sand grains. The flocs move deeper and deeper into the bed. At regular intervals, the bed is back-washed to remove the attached flocs and the cycle is repeated.

9.4 Basic mechanisms of filtration

It is envisaged that many of the mechanisms involved in trapping the fine detritus particles in natural fractures can be related to observations and interpretation of experiments in membrane filtration as well as in deep bed filtration.

Figure 9-1 illustrates an entrance to a variable aperture fracture and how different size particles can be hindered from entering the fracture while other particles will enter the fracture and will have to be trapped deeper in the fracture. The particles trapped at the entrance will help to prevent other particles to enter. When a large fraction of the particles are larger than the largest aperture of the fracture it can be expected that a bed of particles rapidly builds up at the entrance, grows in thickness as for membrane filtration and increasingly hinders further loss of the Mt pushing the detritus to enter.

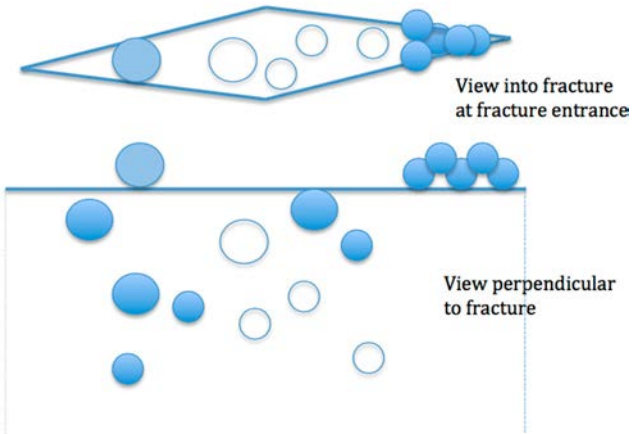

Figure 9-1. *Detritus particles, some hindered from and some entering a variable aperture fracture. Filled circles show trapped particles and open circles show particles moving in the fracture*

The particles that are not captured at the inlet of the opening can be strained in narrow passages in the conduit. They can also attach to the walls by different processes and mechanisms.

9.5 Overview of concepts and mechanisms

In conventional modelling of membrane or cake filtration, the aim is to derive a relation between pressure drop and flowrate in a filter bed with a thickness growing over time. It also includes modelling of how the bed is compressed by the pressure difference between in- and outlet. Overviews of the processes and modelling can be found in Olivier et al. (2007), Tien (2012) and Iritani (2013).

In deep bed filtration, if one could follow the trajectory of the suspended particle in the winding paths in the bed it would be possible to determine when the particle comes in contact with the wall of the pores. If it has a given probability of becoming attached to the wall one can determine the distribution of attached particles along the bed over time and with the volume of suspension that has entered the bed.

The particle trajectory could in principle be determined by solving the hydrodynamic equations for the flow field in the pores accounting also for other forces such as gravity and inertia of the carried particles. Tiny particles carried by the flow will also move by Brownian motion, which adds a stochastic component superimposed on the hydrodynamic trajectory. The probability for a particle to become attached to the surface is influenced by a variety of mechanisms, among them attraction by der Waals force, by repulsive DDL forces for charged surfaces and/or particles, by the slope of the wall, by the impact velocity of the particle and many other effects. Generally, it is not possible to determine trajectories or the attachment probabilities without resorting to experiments.

In practical applications, all these effects are lumped into one parameter, the specific collector efficiency η_i in section "i" of the bed. This states what fraction of the incoming particles will be collected in that section in the bed. This is conceptually simple but has the problem that η varies with location "i" and over time. It also depends on the size of the particles. In practical application these variations are not possible to determine except by direct experiments for a specific application. One important reason for these difficulties, of specific importance for present problem, is that the captured particles will influence the porosity and pore structure of the bed itself. This is seldom a major concern in deep bed filtration applications because when the bed becomes clogged, the operation is stopped and the bed is cleaned. The final stages of the clogging have therefore not been investigated and reported in much detail in the deep bed filtration literature.

The basic model concept, described by mass balance equations for particle accumulation on or in a filter, is based on the idea that particles attach and accumulate with a rate that is proportional to the particle concentration and the fluid velocity. The rate coefficient will have to account for the rate of primary impact of particle to medium surface and the frequency of attachment compensated by the rate of detachment. This, in turn, can be influenced by the underlying attachment mechanisms binding forces involved. It also has to account for the rate of physical straining. The rate coefficients will vary with time as more and more particles attach and change the pore sizes. This is sometimes not so problematical in industrial applications where the membrane of the material of the deep bed, as well as the properties of filtered particles are well known. In natural systems e.g. gas and oil extraction from deep wells where the properties of rock and of the released small particles are not as easily assessed the problem is more challenging and essentially only empirical model are used, see e.g. Yang et al. (2016).

These models do not seem to be directly applicable to the present problem where the swelling pressure of the expanding clay develops due to the repulsion between the Mt sheets in compacted clays and not only by hydrodynamic or gravity forces. The expanding clay enters into the fracture as it takes up water and swells. However, as the clay swells by taking up water the process is much different than when clay is pressed by water "from behind" as in cake filtration. The difference is sometimes not fully appreciated and we wish to point out a few important differences. The montmorillonite particles repel each other by the osmotic pressure caused by the presence of cations attached to the negatively charged surface of the Mt sheets. This makes them distance themselves from each other. There is no need for hydraulic gradient to drive them into the pores.

Furthermore, the Mt sheets do not readily attach themselves to the mineral surfaces of crystalline rocks, which are mostly neutral or negatively charged. On the contrary, they are repelled. It has been suggested that low pH conditions the edges can be positively charged which would lead to attachment (Birgersson et al. 2009). On the other hand, it has been shown that the negative charges on the faces of the Mt sheets spills over on the edges and prevents this (Secor and Radke 1985).

The un-charged detritus particles are pushed along by the expanding clay until this has become so dilute that the detritus particles are released from dilute Mt suspension when this forms a sol. This happens in waters with an ionic strength below the CCC. The detritus particles will be left behind already before sol formation if they are strained in narrow passages.

9.6 Colloid transport in porous media and fractured rocks

Zhang et al. (2012) give a review of colloid transport in fractured rocks. They mention the same retention mechanisms of nano-scale particles as in other porous media and conclude that colloidal size particle often can travel long distances without being captured.

9.6.1 Experimental evidence for clogging of pores by expanding bentonite

It has been experimentally found that montmorillonite passes 2 and 10 µm pores in filters with the same ease but practically do not pass 0.5 µm filters (Birgersson et al. 2009). It has also been demonstrated that compacted natural bentonite clays containing detritus, after a short initial period (50 to 200 days) in practice stop further penetration of montmorillonite through sintered metal filters with up to 100 µm pore size. This is illustrated in Figure 9-2. Filters with 100, 10 and 2 µm pore size gave similar results provided the porosity was the same (Missana et al. 2011).

Similar experiments with flow through and outside of filters surrounding compacted clay pellets show that clays with detritus let through much less colloids than clays from which the detritus has been removed (Birgersson et al. 2009, BELBaR 2015).

It should be noted that Nanocor clay contains very little detritus but still clogs the filters in the same way as the detritus containing clays do. This is contrary to the findings in Birgersson et al. (2009) who used MX-80 carefully separated from its detritus under similar conditions and found a considerable loss. The observed rate of loss agreed well with that predicted by the dynamic expansion model (Neretnieks et al. 2009).

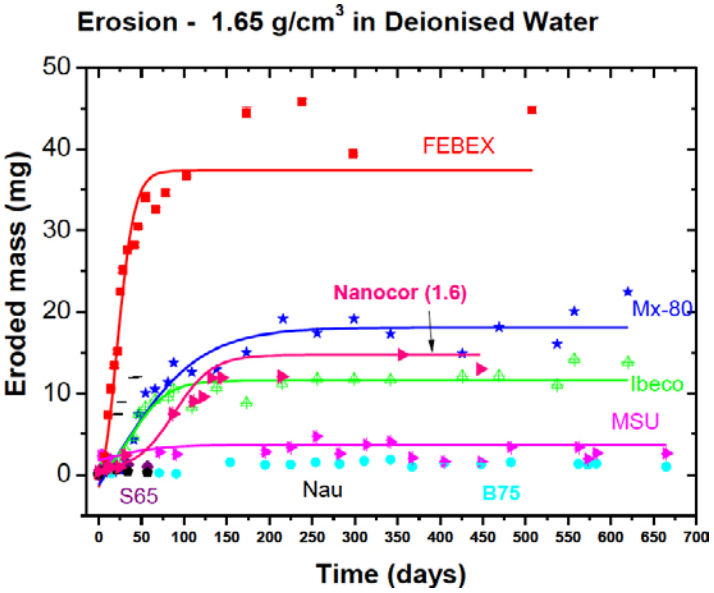

Figure 9-2. *Eroded mass measured as function of time in de-ionised water from different raw bentonites compacted to 1.65 g/cm³ in non-flow tests (BELBaR 2015).*

Another set of experiments with filters is reported in Huber at al. (2016). The filters have 20 µm pores with a porosity of 29.4 %. Compacted clay pellets were placed between filters and a synthetic groundwater was circulated outside the filters. The water had pH = 8.3 and contained 1.2 mM Na, 0.05 mM Ca and chloride, sulphate, and carbonate as anions. MX-80 bentonite was used as received and also as filtered and homo-ionic. Homo-ionic bentonite with Na, Ca and a 50/50 mixture of these were used. The homo-ionic, filtered clays did not contain detritus particles larger than 63 µm. The effluent water with colloids was analysed for Al, Si, Mg, and Fe to determine the mass of colloids that penetrated the filters. The results are shown in Figure 9-3.

It is seen that the homo-ionic Na-smectite allows much more smectite to pass before the filter is clogged by the detritus material than the raw MX-80, which is clogged almost immediately. The 50/50 mix of Na- and Ca-clay releases less than the Na-clay and the Ca-clay releases very much less clay.

These results show that clogging can dramatically influence the expansion of natural bentonite into narrow pores and fractures.

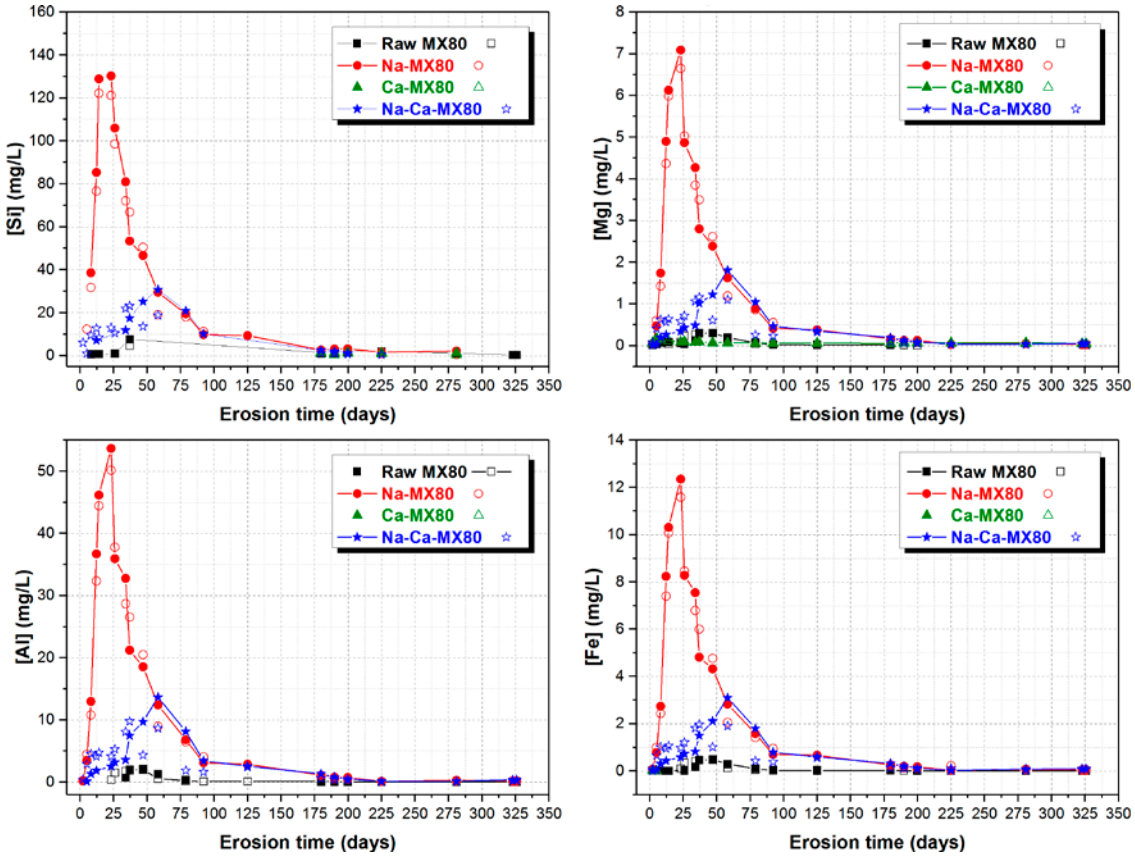

Figure 9-3. *Amount of colloids that penetrated the filters expressed as concentration of main smectite constituents.*

10 Quantitative modelling of filtration

10.1 Continuum-based models

In the continuum-based models, the medium is conceived as a homogeneous continuum consisting of small pores in which the suspension can flow and in which the particles can be retarded or even irreversibly attached to pore surfaces or in the pores themselves in narrow passages.

10.1.1 Filtration coefficient concept

The bed is conceived as a continuous porous medium in which the fluid that carries the particles flows with a given flux. In the simplest case, the particles can attach by one or more mechanisms to the pore walls. The rate of attachment is proportional to the water flowrate and concentration of suspended particles, SP, particles in the mobile pore water.

The differential mass balance of the SP can be written (Herzig et al. 1970)

The mass balance is

$$\frac{\partial \varepsilon c_{SP}}{\partial t} + \frac{\partial s}{\partial t} = -U\frac{\partial c_{SP}}{\partial z} \tag{10-1}$$

U is the flux of the suspension (m^3 suspension/m^2 medium/s). It is usually taken to be constant in the filtration literature because in deep bed filtering U is given by the constant pumping flowrate of the slurry. c_{SP} is the concentration of SP in the flowing water (m^3 SP/m^3 water), s is the concentration of attached particles (m^3 SP/m^3 bed), ε is the bed porosity and z the distance in the flow direction. It is assumed that the concentration of SP in the water is low.

The straining kinetic equation, based on experiments is often taken to be

$$\frac{\partial s}{\partial t} = kUc_{SP} = ku_z\varepsilon c_{SP} \tag{10-2}$$

where u_z is the interstitial velocity. k is the filtration coefficient. It has the unit m^{-1}. It could include the effects of re-suspension of attached particles.

It is noted that Uc_{SP} is the flux J_{SP} of SP (m^3 SP/m^2 medium/s) and u_z is the velocity of SP.

The velocity will depend on the expansion rate of the bentonite into the volume considered. It will change over time and space.

At high accumulation of solids the change of porosity by settling of the particles can be accounted for by Equation (10-3).

$$\frac{\partial \varepsilon}{\partial t} = -\frac{\partial s}{\partial t} \tag{10-3}$$

The filtration coefficient depends on s and has to be determined by experiments. Herzig et al. (1970) compiled some experimental data on the filtration coefficients for different SP and porous media materials. They span several orders of magnitude.

For constant k, ε and U, the solution to Equations (10-1 and 10-2) with good approximation when the accumulation in the water, $\frac{\partial c_{SP}}{\partial t}$, is negligible (Herzig et al. 1970)

$$c_{SP}(z) = c_{SP,o}e^{-z\,k} \tag{10-4}$$

Herzig et al. (1970) also present some other analytical solutions in which k depends on s in different ways. Recently Babakhani et al. (2017) published a review of the state of the science for what they call the continuum-based models in which they present 16 different models used in different applications for colloid transport and SP capture mechanisms.

For well-defined systems such as sand filters that are to filter SP with essentially similar properties, this approach has been found to work as long as the bed has not been overly filled with particles. The use of this simple concept for more complex systems, where the attachment is not irreversible, the attachment/detachment mechanisms must be described in different, and often considerably more complex ways. A major problem is to assess the filtration coefficient k, which can differ by many orders of magnitude for different systems.

An example of the complexities encountered in natural systems is described below. Yang et al. (2016) discuss clogging of gas, oil and water production wells. The main sources of movable fine particles in natural reservoirs are kaolinite and illite clays. These clay particles consist of stacks of thin sheets from which individual sheets can be detached and migrate with the fluid. The thin sheets contribute considerably to the clogging of the flow paths by straining. Straining has a larger effect on permeability decrease than the attachment of the particle to the pore surfaces. An important part of the modelling is how gravity and the hydrodynamic force by Stokes equation generated by the flowing water can detach particles that have attached to the pore walls. The forces between the pore surface and the particle are modelled by the DLVO (Derjaguin-Landau-Verwey-Overbeek) theory, which includes the diffuse double layer repulsion and the van der Waals attractive forces (Evans and Wennerström 1999). The implementation of the model needs considerable experimental information to obtain data for the parameters involved.

Furthermore, when more and more particles are trapped this influences the transmissive properties of the porous medium. This can change the flow field. In principle, this could be handled by recalculating the flow field accounting for the increased flow resistance by the presence of the particles as mentioned by Yang et al. (2016).

One aim of that paper was to understand the impact of flow velocity or flux on the remobilisation of the colloidal particles. A considerable number of assumptions were made to formulate the model, which may not be applicable to the main theme of the present report. Among them may be mentioned the dominating effect of flow and that the suspension is dilute so that the colloidal particles do not interfere with each other. These assumptions are in direct contradiction to that for the swelling montmorillonite, which generates the SP movement by the swelling of the bentonite clay, which is caused by repulsion between the colloids. For the bentonite expansion, there is no flow of the suspension driven by pumping or by an existing hydraulic gradient, which is a recent assumption in the deep bed filtering models.

When more and more particles are trapped this influences the transmissive properties of the porous medium. This can change the flow field. In principle, this could be handled by simultaneously solving the Darcy equation. Such coupling of the flow equation to the transport equation is reported in Bianco et al. (2016). They describe a 3-dimensional micro- and nanoparticle transport and filtration model in porous media. Their work is based on coupling a modified advection-dispersion model, AD, to a conventional 3-dimensional flow model. The interaction between the colloid particles is described by a combination of kinetic processes and equilibrium conditions and can contain several processes competing simultaneously. Ion concentrations can influence the interaction equilibria. Attachment and detachment rate parameters have to be determined by experiment. The model was successfully used to describe experiments with carbon-based nano-materials. Also in this model, the fluid velocity drives the transport of the particles, which are not influencing each other. This is common for a number of similar models mentioned in the paper. The large number of parameters whose values must be determined experimentally makes it difficult to use such complex models and to ensure that the results can be used to reasonably predict the filtering effects.

Numerous other papers have used different modifications of Equation (10-1 and 10-2).

Leij et al. (2016) present analytic solutions for colloid transport with time- and depth-dependent retention in porous media. Analytical solutions are only possible to obtain when the interaction mechanisms can be described by simple first-order attachment/detachment relations.

Another extension of the simple transport Equation (10-1) is to include dispersion as a transport mechanism and to allow the attached particles to be mobile (Yuan and Shapiro 2011). However, this is a questionable addition because dispersion, except on the micro-scale, where the dispersion is caused by molecular diffusion or for the SP caused by Brownian diffusion, is not a transport mechanism but is caused by velocity variations and should be treated as such.

Sacramento et al. (2015) consider deep bed filtration of a mixture of two particle sizes, one larger than the pore-size in the bed, the other smaller. The larger particles can build up a bed at the entrance of the original bed with smaller pores than the original. It is similar to the idea applied in industry to use a "pre-coat". A coarse-pored membrane is first subjected to a slurry of particles that just do not penetrate the membrane pores. These form a coating with much smaller pores than those of the membrane. The pre-coat in turn strains the small particles. This is in line with the conditions expected for the bentonite clay with detritus material.

Iritani (2013) give a Review on modelling of pore-blocking behaviours of membranes during pressurized membrane filtration. Illustrative figures are used to show how blocking occurs under different conditions. Iritani and Katagiri (2016) discuss various blocking mechanisms including complete blocking, standard blocking, intermediate blocking, and cake filtration. They give an overview of the developments of blocking filtration laws and equations under constant pressure and constant rate conditions reported for the filtrate flow of Newtonian and non-Newtonian fluids. In both papers, a variety of simple models that all rely on empirical parameters to be determined by experiments are presented.

We conclude that the models for deep bed filtration cannot be directly used to model straining of detritus particles pushed by swelling montmorillonite in variable aperture fractures because the transport mechanism is different in important respects. The filtration coefficient cannot be determined from first principles and extensive experiments to determine how the filtration coefficient varies with the amount of accumulated SP and with other conditions are needed.

10.1.2 Filtration coefficient magnitude

If we only consider straining by size exclusion, neglecting settling by gravity and attraction of SP to pore walls by any of the possible mechanisms, one would expect the filtration coefficient to be mainly influenced by the size of the particles that make up the porous bed. This defines the pore size. The size of the SP is also expected to influence the rate of capture. Herzig et al. (1970) present some data on the magnitude of filtration coefficients in porous bed with different bed particle sizes for the capture of different suspensions.

10.1.3 Tentative conclusion regarding the use of filtration coefficient models

We conclude that the models for deep bed filtration cannot be directly used to model straining of detritus particles pushed by swelling montmorillonite in variable aperture fractures because the transport mechanism is different in important respects. The filtration coefficient cannot be determined from first principles and extensive experiments to determine how the filtration coefficient varies with the amount of accumulated SP and with other conditions are needed.

10.2 Population balance models

The filtration coefficient model, when applied to systems where the main fracture mechanism is physical straining of SP in narrow passages, e.g. pore throats, does not give consistent results between the breakthrough curve of SP at the effluent and the concentration profile of retained particles in the bed. This has been interpreted as being caused by the fact that small particles are strained differently from larger particles and that they are captured in pores of different size, which makes it impossible to lump these effects into one global coefficient. This has stimulated the development of models that account for the presence of different pore sizes and different SP sizes. The distinct advantage over the filtration coefficient model is that instead of assuming that the particle suspension is more or less homogeneous it acknowledges that SP has a size distribution and that small particles are attached by at least partly different mechanism than large particles. This approach also acknowledges that particles of a given size that have been strained will influence the passage or attachment of other sizes of particles in the variable aperture pores. One such model was proposed about a decade ago for the case where the main mechanism is size exclusion in which particles just larger than a pore are captured clogging that pore. Population balances of numbers of pores of different sizes and of SP of another size distribution are used to follow how the pores are clogged at

the inlet of the pores by particles of that size. One can think of the system as consisting of a number of "sieves" or bundle-of-tubes interspersed by a "mixing chamber". The particles in the effluent from one sieve can choose any of the openings in the next sieve etc.

The idea is well presented by Bedrikovetsky (2008). He reviews the applications and use of the conventional filtration models and modelling based on the concept of the filtration coefficient and filtration function. He points out several fundamental weaknesses of these approaches and proposes an alternative approach based on population balances and upscaling of a stochastic micro-model for suspension transport and capture by different mechanisms. His work is built on previous work by Sharma and Yortsos (1987a, b, c) and Shapiro et al. (2007). These authors, however, also included other retention mechanisms than straining in a generalized way. Part of the capture can be in dead-end pores from which the particles can re-emerge into the flowing part of the pores. This could emulate attachment/detachment by e.g. DLVO forces. We will, however, only consider capture by straining in the following because we deem this to be an overarching mechanism and should be conservative in the sense that other mechanisms can add to capture, not detract from it.

In the pure straining model, the suspension with different particle sizes approaches the porous medium, which also has a distribution of pore sizes not entirely different from that of the particles. In the Bedrikovetsky conceptualization, the medium consists of a bundle of parallel tubes with different radii. They end in a mixing chamber from which the next tube bundle starts. The smallest particles in the fluid that carries them can pass essentially all pores. Larger particles pass only pores with pores larger than the specific particle size. When the particle size distribution H_{SP} and the pore-size distribution H_p are known one can define the fraction of the total flowrate $f_n(H_p, r_{SP})$ that carries particles of the same size as the pore and thus will be captured. Smaller particles have access to a larger fraction of the flowrate than can pass the tube-bundle

The particle size distribution in the water leaving the sieve is now different. This fluid with the remaining suspended particles (SP) continues into the next tube-bundle, and so on (Bedrikovetsky 2008).

When a tiny water volume has passed, the pores size distribution H_p in the first tube-bundle has changed slightly because some pores were clogged by the retained particles. So has the fraction of flowrate $f_n(H_p, r_{SP})$ that contains particles not allowed to pass the first tube-bundle. The effluent from the first tube-bundle will have constantly changing SP distribution. The water will contain a decreasingly fraction of large particles. This will also be the case in subsequent tube-bundles. The model must therefore keep track on the SP size distribution as it changes over time and along the flowpath. Also, the still un-clogged pores-size distribution must be followed in the same manner. This can be formulated as a set of coupled partial differential equations, PDE's, keeping track of the mass balance of the concentration of each SP and pore size.

The population balance models can be combined into an integro-differential equation formally written as a partial differential equation, PDE, of the distribution of pore sizes. It can alternatively be conceived as the simultaneous solution of a large number (infinite) number of coupled PDE's for different sizes of the SP's. The unknowns in the differential equations are suspended particle and vacant pore concentration size distributions respectively. In the simplest form when only physical straining by size exclusion is modelled only these two size distributions are needed. Both can probably be determined from independent experiments. Yuan et al. (2013) call the model the PTMC model (parallel tube with mixing chambers).

The model needs information on the pore-size distribution also in order to calculate the flowrate, assumed to be governed by Poiseuille flow in each pore/tube. Furthermore, as presented by Yuan et al. (2013), the length of the tube bundles is needed. In the basic model, it was thought to be on the order of the length of the pores between the bed particles. However, it was found that this entity is different for different particle sizes and cannot be determined by independent means at present. We think that this information possibly can be obtained from the aperture distribution of variable aperture fractures and the correlation length structures. This will have to be explored.

As noted above, for instationary modelling where the retention properties constantly change over time is rather complex and demanding on computer resources. For very early times the model can be considerably simplified. Then very little accumulation of SP and clogging has to be accounted for,

while still retaining the change in SP size distribution, as larger SP's always will be more retained than smaller. Under these circumstances, an analytical solution exists for how a given SP size fraction varies with the depth of the bed. Not surprisingly, the concentration follows an exponential function

$$c_{SP}(r_{SP}, x) = c_{SP}(r_{SP}, 0)e^{-z/lf_n(r_{SP})} \tag{10-5}$$

l is the length of the tube bundle and $f_n(r_{SP})$ is the fraction of flow through the tubes that does not permit particles larger than r_{SP} to enter. For the steady-state case where accumulation of SP is negligible and for circular tubes with a pore-size distribution $H(r_P)$ in which the flowrate of the suspension is driven by a hydraulic gradient and in which the flow velocity in each pore follows the Poiseuille law

$$f_n(r_{SP}) = \frac{\int_0^{r_{SP}} r_p^4 H(r_p)dr_p}{\int_0^{\infty} r_p^4 H(r_p)dr_p} \tag{10-6a}$$

For later use it may be noted that when the suspension is driven by the expanding Mt this expands with the same velocity in all pore sizes and then non-accessible flowrate fraction instead is

$$f_n(r_{SP}) = \frac{\int_0^{r_{SP}} r_p^2 H(r_p)dr_p}{\int_0^{\infty} r_p^2 H(r_p)dr_p} \tag{10-6b}$$

It may further be noted that Equation (10-5) for a given SP size fraction is the same as Equation (10-4). The instationary PTMC model based on population balances is considerably more complex than the filtration coefficient model. Neither of the models in their basic form are directly applicable to the straining of SP pushed by expanding montmorillonite but the PTMC is better based on fundamental physical processes and therefore potentially better suited for further development and adaption to the expanding bentonite case.

One major problem with the PTMC model is that although it is based on the physically reasonable notion that SP of a given size can only pass through pores that are larger than the SP the model introduces a correlation length l, which is an unknown entity that possibly will depend on the SP size. It will have to be determined by experiments. Although the equations can be elegantly formulated, Bedrikovetsky (2008), there is at present little information on how the correlation length can be assessed from experiments. You et al. (2014) propose an experimental approach but acknowledge that it only will be useful for the very early phase of accumulation of strained particles.

As discussed later, we will at present avoid this difficulty and also the need to consider the processes in the mixing chamber by limiting the problem to how the entrance to the first layer of pores, i.e. entrance to a variable aperture fracture is gradually being clogged. At present we think that this is sufficient to find if the PTMC concept is worth to pursue further.

10.2.1 Example to illustrative the idea of the PTMC

To illustrate how particles of different sizes would behave under dilute and early time conditions, let us consider a two-dimensional fracture with a log-normal aperture distribution, which we model as a bundle of tubes. A log-normal distribution of tube sizes is used to model the inlet of the channels in the fracture.

$$H(r_p) = \frac{1}{r_p\,\sigma\sqrt{2\pi}} e^{-\frac{((\ln r_p - \mu)^2)}{2\sigma^2}} \tag{10-7}$$

μ is the mean of $\ln r_p$ (in mm) and σ the standard deviation. Figure 10-1 shows the $H(r_p)$ for $\sigma = 1$ and $\mu = -2.8$. The arithmetic mean for these values is 0.1 mm

Figure 10-2 shows the fraction of the flowrate carrying SP larger than a given size that will lose the particles by clogging. This illustrates the concept of non-accessible pores. Only the largest particles will be strained in this example. Colloidal particles will practically not be strained in the early phases of the filtering. After having been subjected to inflow of particles some pores will have been clogged and the pore-size distribution $H(r_p)$ will be different, as will the fraction of flowrate $f_n(r_{SP})$ that cannot carry particles of size r_{SP} through the tube-bundle. The SP size distribution will strongly influence how $f_n(r_{SP})$ changes when more and more suspension is forced through the tube-bundle.

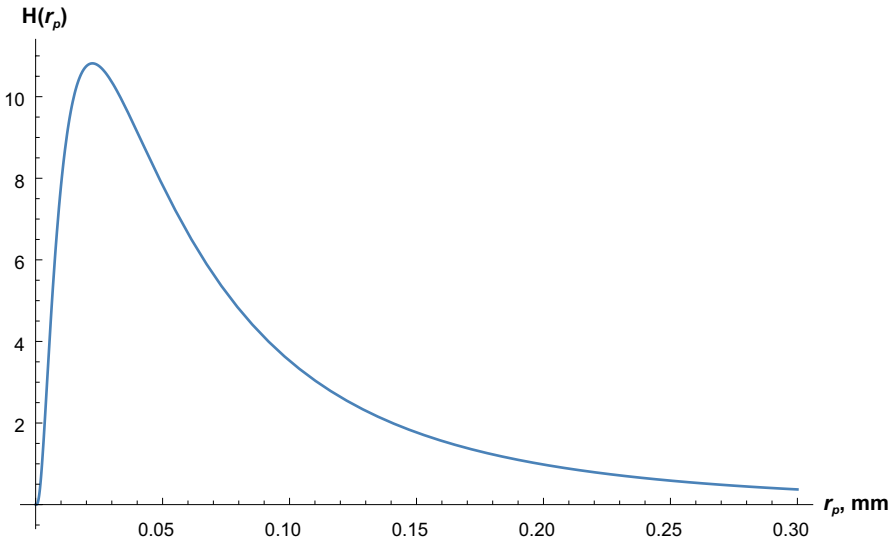

Figure 10-1. *Log-normal distribution of radii for $\sigma = 1$ and $\mu = -2.8$.*

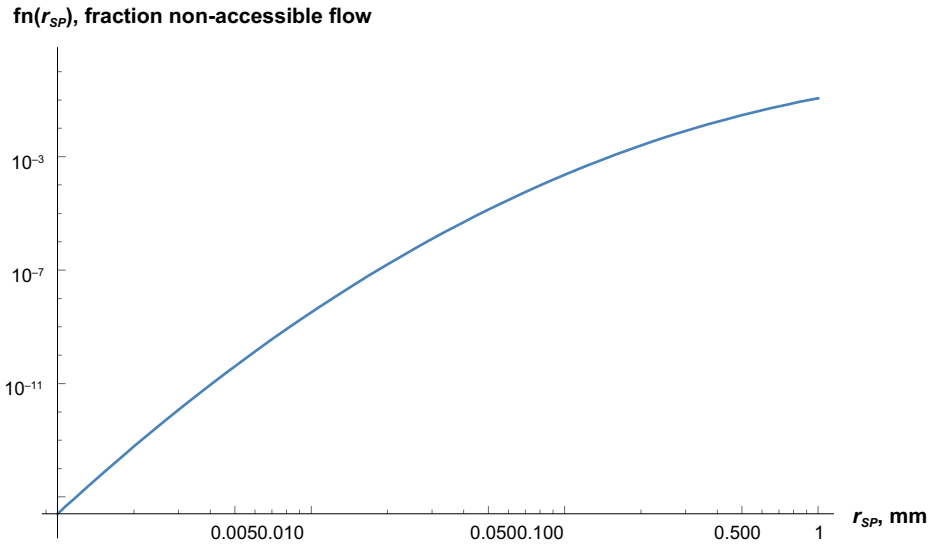

Figure 10-2. *Fraction of the flowrate carrying SP larger than a given size that will lose the particles by clogging.*

The PTMC model concept is attractive in the sense that it captures the physic that are considered to be responsible for straining of individual particles in pores of given size and that both pore and particle size distribution can be determined based on reasonably direct measurements. There are of course a number of assumptions and simplifications, the validity of which must be further studied.

10.3 Discrete pore network modelling

Another modelling approach based on simulation of individual particle transport and capture in individual pores in a network of pores has also been used and discussed in the literature. It is only briefly outlined here because although it is based on simple physical processes the description of the network has to be realistic and credible. This seems not to a straightforward task to accomplish for a porous medium made up of conduits of different sizes and different other properties.

A short description of the main ideas behind the channel or pore network modelling is summarily described below. Pore network models describe the pore system as a 2- or 3-dimensional network of

pores with different pore sizes. Flow in such a network is determined by solving for the flowrate in each channel in the network with flow resistance in each channel given by its aperture. This is similar to solving for the electrical current in a network of electrical resistances and is done by standard numerical techniques using matrix algebra. With flowrate known a particle can be injected one by one at a random location and propagated by the flow in that location (pore). At an intersection with other pores, typically the particle chooses to go to the next pore at the intersection with a chance proportional to the flowrate in the two or more effluent pores. A particle larger than the selected pore can block this. It is directed to one of the other pores if they are large enough to accept. The consequences of if none of the exit pores will accept the particle are not apparent.

If a pore is blocked it will change the local flow resistance. This implies in principle that the entire flowrate distribution in the network will have to be recalculated. This is prohibitive as to computer resources in large networks and such re-calculations will be made only after some number of particles has been strained.

In the study by Yuan et al. (2013) comparison were made with a 2-dimensional pore network model into which individual particle of different sizes were injected sequentially. The simulations were used to show that the global correlation length in the PTMC model depends on particle size. Similar modelling was also used recently by Ding et al. (2015a, b, 2017, 2018). Network models, NM, need considerable computer resources and at present, we see no obvious advantages compared to the filtration coefficient and the PTMC approaches as many of the disadvantages with the latter also apply to the NM model. Also, the need to generate realistic networks based on measured data is not trivial at present. Nevertheless, such modelling may support and give some insights that may not be possible for the two other model concepts described earlier. However, it may be interesting to test NM on variable aperture fractures in which the pore size distribution actually can be measured on transparent, cast replicas of real fractures.

10.4 SP flux driven by expanding Mt

In the model concepts described above a central mechanism and parameter is the imposed flux, U, of the entering suspension. In the problem we are interested in there is no imposed flow. Instead, it is the expansion of the bentonite driven by the repulsion between the Mt sheets that drives the SP with it until the Mt suspension becomes so dilute that the SP is released and sediments to the lower side of the fracture, or down along it if the fracture is sufficiently sloping. Before the Mt suspension has been so diluted the SPs are driven along by the expanding Mt paste.

In this section, a simplified approach is used to assess the expansion velocity of the Mt and from this to estimate the flux of SP carried by the Mt.

The expansion of the bentonite with the SP can be described by a diffusion equation. The bentonite expansion model is described in Neretnieks et al. (2009). ε is the porosity of the fracture as it fills with detritus (the strained particles). c_{Mt} is the concentration of Mt in the expanding bentonite. See Section 10.1.2 for more information.

$$\frac{\partial \varepsilon c_{Mt}}{\partial t} + \frac{\partial s_{Mt}}{\partial t} = \frac{\partial}{\partial x}\left(D_{Mt}\varepsilon \frac{\partial c_{Mt}}{\partial x}\right) \tag{10-8}$$

and

$$\frac{\partial s_{Mt}}{\partial t} = k_{Mt} U c_{Mt} \tag{10-9}$$

The Mt may also be slowed down when the strained SP decreases the bed porosity ε, which decreases as more and more SP settles in the flowpath. Equations (10-8 and 10-9) must be solved together with Equations (10-1, 10-2 and 10-3). It is acknowledged that k_{Mt} can depend on s but this dependence must be determined by experiments or possibly by other modelling in which the pore size distribution of s is described. Possibly the PTMC approach described in Section 10.2 could be used. The flux U is given by the solution of (10-8), which gives the Mt flux which carries the SP.

For the examples presented below, it is assumed that k_{Mt} is small, which implies that Mt unhindered can pass the non-clogged pores of the strained SP filling up the system. The Mt and thus the SP flux will decrease with decreasing porosity, however.

For a bed of constant porosity the swelling Mt, which carries the SP, with an inlet concentration c_{Mto} is given from the solution of (10-8) which for constant D_{Mt} and ε is given by

$$\frac{c_{Mt}}{c_{Mto}} = erfc\left(\frac{x}{2\sqrt{D_{Mt}t}}\right) \tag{10-10}$$

However, when the porosity changes with time and the flux U as used in (10-1) is not constant, this equation is not valid. The mass balance for SP must account for the changing porosity.

The Mt flux at a location x is

$$U_{Mt} = J_{Mt} = -D_{Mt}\varepsilon\frac{\partial c_{Mt}}{\partial x} \tag{10-11}$$

The flux of SP carried by the expanding Mt is

$$J_{SP} = J_{Mt}\frac{c_{sp}}{c_{Mto}} \tag{10-12}$$

The mass balance for SP accounting for the changing flux then is

$$\frac{\partial \varepsilon c_{SP}}{\partial t} + \frac{\partial s}{\partial t} = -\frac{\partial J_{SP}}{\partial x} \tag{10-13}$$

Also (10-2, 10-3) are re-written to

$$\frac{\partial s}{\partial t} = -\frac{\partial \varepsilon}{\partial t} = J_{SP}\, k \tag{10-14}$$

From the above equations, it is seen that there are three dependent variables, the Mt and the SP concentrations and the porosity, which all change over time and in space. The equations are summarized in Appendix A. Solutions of these coupled differential equations can be obtained by numerical methods.

To solve the coupled differential equations for the three independent variables c_{Mt},c_{SP} *and* ε in the three Equation (10-8, 10-13, 10-14) initial and boundary conditions are needed. The initial conditions are

$$\begin{aligned} &\varepsilon(0,x) = 1 \\ &c_{SP}(0,x) = 0 \\ &c_{Mt}(0,x) = 0 \end{aligned} \tag{10-15 a, b, c}$$

and the boundary conditions are

$$\begin{aligned} &c_{SP}(t,0) = c_{SPo} \\ &c_{Mt}(t,0) = c_{Mto} \\ &\varepsilon(t,x_o) = 1 \\ &c_{Mt}(t,x_o) = 0 \end{aligned} \tag{10-16 a, b, c, d}$$

c_{SPo} is the volume fraction, β, of SP in the bentonite $c_{SPo} = \beta c_{Bto} = \beta\,\dfrac{c_{Mto}}{1-\beta}$

c_{Bto} is the volume fraction of bentonite at the inlet. The distance x_o is chosen to be large enough for no clogging to occur there.

10.4.1 Example with filtration coefficient model

In this example, a case is illustrated in which bentonite expands into a water-filled fracture. The diffusion coefficient for bentonite is 0.01 m^2/yr, a typical value for expansion in below CCC water. The solids volume fraction of Mt in the bentonite is 0.9.

The pure Mt expansion is used to illustrate the flux of the SP for a case with constant porosity in time and space. Figure 10-3 shows the penetration depth of Mt into the fracture as function of time for different Mt volume fractions at the locus that is followed.

The tip of the swelling paste, before the paste turns to sol has a volume fraction of smectite = 0.01. The tip would reach 11 m after 1 000 years. Only time up to 1 000 years is shown in the figure because most SP will be strained at shorter distances than 11 m even after very long times, as will be shown later in the example.

First, a case is illustrated in which the filtration coefficient k is 1 m^{-1}. This can also be expressed as a half-length $z_{1/2}$ at which the SP concentration has dropped by a factor of 2. This implies that if the SP flux were driven by a constant pumping rate, about every $z_{1/2}$ = 0.7 m the SP concentration would decrease by a factor of two according to (10-4) if the straining did not influence the porosity.

For the Mt driven expansion, the solution to the three-coupled equations gives the following results. Figure 10-4 shows how the porosity along the fracture and at the inlet of the fracture vary. After 11 000 years the porosity at the inlet has dropped to zero. Porosity, in this case, means that all settled PS has arranged itself so that the strained SP fills the void without any water between them. Smaller particles fill the voids between the larger and even smaller fill the smaller voids, etc. Then also Mt will not pass. Approximately the first few metres from the inlet are affected. The porosity becomes zero at the inlet after 11 000 years.

Figure 10-5 show the same plots for k = 10 m^{-1}

Figure 10-6 shows the Mt flux over time and compares it with the Mt flux if there were no SP straining for k = 10 m^{-1}. The Mt flux stops after 140 years as the porosity has dropped to zero at the inlet.

Increasing the filtration coefficient to 100 m^{-1} ($z_{1/2}$ = 7 mm) decreases the time to stop further penetration of Mt to less than 10 years. The porosity drops to zero after about 1 cm.

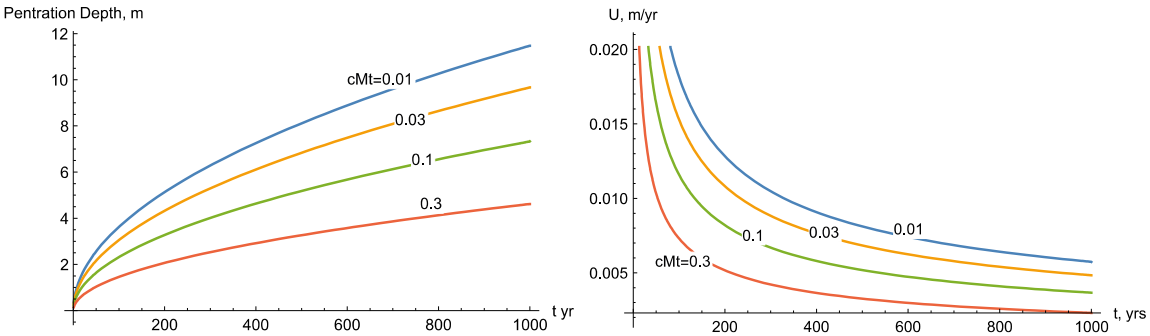

Figure 10-3. *Penetration depth (left) and velocity (right) of Mt into the fracture as function of time for different Mt volume fractions at the locus that is followed. (Straining PDE's.nb)*

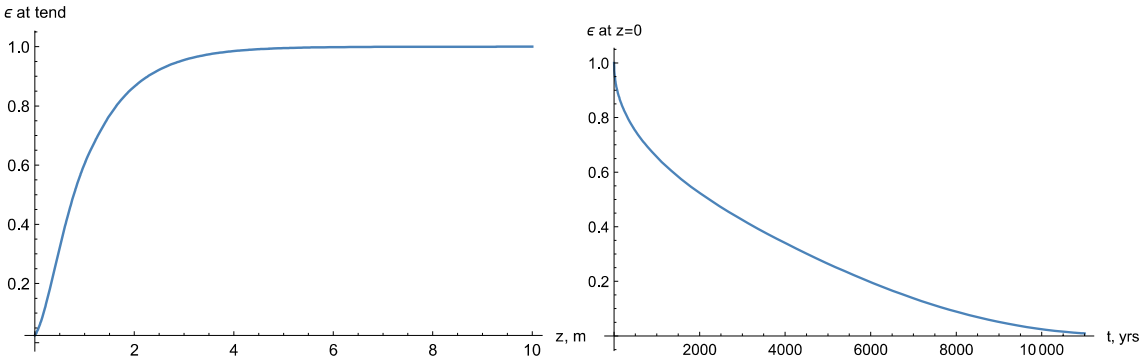

Figure 10-4. *Porosity evolution in fracture for k = 1 m^{-1}. (Straining PDE's.nb)*

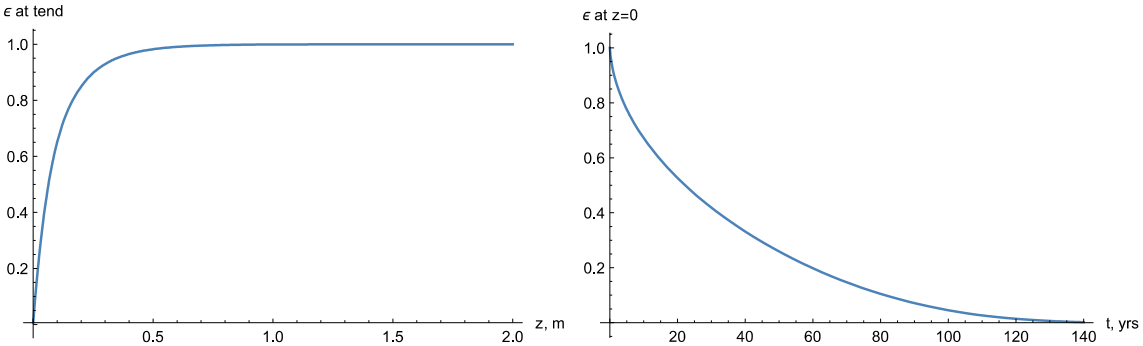

Figure 10-5. *Porosity evolution in fracture for k = 10 m^{-1}. $z_{1/2}$ = 7 cm. (Straining PDE's.nb)*

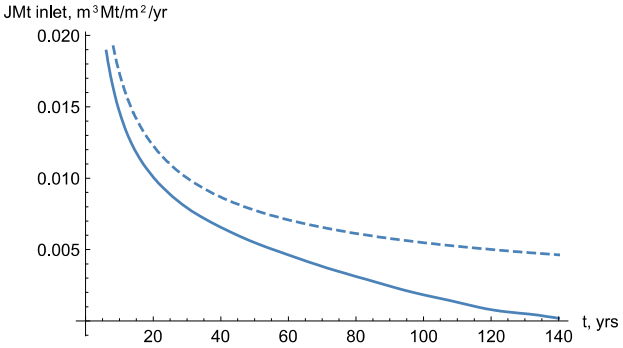

Figure 10-6. *Mt flux over time with and without, dashed line, SP straining. k = 10 m^{-1}. (Straining PDE's.nb)*

We have as yet found no way to assess how the filtration coefficient can be derived for a variable aperture fracture. It seems reasonable to assume the correlation length of the aperture distribution, simply put, some kind of measure of the distance between the locations between larger apertures could be used for 1/k. The choice of *k* in the interval 1 to 100 m^{-1} at present seems to be a reasonable range, considering that observed *channel* widths in fractures range from a few mm to several tens of cm (Tsang and Neretnieks 1998).

A test was also made to see if the much simpler approach using the approximate analytical solution to the PDE describing the expansion of the bentonite, Equation (10-10) could be used to describe the SP flux. One can possibly neglect the impact of the slow change of porosity on the form of the Mt concentration profile because $c_{Mt}\frac{\partial \varepsilon}{\partial t} \ll \varepsilon \frac{\partial c_{Mt}}{\partial t}$ when $\frac{\partial s}{\partial t}$ is small because s is a small fraction of c_{MT}. With this approximation, the time to clog the fracture decreased by less than a factor of 2.

10.4.2 Example to illustrate Population balance model.

For this, we need information on pore size and SP distributions. Fractures in crystalline rocks have variable apertures. Sahimi (2011) describes some ways to model the aperture variations and the correlation structures in them and refers to many papers in the open literature that describe measurements techniques and results. Hakami and Larsson (1996) measured the aperture structure of a large sample (190 × 410 mm) from the Äspö Hard Rock Laboratory obtained by over-coring the fracture. The hydraulic aperture, measured prior to injecting resin was 250 µm. Apertures were measured after sawing the rock cylinder with its fracture along the middle of the cylinder in segments. A total of 30,000 aperture data were recorded. Eight subareas of the fracture showed mean aperture between 307 and 384 µm. The standard deviation in the subareas varied between 133 and 231 µm. The mean aperture and standard deviation for all points were 360 and 150 µm respectively. The ratio of standard deviation and mean aperture varied between 0.36 and 0.64 in the subareas and is 0.42 for the entire ensemble. The ratio between mean aperture and hydraulic aperture is 1.4, which is similar to what is reported in other studies according to the authors. The aperture histograms for the eight subareas show a slight asymmetry suggesting that a log-normal distribution might be better used to describe the distribution.

In the Forsmark site at repository depth, the hydraulic apertures varied between about 2×10^{-6} and 0.8×10^{-4} m (SKB 2010). In the performance assessment calculations for the long-term safety for the final repository for spent nuclear fuel at Forsmark (SKB 2011), a slightly wider range was used.

We use the Hakami and Larsson (1996) data but adapted them to a log-normal distribution to catch the longer tailing. Also, a cut-off at 1.2 mm is used, which agrees well with the largest apertures recorded in the histograms. We refer the reader to Appendix B and Equation (B-8) for Mt driven flow. In this example, the pore size distribution is derived from a log-normal distribution with μ_p = ln(r = 100 µm) and a standard deviation s = 0.42. A discretised distribution is generated with 100 bins in a geometric progression starting with the smallest pore 0.5 µm. This will allow the colloid size Mt particles to pass.

The SP volume fraction size distribution has μ_{SP} = ln(r = 10 µm) and s = 1. This is based on the measured data shown in Figure 2-3. This volume fraction distribution is then converted to a number fraction distribution. The pore size distribution is shown in Figure 10-7, left frame, and the particle size distribution in Figure 10-7, right frame.

To simplify the simulations a dimensionless time is used and the time steps chosen such that there is only a slight change in the number of clogged pores in each step in order not to induce large errors in the simple Euler integration. Later we will convert this to real-time units.

Figure 10-7 shows the pore and SP size distribution.

Figure 10-8, shows how the pore size distribution at the entrance to the medium changes over time. This is for initial Mt expansion rate of 0.01 m/yr. See Figure 10-3 for information of Mt expansion rate. The porosity evolution over time is shown in Figure 10-9.

In this example, the porosity would eventually become so small that practically no particles can be carried into the fracture by the expanding Mt.

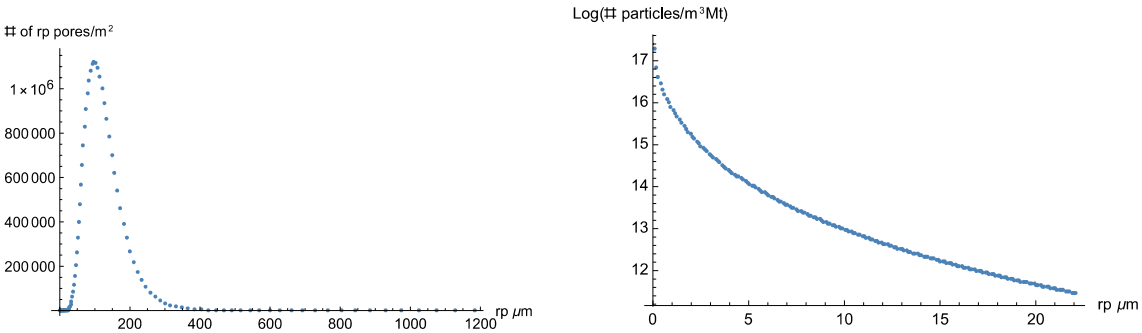

Figure 10-7. *Number of pores/m² bed (left) and number of particles/m³Mt (right). (PTMC first entrance.nb).*

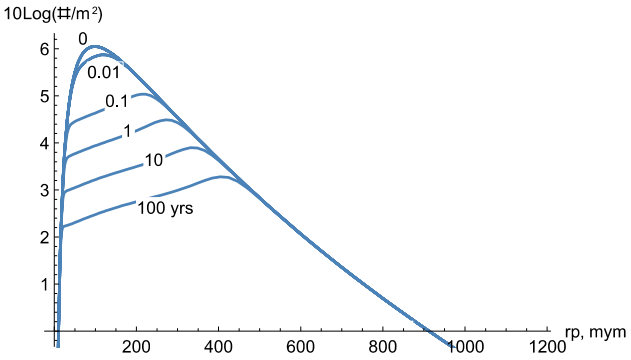

Figure 10-8. *Pore size distribution evolution of open pores*

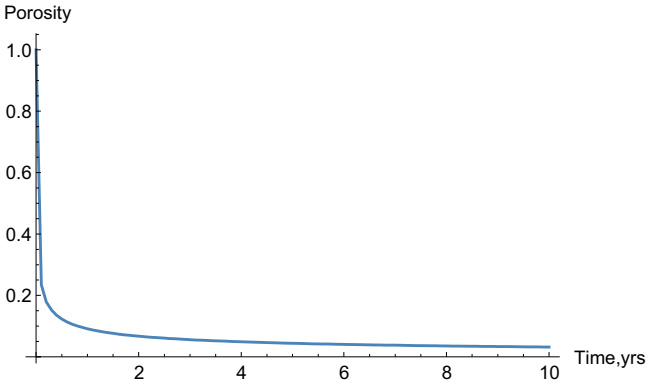

Figure 10-9. *Evolution of porosity over time.*

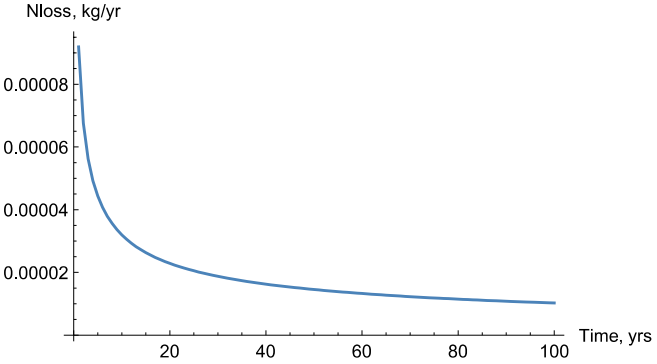

Figure10-10. *Smectite loss rate from a deposition hole with 1 m radius intersected by a 0.1 mm aperture fracture.*

Figure10-10 shows the smectite loss rate from a deposition hole with 1 m radius intersected by a 0.1 mm aperture fracture. Initial loss rate is 0.0010 kg/yr driven by the expansion of swelling bentonite.

After 100 years 0.29 kg bentonite has been lost. Of this, 0.029 kg detritus has gone into the fracture. Most of it has together with the montmorillonite moved further in the fracture but a small amount clogs the pores at the entrance of the fracture.

10.4.3 Further comments on the PTMC model

It is in principle possible to follow the mass of montmorillonite and detritus that moved into the fracture and assess its fate further along the fracture by the PTMC model. It suffices for the aims of the present study to determine what happens at the inlet of the fracture because that fully determines the rate of bentonite loss. However, it can be of considerable interest to determine how far into the fractures these are filled with immobile gel and/or detritus material because distances larger than a few tens of cm will considerably decrease the mass transfer between the waste protected by bentonite and the seeping water outside. The PTMC model is formulated in a way that it would allow the clogging in depth to be assessed. Additional work is needed to implement this in a numeric code. Reliable data on the correlation lengths in real variable aperture fractures must also be obtained.

It should be noted that the PTMC model only considers how the original pores of the medium are clogged. Any potential build-up of new narrow passages between the retained particles, that will form a pre-coat like layer is not accounted for. The PTMC model is therefore conservative not only due to this but also because only size exclusion is accounted for and not effects like attachment on pore walls or settling by gravity forces.

11 Discrete element modelling of particle transport

In this chapter, we describe a method that in principle can account for a large number of interaction mechanisms. It can follow each individual particle through a network of channels such as exist in variable aperture fractures.

The discrete element method(s), DEM, has become a popular and useful tool in many areas where many solid structures move and interact simultaneously with each other and with solid walls. An overview of DEM can be found at https://en.wikipedia.org/wiki/Discrete_element_method

In short, the method(s) can treat the simultaneous movement of a multitude of particles that can interact in many different ways with each other and with other objects such as walls of vessels. The particles can have different sizes and shapes and can be rigid, elastic or elasto-plastic and even brittle. They can break into smaller particles or build larger particles. The method is closely related to molecular dynamics modelling, MD, and can be extended to include other processes such as complex fluid flow. It can be coupled to computational fluid dynamics, CFD, and finite element, FEM, methods. One of the advantages is that the code(s) for many applications can be mesh free. This avoids the problems that space discretisation often causes when large differences in scale and material properties must be considered.

Discrete element methods are computationally intensive, which limits either the length of a simulation or the number of particles, or both, when running on computers with few cores. Very large problems can and must be solved on parallel processor computers. Some examples can be found at http://jenike.com/discrete-element-modeling/

11.1 Possible clogging simulations of a variable aperture fracture

We have found no papers that use DEM to simulate clogging by particles of a variable aperture fracture. But some ideas that should be directly transferable to the present problem can be found in a DEM overview paper by a recent Guo and Curtis (2015) Below we outline some possible approaches, starting with some simple cases.

We wish to model how the clay expanding into and in variable aperture fractures brings with it the detritus particles and how these are captured inside the fractures. A simple and probably very conservative case is when size exclusion is the only capture mechanism. For the modelling, a variable aperture could be generated based on observations of aperture statistics. Variable apertures have been found to be well described by a log-normal distribution. From measurements, it is possible to determine correlation lengths on scales up to a fraction of the size of the object measured. This information is used to generate model fractures with the desired properties in the computer. Particle size distributions can be selected from measured data. An example is shown in Figure 2-3.

As a test, a simulation could be made without considering that the particles have to follow the direction of the Mt in the expanding clay. A particle larger than the local aperture is captured at that location. Smaller particles are captured in narrower locations. Subsequent smaller particles that hit a captured particle “roll” left or right to find a sufficiently wide aperture to move into. The captured particles themselves thus build up increasingly narrower pores.

It is expected that for typical particle size distributions either the collected particle bed at the inlet of the fracture has developed which allows only the smallest particles to pass into the fracture, or that the fracture itself will eventually have been filled with a “bed” of particles. Which of the two cases will happen is expected to depend on the mean size of particles in relation to the mean aperture size as well as on the size distribution of apertures and of particles.

It may not be important to follow the process in detail over time because we are interested in how clogging evolves with captured mass of particles. This tells us how the loss of clay changes with the amount of clay lost. When in time this occurs may be of secondary importance, unless there is only little clogging.

When a bed forms the pore size distribution of the captured particles can be followed. If the mean pore size is smaller than 0.5 μm it can be expected that the colloidal size montmorillonite particles will pass only in negligible quantities. If the pore size is larger than 2 μm the smectite will pass but the flux will be governed by the porosity, which decreases as more and more particles are captured.

In the simulations outlined above the actual rate of bed formation has not been considered. This will depend on the rate at which the Mt particles pass through the bed and that will decrease over time because the intrusion rate decreases due to the decreasing porosity. The intrusion rate also decreases over time because the further the Mt expansion has progressed the lower will be intrusion rate.

Such simulations are expected to show how the loss-rate of Mt decreases over time. They will also show how far from the source the fracture is filled with the porous detritus bed.

This implies that the radionuclide escape from the waste to the seeping water will be increasingly controlled by the diffusion through the growing detritus bed in the fracture, and not by the flowrate of water in the fracture. Already a few cm bed depth would decrease the equivalent flow rate Q_{eq} that can carry escaping nuclides considerably. Although this may not be important for KBS-3 repository it could have a considerable impact on long vault repositories in which larger fractures and fracture zones are difficult to avoid. This may be important for the SFL repository.

12 Some possible future modelling approaches and experimental demonstrations of clogging of rock fractures around a repository

12.1 Sol flocculation, gel formation and clogging of fractures

The bentonite intrusion into fractures over time and in space is governed by several processes, two of which, had not been considered previously.

One is based on the observation that smectite sol, even under below CCC conditions is not stable and that it separates into an immobile gel and essentially colloid free water. This has the following implications.

Sol that forms at the bentonite/water interface is transported away by the seeping water. After some time and somewhere downstream the individual smectite particles form small agglomerates that later attach to other flocs and form larger agglomerates filling the aperture. The friction against the walls slows down their migration. The flowrate of the slurry decreases. The aging agglomerates phase separate into a gel and essentially smectite free water. New small agglomerates carried by the water are captured, eventually filling a large part of the conductive parts of the fracture somewhere downstream. This essentially stops further flow in the gel-clogged region. Much less or essentially negligible amounts of colloids are carried downstream because the phase-separated gel does not release smectite particles. If the expanding clay from the source catches up with the gel this will either be pushed along or it will break the gel, which will reform to a swelling paste that can release colloids. The distance between the location of the gel formed by phase separation and the clay/ water interface will depend on how far the flocs migrated from the clay/ water interface before phase separation generated the gel.

In the experiments described earlier, it was found that flocculation was noticeable and phase separation happened from days to weeks to perhaps months. For illustration consider the following. With a water velocity of 1 m/yr and a gelation time of 0.1 year, the clogging would commence 0.1 m downstream from the bentonite/water interface. For a velocity of 10 m/yr it would commence at 1 m downstream. Similarly, in stagnant waters the flocs sediment downward by buoyance forces and clog the fractures below the source.

Eventually, the entire region between the clay/water interface fills with gel Modelling these processes may be possible but must be supported by additional experiments to study the kinetics of floc formation and phase separation in detail. Also the compaction and breakdown of the formed gel subject to shear must be further studied.

12.2 Clogging by detritus

Clogging porous filters was shown experimentally in Section 9.6. This was also demonstrated in experiments by Richards and Neretnieks (2010) with detritus material assembling and forming filters. The simple modelling presented in Chapter 10 gives support to the phenomenon on theoretical grounds. The simple and rather crude filtration coefficient model has a merit in that it is simple. It can possibly be used if supported by clogging experiments in variable aperture fractures. The strength of the population balance model is that it in principle can use independent data on pore and particle size distributions to make predictions. However, it will also have to be supported by validation experiments. The DEM method is by far the most sophisticated as it can account for a large number of detailed mechanisms and directly use measured fracture aperture information. Some more aspects of the three models are given below.

12.2.1 Filtration coefficient concept

Conventional modelling of deep bed filter properties may be used to simulate the clogging of variable aperture fractures but this must be done in parallel with direct experiments in fractures with variable aperture, similar to real fractures in granite to determine the “filter coefficient ”, which at present cannot be derived from first principles. Such experiments could be performed in transparent replicas of fractures similar to those made by Reid et al. (2015). The modelling is essentially trivial, as it needs only one parameter, which must be determined by experiments. The model can be used to simulate the rate of change of bentonite loss as well as of the evolution of detritus intrusion over time and in space.

12.2.2 Population balance model(s)

This approach uses independently derived data of particle size distribution and of pore size distribution. The latter can be derived from measurements and of modelling fracture aperture distributions and correlations. This is a potentially important strength because it does not rely on the clogging experiments to obtain data for the modelling. Experiments can, and must, be used to validate the simulation results. Additional information on real variable fracture aperture distributions and particle size distributions would be of value. It is obvious that if most particles are smaller than most pores less clogging is expected than when the relation is the opposite. Simulations using different size distributions of both pores and particles can be used to assess how rapidly clogging sets in and how effective it is. It has considerable theoretical merits.

12.2.3 Discrete element modelling of particle transport

This technique does not seem to have been used to simulate fracture clogging. It is a powerful technique based on first principles, which makes it very attractive. Considerable development work will be needed. For good performance and detailed modelling of clogging of variable aperture fractures, large parallel computers must be used. However, simulation of the build-up and compaction of a detritus filter at the inlet to a section of a fracture with constant aperture and penetration of this by smectite particles should be easier. It could illustrate and illuminate the different processes involved.

13 Discussion and conclusions

A literature survey has shown that flocculation processes and floc capturing mechanisms in fractures are not sufficiently well understood to be able to do quantitative predictions based on available data and on conventional modelling tools. The observed formation of montmorillonite flocs in seeping water with an ionic concentration below the CCC and the results of the scoping experiments suggest that their transport could be slowed down and, even stopped, as flocs grow stronger with time. The agglomerate fluid, AF of flocs and sediment seem to behave like a Bingham solid/fluid or Herschel-Bulkley fluid, which need a minimum pressure gradient to be mobilised. On theoretical grounds and supported by earlier derived viscosity models for montmorillonite suspensions it is expected that, even when mobilised, the viscosity of the AF should be vastly larger than water without flocs and particles. Experiments of the rheology of aged AF under the low shear rates and the low ion concentrations expected under repository conditions have not been reported in the literature. Earlier observations and those in the simple scoping experiments suggest that the floc sediments will clog variable aperture fractures.

Furthermore, the accessory mineral particles in the expanding clay have been observed to clog fractures. Conventional filtration models based on the notion of a filtration coefficient are not capable to quantify this in a way useful for predictive simulations without additional direct experimental support. A rather recent modelling approach based on population balances of pore sizes and of particle sizes has a potential to do predictive modelling based on independent measurement of pore and particle size distributions. Different modelling approaches based on following individual particles and their capture in variable aperture fractures modelled as pore networks are evolving. A powerful technique called discrete element modelling, DEM, which is based on first principles has the potential to follow individual particles in variable aperture fractures.

The further adaptation and development of a model must be accompanied by experiments, both to derive independent data on the geometry of fractures and for validation experiments. Additional experiments with natural clays with detritus materials could be made in transparent synthetic variable aperture fractures and in replicas of real fractures.

In conclusion, we think that the likelihood that it can be credibly demonstrated that natural fractures at repository depth will be clogged by gel-like sediments of flocs is large. We also think that clogging can be convincingly demonstrated to result from the capture of the natural detritus material in clay by a combination of modelling and additional experiments.

References

SKB reports can be downloaded from http://www.skb.com/publikationer/

BELBaR reports, referred to as Dx.y… can be downloaded from
http://www.skb.se/belbar/public-deliverablesreports/

Alonso U, Missana T, Garcia M, Morejón J, Mingarro M, López T, 2018. POSKBAR Erosion Results, CIEMAT Technical Report M15 / 2017/ 10.

Angelini R, Zaccarelli E, de Melo Marques F A, Sztucki M, Fluerasu A, Ruocco G, Ruzicka B, 2014. Glass–glass transition during aging of a colloidal clay. Nature Communications 5, 4049. doi:10.1038/ncomms5049

Babakhani P, Bridge J, Doong R, Phenrat T, 2017. Continuum-based models and concepts for the transport of nanoparticles in saturated porous media: a state-of-the-science review. Advances in Colloid and Interface Science 246, 75–104.

Bedrikovetsky P, 2008. Upscaling of stochastic micro model for suspension transport in porous media. Transport in Porous Media 75, 335–369.

Bergaya F, Theng B K G, Lagaly G, 2006. Handbook of clay science. Amsterdam: Elsevier.

Bianco C, Tosco T, Sethi R, 2016. A 3-dimensional micro- and nanoparticle transport, filtration and clogging model (MNM3D) applied to the migration of carbon-based nanomaterials in porous media. Journal of Contaminant Hydrology 193, 10–20.

Bird R B, Stewart W E, Lightfoot E N, 2002. Transport phenomena. 2nd ed. New York: Wiley.

Birgersson M, Börgesson L, Hedström M, Karnland O, Nilsson U, 2009. Bentonite erosion. Final report. SKB TR-09-34, Svensk Kärnbränslehantering AB.

Börgesson L, Hökmark H, Karnland O, 1988. Rheological properties of sodium smectite clay. SKB TR 88-30, Svensk Kärnbränslehantering AB.

Ding B, Li C, Dong X, 2015a. Percolation-based model for straining-dominant deep bed filtration. Separation and Purification Technology 147, 82–89.

Ding B, Li C, Zhang M, Ji F, Dong X, 2015b. Effects of pore size distribution and coordination number on the prediction of filtration coefficients for straining from percolation theory. Chemical Engineering Science 127, 40–51.

Ding B, Li C, Wang Y, Xu J, 2017. Effects of pore size distribution and coordination number on filtration coefficients for straining-dominant deep bed filtration from percolation theory with 3D networks. Chemical Engineering Science 175, 1–11.

Ding B, Li C, Wang Y, Xu J, 2018. Effects of pore size distribution and coordination number on filtration coefficients for straining-dominant deep bed filtration from percolation theory with 3D networks. Chemical Engineering Science 175, 1–11.

Dvinskikh S V, Furó I, 2009. Magnetic resonance imaging and nuclear magnetic resonance investigations of bentonite systems. SKB TR-09-27, Svensk Kärnbränslehantering AB.

BELBaR, 2015. WP2 partners final report on bentonite erosion, B+TECH: Schatz T, Eriksson R; Clay Technology AB: Ekvy-Hansen E, Hedström M; CIEMAT: Missana T, Alonso U, Mayordomo N, Fernández A M; KIT-INE: Bouby M, Heck S, Geyer F, Schäfer T. BELBaR deliverable D2.12.

Evans D F, Wennerström H, 1999. The colloidal domain: where physics, chemistry, biology, and technology meet. 2nd ed. New York: Wiley-VCH.

Guo Y, Curtis J S, 2015. Discrete element method simulations for complex granular flows. Annual Review of Fluid Mechanics 47, 21–46.

Hakami E, Larsson E, 1996. Aperture measurements and flow experiments on a single natural fracture. International Journal of Rock Mechanics and Mining Sciences & Geomechanics Abstracts 33, 395–404.

Hedström M, Ekvy Hansen E, Nilsson U, 2016. Montmorillonite phase behaviour. Relevance for buffer erosion in dilute groundwater. SKB TR-15-07, Svensk Kärnbränslehantering AB.

Herzig J P, Leclerc D M, Le Goff P, 1970. Flow of suspensions through porous media – Application to deep filtration. Industrial and Engineering Chemistry 62, 8–35.

Huber F, Noseck U, Schäfer T (eds), 2016. Stability of compacted bentonite for radionuclide retardation – Experiments and modelling (Project Kollorado-e; Final Report). Karlsruhe Institut für Technologie (KIT). doi:10.5445/IR/1000059756

Iritani E, 2013. A review on modeling of pore-blocking behaviors of membranes during pressurized membrane filtration. Drying Technology 31, 146–162.

Iritani E, Katagiri N, 2016. Developments of blocking filtration model in membrane filtration. KONA Powder and Particle Journal 2016, 179–202.

Israelachvili J N, 2011. Intermolecular and surface forces. 3rd ed. Burlington: Academic Press.

Jansson M, 2009. Bentonite erosion. Laboratory studies. SKB TR-09-33, Svensk Kärnbränslehantering AB.

Jarvis P, Jefferson B, Gregory J, Parsons S A, 2005. A review of floc strength and breakage. Water Research 39, 3121–3137.

Kranenburg C, 1999. Effects of floc strength on viscosity and deposition of cohesive sediment suspensions. Continental Shelf Research 19, 1665–1680.

Kuzmina L I, Osipov Y V, 2016. Deep bed filtration asymptotics at the filter inlet. Procedia Engineering 153, 366–370.

Leij F J, Bradford S A, Sciortino A, 2016. Analytic solutions for colloid transport with time- and depth-dependent retention in porous media. Journal of Contaminant Hydrology 195, 40–51.

Liu L, 2011. A model for the viscosity of dilute smectite gels. Physics and Chemistry of the Earth, Parts A/B/C 36, 1792–1798.

Liu L, Moreno L, Neretnieks I, 2009. A novel approach to determine the critical coagulation concentration of a colloidal dispersion with plate-like particles. Langmuir 25, 688–697.

Missana T, Alonso U, Albarran N, García-Gutiérrez M, Cormenzana J-L, 2011. Analysis of colloids erosion from the bentonite barrier of a high level radioactive waste repository and implications in safety assessment. Physics and Chemistry of the Earth, Parts A/B/C 36, 1607–1615.

Neretnieks I, Moreno L, 2018. Revisiting bentonite erosion understanding and modelling based on the BELBaR project findings. SKB TR-17-12, Svensk Kärnbränslehantering AB.

Neretnieks I, Liu L, Moreno L, 2009. Mechanisms and models for bentonite erosion. SKB TR-09-35, Svensk Kärnbränslehantering AB.

Neretnieks I, Moreno L, Liu L, 2017. Clay erosion – impact of flocculation and gravitation. SKB TR-16-11, Svensk Kärnbränslehantering AB.

Olivier J, Vaxelaire J, Vorobiev E, 2007. Modelling of cake filtration: an overview. Separation Science and Technology 42, 1667–1700.

Pujala R K, 2014. Dispersion stability, microstructure and phase transition of anisotropic nanodiscs. Cham, Switzerland: Springer International Publishing.

Reid C, Lunn R, El Mountassir G, Tarantino A, 2015. A mechanism for bentonite buffer erosion in a fracture with a naturally varying aperture. Mineralogical Magazine 79, 1485–1494.

Richards T, Neretnieks I, 2010. Filtering of clay colloids in bentonite detritus material. Chemical Engineering & Technology 33, 1303–1310.

Rinderknecht F R, 2017. Bentonite erosion and colloid mediated transport of radionuclides in advection controlled systems. PhD thesis. Karlsruher Institut für Technologie, Germany.

Ruzicka B, Zulian L, Zaccarelli E, Angelini R, Sztucki M, Moussaïd A, Ruocco G, 2010. Competing interactions in arrested states of colloidal clays. Physical Review Letters 104. doi:10.1103/PhysRevLett.104.085701

Sacramento R N, Yang Y, You Z, Waldmann A, Martins A L, Vaz A S L, Zitha P L J, Bedrikovetsky P, 2015. Deep bed and cake filtration of two-size particle suspension in porous media. Journal of Petroleum Science and Engineering 126, 201–210.

Sahimi M, 2011. Flow and transport in porous media and fractured rock: from classical methods to modern approaches. 2nd ed. Hoboken, NJ: Wiley.

Sato D, Kobayashi M, Adachi Y, 2004. Effect of floc structure on the rate of shear coagulation. Journal of Colloid and Interface Science 272, 345–351.

Schatz T, Akhanoba N, 2017. Bentonite buffer erosion in sloped fracture environments. Posiva 2016-13, Posiva Oy, Finland.

Schatz T, Kanerva N, Martikainen J, Sane P, Olin M, Seppälä A, Koskinen K, 2013. Buffer erosion in dilute groundwater. Posiva 2012-44, Posiva Oy, Finland.

Secor R, Radke C, 1985. Spillover of the diffuse double layer on montmorillonite particles. Journal of Colloid and Interface Science 103, 237–244.

Shalkevich A, Stradner A, Bhat S.K. Muller F, Schurtenberger P, 2007. Cluster, glass, and gel formation and viscoelastic phase separation in aqueous clay suspensions. Langmuir, 23, 3570–3580.

Shapiro A A, Bedrikovetsky P G, Santos A, Medvedev O O, 2007. A stochastic model for filtration of particulate suspensions with incomplete pore plugging. Transport in Porous Media 67, 135–164.

Sharma M M, Yortsos Y C, 1987a. Fines migration in porous media. AIChE Journal 33, 1654–1662.

Sharma M M, Yortsos Y C, 1987b. Transport of particulate suspensions in porous media: model formulation. AIChE Journal 33, 1636–1643.

Sharma M M, Yortsos Y C, 1987c. A network model for deep bed filtration processes. AIChE Journal 33, 1644–1653.

SKB, 2010. Data report for the safety assessment SR-Site. SKB TR-10-52, Svensk Kärnbränslehantering AB.

SKB, 2011. Long-term safety for the final repository for spent nuclear fuel at Forsmark. Main report of the SR-Site project. SKB TR-11-01, Svensk Kärnbränslehantering AB.

Tien C, 2012. Principles of filtration. Amsterdam: Elsevier.

Tsang C-F, Neretnieks I, 1998. Flow channeling in heterogeneous fractured rocks. Reviews of Geophysics 26, 275–298.

van Olphen H, 1977. An introduction to clay colloid chemistry: for clay technologists, geologists and soil scientists. 2nd ed. New York: Wiley.

Yang Y, Siqueira F D, Vaz A S L, You Z, Bedrikovetsky P, 2016. Slow migration of detached fine particles over rock surface in porous media. Journal of Natural Gas Science and Engineering 34, 1159–1173.

You Z, Bedrikovetsky P, Kuzmina L, 2013. Exact solution for long-term size exclusion suspension-colloidal transport in porous media. Abstract and Applied Analysis 2013, 680693. doi:10.1155/2013/680693

You Z, Osipov Y, Bedrikovetsky P, Kuzmina L, 2014. Asymptotic model for deep bed filtration. Chemical Engineering Journal 258, 374–385.

Yuan H, Shapiro A A, 2011. A mathematical model for non-monotonic deposition profiles in deep bed filtration systems. Chemical Engineering Journal 166, 105–115.

Yuan H, You Z, Shapiro A, Bedrikovetsky P, 2013. Improved population balance model for straining-dominant deep bed filtration using network calculations. Chemical Engineering Journal 226, 227–237.

Zhang W, Tang X, Weisbrod N, Guan Z, 2012. A review of colloid transport in fractured rocks. Journal of Mountain Science 9, 770–787.

Appendix A

Summary of the equations used to simulate straining of SP by the filtration coefficient model

Mass balance for Mt. Expansion of Mt, which carries SP

$$\frac{\partial \varepsilon c_{Mt}}{\partial t} = \frac{\partial}{\partial x}(D_{Mt}\varepsilon \frac{\partial c_{Mt}}{\partial x}) \quad \text{(A-1)}$$

Mass balance for SP

$$\frac{\partial \varepsilon c_{SP}}{\partial t} + \frac{\partial s}{\partial t} = \quad -\frac{\partial J_{SP}}{\partial x} = \quad \frac{\partial \varepsilon c_{SP}}{\partial t} - \frac{\partial \varepsilon}{\partial t} \quad \text{(A-2)}$$

Porosity change due to strained SP

$$\frac{\partial s}{\partial t} = -\frac{\partial \varepsilon}{\partial t} = k\, J_{SP} \quad \text{(A-3)}$$

$$J_{SP} = -D_{Mt}\varepsilon \frac{\partial c_{Mt}}{\partial x}\frac{c_{sp}}{c_{Mto}} \quad \text{(A-4)}$$

Initial conditions

$$\varepsilon(0,x) = 1$$
$$c_{SP}(0,x) = 0 \quad \text{(A-5a, b, c,)}$$
$$c_{Mt}(0,x) = 0$$

Boundary conditions

$$c_{SP}(t,0) = \ c_{SPo}$$
$$c_{Mt}(t,0) = c_{Mto} \quad \text{(A-6a, b, c, d)}$$
$$\varepsilon(t,x_o) = 1$$
$$c_{Mt}(t,x_o) = 0$$

β is the volume fraction of SP in the bentonite, which gives $c_{SPo} = \beta c_{Bto} = \beta \frac{c_{Mto}}{1-\beta}$ where c_{Bto} is the volume fraction of bentonite at the inlet.

The equations are solved numerically by Wolfram "Mathematica" routine NDSolve, which gives the results as interpolation functions in (*t,x*) space.

Appendix B

Summary of the central equations for the population balance model

SP flux driven by constant pumping rate U

The following essentially follows the notation in Bedrikovetsky (2008) and Yuan et al. (2013). There are two populations to keep track of, $H_p(r_p, x, t)$ for the pores and $c_{SP}(r_{SP}, x, t)$ for the suspended particles. SP's. Both change with time and in space. r_p is the radius of pores and r_{SP} is the radius of SP's.

The pores size distribution in a given cross-section of bed or fracture is denoted by

$H_p(r_p,x,t)$ [m^{-3}]

The porosity of the cross section is

$$\phi(x,t) = \pi \int_0^\infty r_p^2 H_p(r_p,x,t) dr_p \tag{B-1}$$

The fraction of pores available to particles with radius r_{SP} is

$$\phi_a(r_{SP},x,t) = \pi \int_{r_{SP}}^\infty r_p^2 H_p(r_p,x,t) dr_p \tag{B-2}$$

The number concentration in the water of suspended particles is denoted by

$c_{SP}(r_{SP}, x, t)$ [m^{-3}]

It has a concentration distribution of particles with radii r_{SP} at the inlet $c_{SP}(r_{SP}, 0, t)$, assumed to be constant over time.

The fraction of flow that is not accessible to flow carrying particles larger than r_{SP} when flow velocity in the pores is pressure driven and governed by Poiseuille flow (parabolic velocity profile) in the circular tubes of the pores is

$$f_n(H_p, r_{SP}) = \frac{\int_0^{r_{SP}} r_p^4 H_p(r_p,x,t) dr_p}{\int_0^\infty r_p^4 H_p(r_p,x,t) dr_p} \tag{B-3}$$

The number concentration of strained particles per volume of bed is denoted by $\sum(r_{SP}, x, t)$

The partial differential equation, PDE for the mass balance for each particle size in the population is

$$\frac{\partial(\phi_a(r_{SP})C(r_{SP},x,t))}{\partial t} = -U\frac{\partial C(r_{SP},x,t)}{\partial x}(1 - f_n(H_p, r_{SP})) - \frac{\partial \Sigma(r_{SP},x,t)}{\partial t} \tag{B-4}$$

Note that this applies when there is a constant flux of water U carrying the SP in the porous medium. When the SP is carried by the expanding montmorillonite (Mt) the second term in (B-4), which means how the flux of SP changes over the distance dx, instead must be determined by the Mt flux, which changes both in time and in space.

The accumulation of strained particles is obtained by

$$\frac{\partial \Sigma(r_{SP},x,t)}{\partial t} = U\frac{C(r_{SP},x,t)}{l} f_n(H_p, r_{SP})(1 - f_n(H_p, r_{SP})) \tag{B-5}$$

l is a correlation length. Conceptually l it is connected to the length of pores but will have to be treated as an adjustable parameter until it will be possible to determine it from independent information. In the PTMC model, it is at present not entirely clear how the mixing chamber volume is to be included in the first term in Equation B-4 and how it can be used by the SP to accumulate in. In our present modelling, it is not needed to define it because the number of strained particles at the inlet of the pores can be obtained from the number of pores clogged, which is not influenced by l. We will actually not need to solve the PDE, Equation B-4, for the purposes of this report.

Finally the rate of change of the pore size distribution is

$$\frac{\partial H_p(r_p x,t)}{\partial t} = -\frac{r_p^4}{\int_0^\infty r_p^4 H_p(r_p x,t) dr_p} \boldsymbol{U H_p(r_p x, t)} \times \int_{r_{SP}}^\infty \boldsymbol{C_{SP}(r_{SP}, x, t)(1 - f_n(H_p, r_{SP}))} \boldsymbol{dr_{sp}} \qquad \text{(B-6)}$$

For the Mt expansion case, U must be changed to account for this.

In addition, initial and boundary conditions must be defined, among them the SP size distribution at the inlet.

When Mt expansion drives the SP, an additional PDE will be coupled to the above equations because the Mt expansion will depend on the available porosity ϕ_a for the Mt particles, which although small, may to some extent be restrained from entering into the pores in the early part of the bed, which clogs first. The original model in the literature implicitly assumes that U can be maintained constant although the pores are increasingly becoming clogged.

The above system of equations must be solved numerically. Some solutions have been presented for simplified cases. You et al. (2013) present an exact solution for long-term size exclusion for mono-dispersed particles. You et al. (2014) give an asymptotic solution for the non-linear stage of colloidal suspension flow. Kuzmina and Osipov (2016) derive an asymptotic solution at the filter inlet. None of these solutions are directly applicable to the problem at hand.

It may be noted that for the purposes of the present investigation it may be as important to assess that the paths will be increasingly clogged anywhere and decrease or stop further flow than to determine the exact evolution over time and in space. Then the problem could be re-formulated to follow how the clogging proceeds as a function of the volume of suspension (or particles) that has entered. Considering that the entrance pores of to the medium will be clogged first we need only to consider their fate.

For the pressure driven flow case, at the inlet the rate of change of accessible pores

$$\frac{dH_p(r_p,0,t)}{dt} = -U \frac{r_p^4 H_p(r_p,0,t)}{\int_0^\infty r_p^4 H_p(r_p,0,t) dr_p} \times \int_{r_{SP}}^\infty C_{SP}(r_{SP},0,t)(1 - f_n(H_p, r_{SP}))dr_{sp} \qquad \text{(B-7)}$$

This is an ordinary differential equation, which must be integrated numerically.

In practice it is convenient to discretize the pore and particle size distributions in n_p bins with number of pores and SP's in ranges between r_p and $r_p + dr_p$.

With n_p number of bins $dr_p = (r_{max} - r_{min})/n_p$ and $ri = r_{min} + \frac{dr_p}{2} + (i-1) \times dr_p$ for $i = 1$ to n_p.
Then the integrals become simple sums and

$\int_0^\infty r_p^4 H_p(r_p,0,t) dr_p = \sum_{i=1}^{n_p} r_i^4 n_i(r_i,0,t)$ where the number of pores $n_i(r_i, 0, t)$ in each bin is

$n_i(r_i, 0, t) = \int_{r_i - dr_p/2}^{r_{i+1} - dr_p/2} H_p(r_p,0,t) dr_p.$

The not accessible flowrate fraction $f_n(H_p, r_{SP})$ Equation (B-3) can be handled in the same way. Also $C_{SP}(r_{SP}, 0, t)$ is discretized in the same bin-sizes. If C_{SP} is constant over time only $f_n(H_p, r_{SP})$ changes in each time step in the $\int_{r_{SP}}^\infty C_{SP}(r_{SP},0,t)(1 - f_n(H_p, r_{SP}))dr_{sp}$ integral.

Then the discretized form of (B-7) becomes $\frac{dn_i}{dt} = \frac{dH_p(r_p 0,t)}{dt}$ = R.H.S of (B-7) and Equation (B-7) can be integrated by Euler-stepping to find the new number of pores of size r_i at time $t + \Delta t$ from

$$n_i(t + \Delta t) = n_i(t) + \frac{dH_p(r_p 0,t)}{dt} \Delta t$$

This illustrates the idea but a more efficient discretization scheme and a more efficient integration method is to be used in which the n_p coupled ordinary differential equations resulting from the discretisation of (B-7) are solved simultaneously. This is done by a numeric solver using adaptive time stepping. NDSolve from Mathematica®.

SP flux driven by Mt expansion

When the flux of the particles is set by the rate of expanding montmorillonite paste the velocity in pores of all sizes is the same and

$$f_n(H_p, r_{SP}) = \frac{\int_0^{r_{SP}} r_p^2 H_p(r_p x, t) dr_p}{\int_0^{\infty} r_p^2 H_p(r_p x, t) dr_p} \quad \text{(B-8)}$$

For the case when the influx of SP is driven by the expanding Mt the influx U_{Mt} (t) changes over time and must be solved by the Mt expansion equation. This must also account for the decrease of flux because the porosity $\varepsilon(0, t)$ at the entrance of the bed, x = 0, decreases over time, allowing less and less Mt to enter. For this case

$$\frac{\partial H_p(r_p 0,t)}{\partial t} = -\frac{r_p^2}{\int_0^{\infty} r_p^2 H_p(r_p,0,t) dr_p} U_{Mt}(t)\phi(0,t)\, H_p(r_p, 0, t) \times \int_{r_{SP}}^{\infty} C_{SP}(r_{SP}, 0, t)(1 - f_n(H_p, r_{SP}))dr_{sp} \quad \text{(B-9)}$$

As $\phi(0,t) = \pi \int_0^{\infty} r_p^2 H_p(r_p, 0, t) dr_p$ the equation simplifies to

$$\frac{\partial H_p(r_p 0,t)}{\partial t} = -\pi r_p^2 U_{Mt}(t) H_p(r_p, 0, t) \times \int_{r_{SP}}^{\infty} C_{SP}(r_{SP}, 0, t)(1 - f_n(H_p, r_{SP}))dr_{sp} \quad \text{(B-10)}$$

Two bounding cases

When the largest SP, r_{SPMax}, is smaller than the largest pore, r_{pMax} the pores larger than SP r_{SPMax} will never be clogged and always allow smaller particles to pass. The fraction of cross-section area of the larger pores ϕ_{open} is in the limit

$$\phi_{open} = \pi \int_{r_{SPMax}}^{\infty} r_p^2\, H_p(r_p x, t) dr_p.$$

When SP $r_{SPMax} >= r_{pMax}$, eventually all pores will be clogged and then no more SP can pass.

Appendix C

Summary of some recent erosion experiments

Figure C-1 summarises the experiments from Schatz et al. (2013), Schatz and Akhanoba (2017), ClayTechnology from (BELBaR deliverable 2.12), Reid et al. (2015) and Alonso et al. (2018). The full lines are based on the model of Neretnieks et al. (2017, Equation A2-7) with a smectite diffusion coefficient 3×10^{-10} m^2/s. The upper line is for a radius of the rim 50 mm and the lower for 10 mm. This figure essentially covers all the experiments. Mx stands for the MX-80 bentonite "as received" and NaSm stands for a detritus-free and homo-ionic smectite with sodium as charge balancing ion. The ovals indicate both the flow velocities and the ranges of results presented in the publications. It should be noted that Schatz found very large smectite losses in sloping, 0.1 and 1 mm fractures, by flocculation and sedimentation. This phenomenon was not seen at all in Ciemat's no-flow experiments under very similar conditions. All the experiments compiled in the figure were made with waters with less than 10 mM NaCl. In Schatz' experiments the synthetic Grimsel groundwater contained 0.68 mM Na and 0.14 mM Ca. All other experiments contained only Na as cation.

For the results in Figure C-1, it should be noted that it has been necessary to make approximations and assumptions when evaluating the reported results. This is because the data are presented in different ways in the different reports. Seldom there is information on the rate of expansion of the rim for each experiment together with the rate of loss. Therefore some averaging estimates had to be used based on information of the general evolution of the expanding rim. Also, it may be noted that similar, and even replica experiments, could vary considerably. The methods to determine the loss of smectite also vary. In all cases, by loss is meant erosive loss or sedimentation, i.e. the amount of smectite that was not present in the source volume or was still within the rim zone at the end of the experiment. In flow experiments, the colloids are collected in the effluent water. In Schatz sedimentation experiments the lost mass is collected in a post-mortem measurement.

Rinderknecht (2017) found an erosion rate of 0.091 kg/ m^2/yr with Febex bentonite in Grimsel groundwater in a 1 mm aperture fracture at a water velocity of about 380 m/yr. The Febex bentonite has a much larger fraction of divalent ions in the exchange positions than MX-80 and contains halite and gypsum as soluble accessory minerals, which according to Rinderknecht (2017) further increase the calcium fraction in the smectite, by ion exchange. His results may therefore not be relevant to compare with those discussed earlier as they may represent a calcium dominated clay, which is known to hardly release colloids.

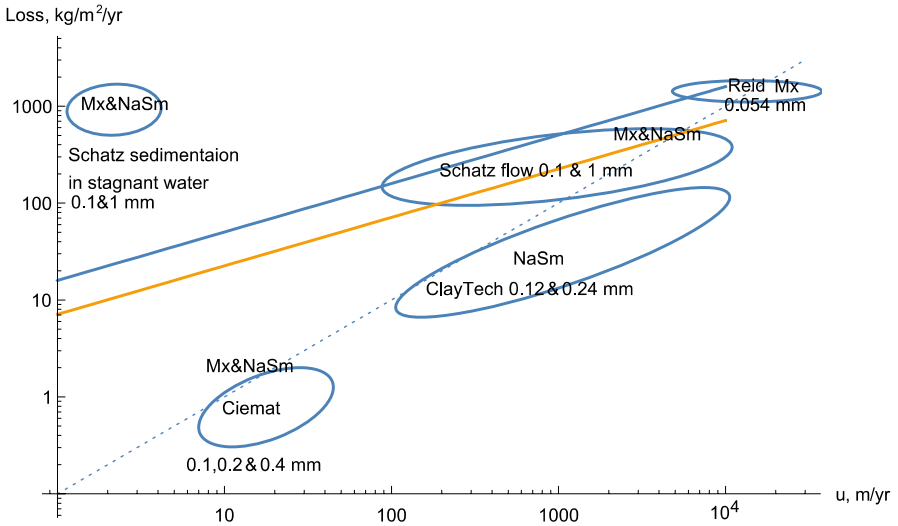

Figure C-1. *Summary of the erosion experiments from four different sources and comparison with the model in Appendix 2 of TR-16-11. These lines have slope ½. The weak dotted line shows slope 1 to guide the eye.*

The model in Appendix 2 of TR-16-11 is based on the assumption that the smectite particles are released at the interface between the expanding paste and the seeping water by diffusion, i.e. due to Brownian motion. The release takes place at a smectite volume fraction of about 1.5 %. As the water passes the interface it picks up more and more particles. This leads to the slope ½ in the log-log diagram. One can speculate that the much lower velocities and the resulting much longer residence in Alonso et al. (2018) experiments have allowed the smectite particles to agglomerate to viscous flocs that fill the fracture and are hindered to move by friction against the walls. This is supported by the circular expansion of the paste in the fracture and by the fact that no sedimentation occurs in sloping fractures.

However, considering that Schatz' experiments used essentially identical clays and waters and show an extensive loss by sedimentation in 1 mm but also 0.1 mm fractures suggest that there are one or more differences in mechanisms that we are not aware of yet. Alonso et al. (2018) reported pH falling from about 8.5 to just over 6 in the flow experiments. Clay Technology report incoming water pH just above 6. We have not found pH reported in the two Schatz reports cited, but the preparation procedures do not suggest that there should be any major differences in pH in those experiments.

We have not succeeded in finding reasons why there are no flocculation and sedimentation in Alonso et al. (2018) experiments when Schatz' experiments, very prominently show these phenomena in what seems to near identical conditions. Flocculation and sedimentation were also reported in Neretnieks et al. (2009) under similar circumstances.

Appendix D

Exploratory modelling of forces in house of cards structures

External forces caused by e.g. shearing can influence the structure and potentially break up the HoC. If the HoC is subjected to a shear force that makes the voids elongated in one direction the faces to come closer in some locations. Within a void, there will be a pressure on the surfaces of the platelets caused by the diffuse double layers, DDL, adjacent to the charged surfaces.

We illustrate this for a void with side length d_p = 200 nm filled with water with NaCl solution. The distances between the platelets in the HoC structure is on the order of 100 nm, if arranged similarly to that shown in Figure 8-1. The diffuse double layer pressure on the walls is about 1 000 Pa according to the DLVO model for 0.1 mM and 10 Pa for 1 mM NaCl, see Figure 7-3. The van der Waals attractive force between two opposing sides is negligible at this distance. In the HoC there is also DDL pressure in the surrounding voids. The DDL pressure in the adjacent voids can be different because the distance between the platelets in those voids can be different and there may be a net force trying to disrupt the HoC.

Assuming that there is only one bond on each of the four EF contacts and that the bonds are purely coulombic, the force holding this side in place can be estimated by Coulombs law

$$F = \frac{1}{4\pi\,\varepsilon_r\varepsilon_o}\,\frac{|q1\,\times q2|}{r_{dist}^2} = \frac{k_e}{\varepsilon_r}\frac{|q1\,\times q2|}{r_{dist}^2} \qquad \text{(D-1)}$$

ε_o is permittivity in vacuum, ε_r is relative permittivity of the medium. *q1* and *q2* are the two charges that attract each other, r_{dist} is their distance. The charges are equal to that of one electron. They are taken to be about 1 nm apart. This distance is on the order of a few atom diameters and is chosen for the following reason. At the EF contact point, the edge charge is located in an atom at the edge of the sheet. The other charge is inside the sheet in the mid-layer of the so-called TOT sheet (Silicon-Aluminium-Silicon oxide configuration). This gives a distance between the charges of about 2 atom diameters. The relative permittivity is 3.9 for SiO_2, which makes up the T-layer of the TOT, separating the two charges. The attractive force for 1 nm is 5.9×10^{-11} Newton. One such bond on each of the four edges of the long side face of the void with an area $2(10^{-7})^2$ m^2 can restrain the pressure difference over the faces of the sheet of 11 800 Pa.

Figure D-1a illustrates how a platelet in a HoC structure is bound to four other platelets with four atom-to-atom edge-to-face bonds. In D-1b the structure is turned 90° and shows how the platelet is stressed by DDL pressure by two other platelets in the HoC, one on each side but at different distances, *h1* and *h2*. With the same dilute water in the voids between the platelets, there will be different DDL-pressure on both sides of the central platelet. When the force difference between the net DDL pressure is larger than the force holding the platelet with EF bonds the structure will break. If the HoC is subject to deformation by shearing the difference in distances *h1* and *h2* decrease and the HoC can disintegrate.

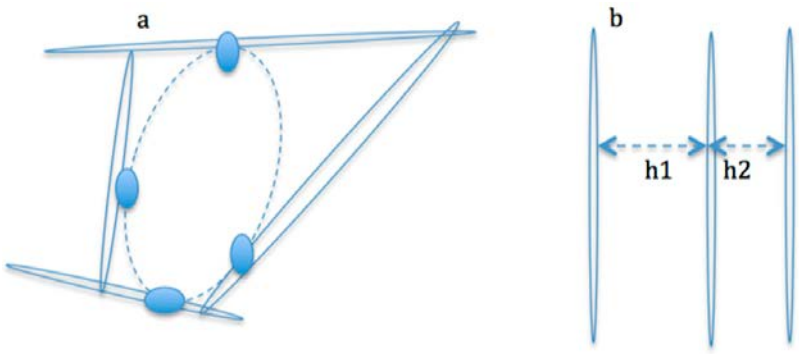

Figure D-1. *Cartoon of platelets in a HoC structure. The filled ovals symbolise one atom-to-atom bond.*

In the example, the mean distance between the 1 nm thick platelets would be $h = 1/\phi = 100$ nm. In very dilute water the DDL pressure can be described by $P_{swell} = 2.5 \times 10^7 \times \phi^{2.4}$. This is also shown in Figure 7-3. If $h1 = 150$ and $h2 = 50$ nm the DDL pressures are 2 100 and 150 Pa respectively. The difference is 1 600 Pa. This is smaller than the force holding the platelet in place by the EF bonds but shearing will deform the structure and decrease the distances, which could lead to disintegration of HoC structure. This example illustrates that it is not in-conceivable that the yield strength of a HoC-like structure could restrain considerable shear forces, even larger than what was estimated from the scoping experiments, especially if the gel is given time to mature.

Similar forces are obtained for EF bond formed by the vdW force when one edge atom comes as close as a few tenths of a nm (Israelachvili 2011). This can be exemplified by the attraction of a molecule e.g. Al_2O_3 with radius r to a thick flat sheet of a Mt. The single molecule, in this case, would represent the tip of the edge of the smectite sheet. It is assumed that the sheet has rough edges and that only atom is in "contact" with the face of a sheet. It is deemed reasonable that a rough edge only can be in contact with a plane sheet in two points. All other atoms on the edge will be at a somewhat larger distance. The attractive force between two atoms is proportional to h^{-7} according to the Lennard-Jones relation. A very strong repulsive force proportional to h^{-13} becomes important at distances about 0.2–0.4 nm, which is comparable to the atoms in the Mt molecule. However, all atoms in the face-sheet as well as in the edge-sheet contribute to the total force attracting the sheets. If the exact shape of the sheets, especially near the contact point were known one could add the contribution from all atoms in both sheets. As this is not feasible we use the results of such summation for one single atom close to an infinite sheet to roughly estimate the impact of the resulting vdW attraction. When the material surrounding these particles is water the Hamaker constant A_H is on the order $1–4 \times 10^{-20}$ Joule (Israelachvili 2011). The energy of this bond depends on the distance h between the surface of the assumed spherical molecule and the surface of the flat sheet.

$$W = \frac{A_H\, r}{6\, h} \tag{D-2}$$

The vdW force F_{vdW} then is

$$F_{vdW} = \frac{A_H\, r}{6\, h^2} \tag{D-3}$$

These expressions underestimate the energy and the force because the edge-sheet has atoms behind the first molecule and these also attract the sheet. However, because these are much further away and the energy contribution is proportional to h^{-6} this will not overwhelmingly contribute to either W of F_{vdW}. Considering that there is also great uncertainty in the value of the Hamaker constant this issue is not further refined here.

In the following example, the radius of the molecule is taken to be 0.5 nm and the distance 0.3 nm. The latter is chosen to be about the distance where the repulsive force in the Lennard-Jones potential is equal to the attractive force. This is the distance at which the EF bond would stabilise.

$W = 0.3$ to1.1×10^{-20} Joule and F_{vdW} 0.3 to1.2×10^{-11} Newton

This suggests that there is no need to stipulate that the edge has a positive charge for EF bonds to exist. It would explain that also neutral or even slightly basic water conditions could have EF bonds and develop HoC structures.

The bond energy W can be compared to the thermal energy $k_B \times T$ where k_B is Boltzmann's constant $1.38064852 \times 10^{-23}$ Joule/K and T is the temperature in K. For $T = 283$ K, the temperature at repository depths, $k_B \times T = 0.39 \times 10^{-20}$ Joule. The thermal energy of the particles is comparable to the binding energy W of the E-F bond. This implies that the smectite particles constantly twisting and bouncing in the water do not have a strong energy barrier to break through to form EF bonds and also that the bonds once formed need some imposed energy to be broken. A rough estimate of the energy needed per volume of gel with a volume fraction 3 % is made as follows. Assume that in the HoC structure each particle, 1 nm thick, and 200 nm in diameter is bonded on two opposite edges to other particles. In one m^3 there is 0.03 m^3 smectite. With the volume of each smectite particle

equal to $\pi\ 10^{-9} \times (1 \times 10^{-7})^2 = 3.14 \times 10^{-23}$ m^3, the number of bonds is 1.9×10^{21}. The total energy in the bonds then is $0.3–1.1 \times 10^{-20}$ J/bond $\times\ 1.9 \times 10^{21}$ bonds/m^3 = 5–21 Joule/m^3= 5–21 N/m^2 = 5–21 Pa. This is surprisingly close to the yield strength estimated from the scoping experiments. In these experiments, the yield strength had reached more than a few Pa after a week. However, this may be a very short time for formation of the full strength of the HoC. The yield strength of older sediment could not be determined with the simple tools at hand for the scoping experiments.

Arkitektkopia AB, Bromma, 2019

SKB is responsible for managing spent nuclear fuel and radioactive waste produced by the Swedish nuclear power plants such that man and the environment are protected in the near and distant future.

skb.se